URBAN FLOOD MODELLING AND ROAD NETWORK VULNERABILITY ASSESSMENT IN BERGEN

Sindre Eikenes

Master's thesis in Human Geography
Department of Geography
University of Bergen

June 2020

ABSTRACT

Increased emissions of greenhouse gases have brought the world's climate into a process of change. The oceans and atmosphere are warming up, which also initiates other negative consequences such as more severe urban floods. This thesis investigates the impacts and vulnerabilities that the city of Bergen, located on the rain-intensive western coast of Norway, experienced after a flood event that occurred the 14th. September 2019, and additionally how such an event would take form in the year of 2100 by adding a linear increase of 30% to the precipitation estimates. Furthermore, an assessment is performed to evaluate the vulnerability of the road network in Bergen from the GIS-modelled scenarios of urban flood. Throughout the analysis, the following questions are being answered: *How well can a major flood event be replicated using hydrological modelling based on high-resolution LIDAR data? What are the potential impacts of a flood based on end of century precipitation estimates? Which parts of the Bergen road network are most vulnerable to flooding; and what are the implications for the whole road network?* The results show that vital infrastructure such as buildings and roads are indeed vulnerable to flood since they receive a large share of the total amount of water within the catchment area. However, while one would expect an increase of flood in these same areas by the end of the century, the results show that this is actually not occurring. This suggests that the excess water has found other, less vulnerable places to accumulate in 2100 since the depressions located in and around the infrastructures are already more or less fully inundated. The level of mobility for motorists in the neighborhoods of Møhlenpris and Sydnes are found to be very reduced since most of the roads leading in and out are blocked by floods. Last but not least, it is proved that the highly trafficked and vulnerable area of Bryggen which is on the UNESCO list (United Nations Educational, Scientific and Cultural Organization) for World Cultural Heritage is also susceptible to large amounts of surface flood. Urban flood modelling is important in order to assess the economic and socio-economic impacts that the society may face. One major limitation to the analysis is that the drainage system and rate of infiltration is modelled by using a dataset of uniform values representing the losses of water instead of applying a dynamic coupling between a surface flood model and drainage model.

ACKNOWLEDGEMENTS

To work on and complete a master's thesis has been a very educational process. An especially important lesson has been to learn how to deal with the challenges of such a large project and find solutions to the obstacles that occurred. During this last year I have gained a much deeper insight into the utilization of GIS and how it plays a vital role in many parts of science.

First and foremost, I would like to thank my main supervisor Benjamin Aubrey Robson who has played a crucial part in navigating me through this uncharted water of producing a master's thesis. He has constantly provided fast, precise and an abundance of feedbacks to my numerous questions regarding every aspect of the thesis, even in these Covid-19 times.

Furthermore, I want to thank my other supervisor Hanna Kvamsås for providing sound advice related to urban flood. Another thanks goes to Håvard Haarstad who was a vicarious supervisor in the early stages of the thesis, and also Peter Andersen and Gidske Andersen for helping me stake out the theme of the master thesis. The employees at the Water and Sewage department in Bergen Municipality also deserves recognition for providing me with relevant information and GIS-data.

Finally, I would like to thank all my fellow co-students at the department, and last but not least my fiancé Karoline who, for better or worse, has had to cope with me these last couple of months of the write up process.

Table of Contents

Abbreviations

IDF – Intensity-Duration-Frequency
NVE - The Norwegian water resources and energy directorate
AOI – Area of Interest
NCCS – Norwegian Carbon Capture and Storage
GIS – Geographical Information Systems
DTM – Digital Terrain Model
1D / 2D – One-dimensional / Two-dimensional
IPCC – Intergovernmental Panel on Climate Change
LIDAR – Light Detection and Ranging

List of figures

List of tables

1. Introduction

1.1 Theme

The world's climate is in a process of change due to an increase in emissions from greenhouse gases (GHG). Climate change has become a familiar phrase throughout the world, both due to the attention it has received in media and science, and by those among us who have experienced the effects of it first handedly (Bulkeley, 2013, pp. 1-2). The Intergovernmental Panel on Climate Change (IPCC) states in their synthesis report of 2014 that climate change can not be misinterpreted. It is happening right now and causing the oceans and atmosphere to warm up (IPCC, Contribution of Working Groups I, II and III to the Fifth Assessment Report of the Intergovernmental Panel on Climate Change, 2014). The climate change risk that will be the main theme of this thesis is extreme weather, more precisely heavy precipitation in an urban context and the floods that emerges from it.

The cities and regions of the world have and will have various encounters with climate change and its consequences. For an instance, tens to hundreds of millions of people in Africa will be affected by increased water stress by 2020, and many of Africa`s coastal areas will be impacted by sea-level rise by the end of the 21st century. By looking at another region, North America is amongst several other potential impacts expected to experience an increase of heatwaves to their urban areas (IPPC, 2007, in Bulkeley, 2013, pp. 3). Downscaling from regions to urban areas, Hunt and Watkiss (2011, in Bulkeley, 2013, pp. 20-21) names five particularly significant risks a city may experience due to climate change and what the direct and indirect impacts they may cause. The severe risks are; accessibility and quality of water, availability and usage of energy, health issues, problems related to increased sea level (coastal cities), and extreme events. The latter includes but are not limited to heatwaves, droughts, and rain-induced floods. As a direct impact, extreme events are able to cause damage to i.e. infrastructure and property, which may affect the economy of the involved actors as an indirect impact (Hunt & Watkins, 2011, in Bulkeley, 2013, pp. 20-21). It is therefore somewhat clear that climate change imposes risks all over the world in various forms. In the following I will take a closer look at the Norwegian context, and thereafter the city of Bergen which is my area of study.

1.1.1 Norwegian context

In 2014 a report was published by NCCS (Norwegian Carbon Capture and Storage) that looked at how the climate change and its risks would affect Norway throughout the 21st century, basing its calculations on the fifth (and latest) assessment report of the IPCC. Precipitation in Norway is largely determined by the greater wind-conditions. Whether it originates from southeast or southwest it will provide lots of precipitation to different parts of Norway (NCCS, 2015, pp. 3 & 49). Changes in the wind-direction or conditions may therefore result in major differences of both the amount and distribution of precipitation in Norway. NCCS (2015, pp. 8 & 103) explain that the annual precipitation in Norway are expected by the end of the century to increase between 7-23% based on different calculations, where 18% is the median value. Another consequence of the climate change is a major increase in days of heavy precipitation (0,5% of the heaviest precipitation events occurred over 24 hours between the years 1971-2000), which NCCS (2015, pp. 108) believes will increase by 49-89% annually across the country based on different calculations. In addition to days of heavy precipitation, the amount of rain on these days are also expected to grow. The western coast where the city of Bergen is located will receive the largest increase of rainfall (in mm) compared to the other regions (NCCS, 2015, pp. 108).

These heavy and intense rainfalls can increase the chance of flash flooding, and it is especially critical to the western coast with its steep topography according to the county authority of Hordaland's climate plan (Hordaland Fylkeskommune, 2014, pp. 19). They estimate that as a direct consequence of the expected heavy precipitation as mentioned above, floods on the western coast will increase in size by 20-60% by the end of the century. These floods due to extreme weather is what Hunt and Watkiss (2011, in Bulkeley, 2013, pp. 20-21) mentioned as one of the most significant risks to urban areas. Seeing that Norway's second largest city of Bergen is located in the midst of this, it will serve as the area of interest in this study.

1.1.2 Urban hydrology in Bergen

In densely built areas it is not the accumulation of heavy precipitation over several days that do the most damage to infrastructure and buildings, it is the shorter, extreme precipitation that occurs within a couple of hours. This has the potential to flood large urban areas where e.g. the drainage system does not have the capacity to keep up with the increasing flood, or it is unable to enter the system as a result of soil and objects brought by the flood which blocks the entrance

to the culvert (NCCS, 2015, pp. 55). In the risk and vulnerability assessment of Bergen from 2014 it is mentioned that the average annual amount of precipitation is at 2500mm, and there are on average 242 days of rainfall per year (Bergen municipality, 2014, p. 14-16). The risk categories included in this assessment are natural disasters, major accidents, critical infrastructure, intentional events, and health. In total there are 31 different risk events within these categories. By looking at the overall assessment of the different events, extreme weather is one of the most severe risks Bergen may face. Extreme weather is critical in four out of five overall assessment categories, these categories are life and health of the citizens, the environment in Bergen, material and economical damage, and the reputation/trust of the municipality (Bergen municipality, 2014, p. 48-54).

Urban-hydrology is the part of the water-cycle connected to urban areas. In a city that contains numerous streets and buildings, like Bergen, precipitation will not be able to infiltrate through the ground as easy as in the nature. As a result, flooding and erosion from heavy precipitation in urban areas contrary to rural areas may happen more rapidly because the runoff rate of the water will be faster due to its dense surface. The floods will also be larger compared to the same amount of precipitation in the nature because both the infiltration and evaporation are reduced (NVE, 2018). Figure 1-1 illustrates this difference between natural and urban hydrological processes.

This mixture of grey infrastructure and heavy precipitation has already caused significant economic and socioeconomic damage to the inhabitants in Bergen. A weather station (rain gauge) in Florida in Bergen recorded 480,7mm of rainfall in September 2018, making it the wettest month in Bergen since the weather station was established in 1983 (Hansen, 2018). During this period a number of buildings and infrastructure were flooded due to large amounts of precipitation, resulting in large sums of insurance compensations to be paid out (Fredriksen & Oldeide, 2018). Flooding may also affect the roads and networks in urban areas. On 26. September. 2018, by the end of the record-breaking precipitation month, many of the roads leading traffic in and out of Bergen were closed due to flooding (Johansen & Kranz, 2018). In addition to damaging the actual infrastructure, the flood has socioeconomical impacts by affecting the movement of the 281 445 inhabitants within the municipality and more on the outskirts (Statistisk Sentralbyrå, 2018).

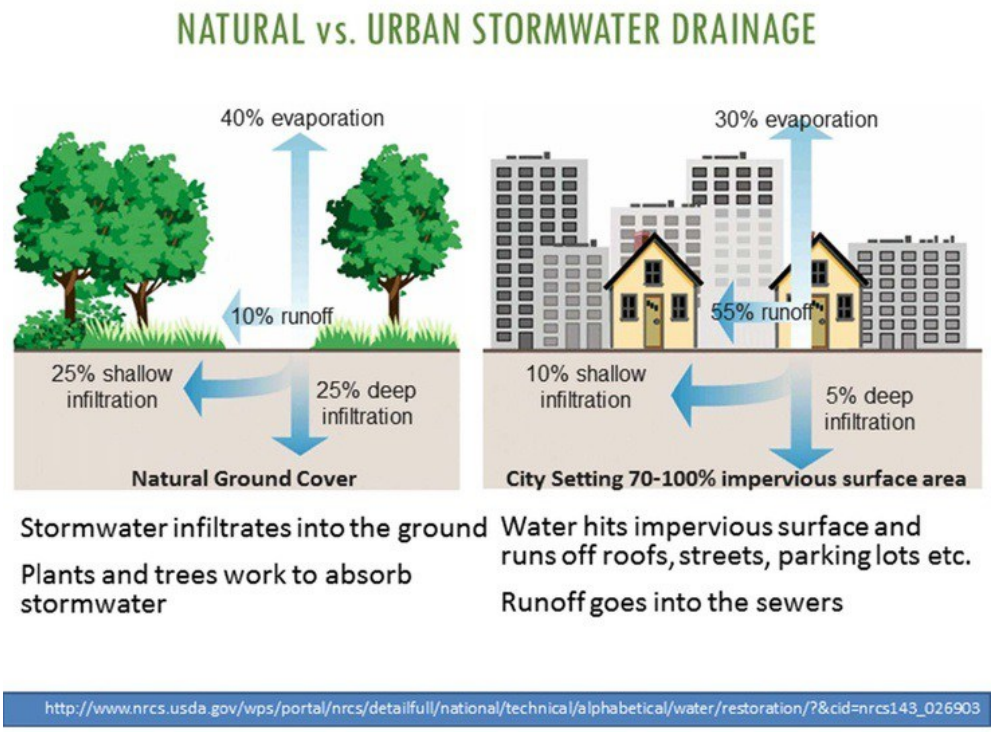

Figure 1-1. Natural vs urban hydrology. Source: Brandon Mississippi (2018).

1.2 Outline and research questions

As it is explained above, Bergen has had severe urban floods in the past, and will receive even more intense precipitation in the future that might lead to much more severe urban floods. Thus, the aim of this thesis is to use a newly developed GIS-tool called Itzï to model both a recent event of heavy precipitation that lead to urban flood in Bergen, and consequently try to aggregate the data to show how much more severe the urban flood might turn out to be by the end of the century. Furthermore, an assessment will be performed by using network-analyses to see how vulnerable the road network in Bergen is to these scenarios of flood.

The area of study in Bergen is, as shown in the overview map of figure 1-2, delimited to the most local watershed covering the city-centre. This figure also presents the location of the rain-gauge at Florida where the precipitation data is collected from.

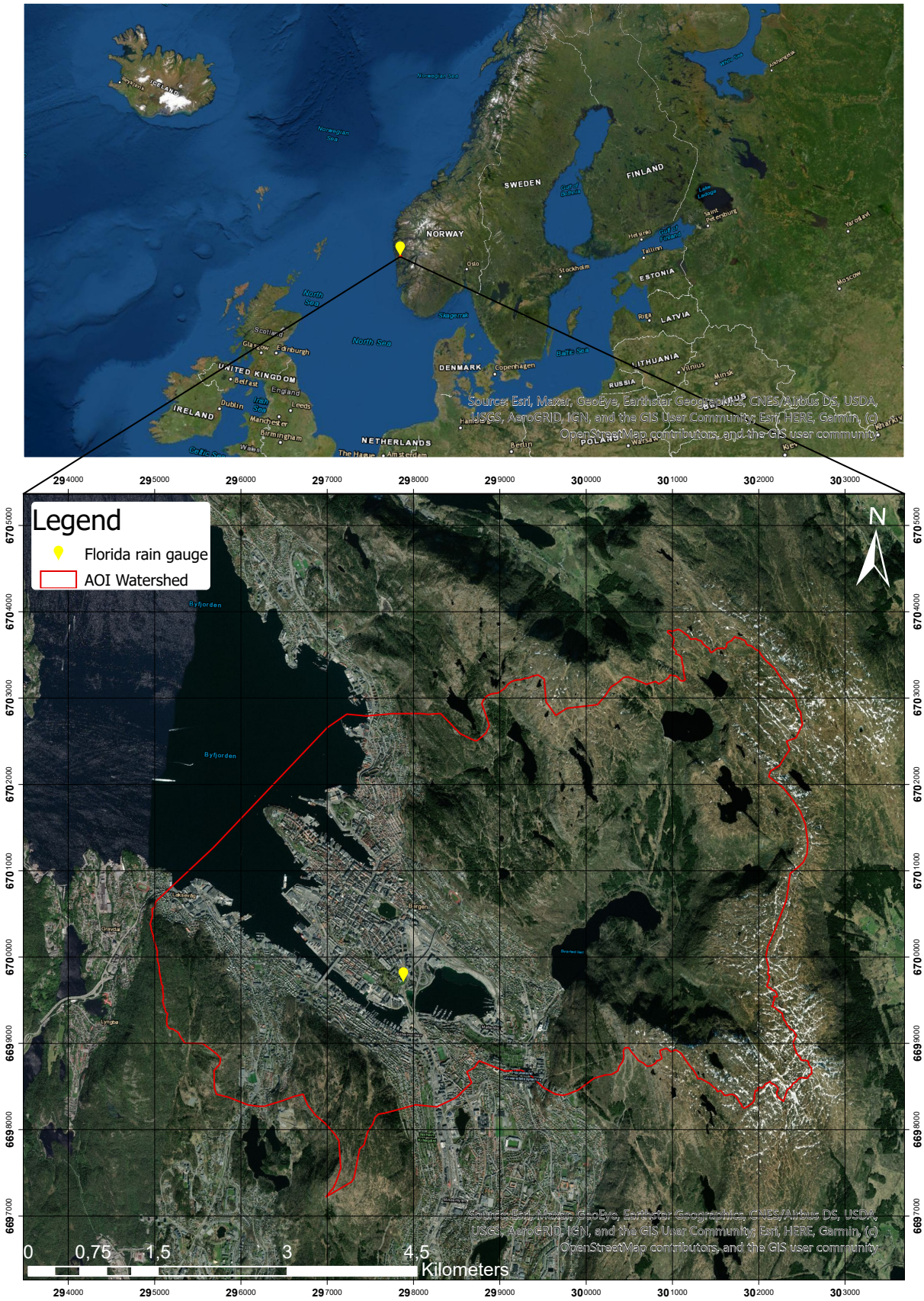

Figure 1-2. Overview map of Bergen and the delineated watershed surrounding the city-centre representing the area of interest (AOI). The location of the rain gauge at Florida is also included.

Hence, in order to fully address the aims of the thesis as stated above, this project will try to answer the three research questions of:

- *How well can a major flood event be replicated using hydrological modelling based on high-resolution LIDAR data?*

- *What are the potential impacts of a flood based on end of century precipitation estimates?*

- *Which parts of the Bergen road network are most vulnerable to flooding; and what are the implications for the whole road network?*

2. Theory

As highlighted in the introductory, this thesis will focus on GIS-modelling of urban floods. Hence, to start this chapter in a more general matter, the theoretical frameworks will first and foremost introduce and provide an understanding of the wider term geohazard and how one may use GIS-modelling to predict such hazards (section 2.1). Following this, an overview on other relevant research using GIS to model urban flood will be outlined (section 2.2). The chapter is concluded by providing a deeper insight into the GIS-tool of Itzï

2.1 Geohazards

A geohazard is a risk or damage stemming from geological sources, and despite there being many various types of geohazards that may occur by either natural or artificial processes, they all have in common that they can potentially pose a great risk to both human lives and the built infrastructure. The occurrence of a geohazard can be developed within a short time period (e.g. minutes or hours), or a very long time period (e.g. thousands of years), all depending on the type of process the geohazard represents. Furthermore, the various hazards can be observed in almost every corner of the planet and are all a part of the endless shaping of the solid earth (Culshaw, 2018). According to Culshaw (2018), the types of geohazards can be categorized into 6 groups based on the processes causing them, or the properties of the substance constituting them. The 6 categories are listed below:

- *Geomorphological hazards:* Activated by natural processes that are close to the surface (e.g. erosion, avalanche, permafrost).

- *Geotechnical hazards:* A geohazard that are activated by the properties of a material (e.g. quick clay, saline soil, acidity).

- *Hydrological or hydrogeological hazards:* Activated by movement of groundwater or water at the surface (e.g. change of groundwater level or surface flood).

- *Geological hazards:* Directly or indirectly impacts from the source (e.g. earthquake. tsunami, volcanic eruption).

- *Marine hazards:* Partial movement of ocean floor or release of gas and/or fluids (e.g. coastal erosion, gas hydrate release, turbidity currents (underwater current moving quickly downwards due to excess weight of sediments)).

- *Artificial hazards:* Human induced hazard by removing or adding fluids, gases, chemicals, or physical materials (e.g. pollution, landfill, contamination).

Having listed the various categories of geohazards included specific examples, it is the hydrological hazards that is of interest here since it represents surface floods. The subsequent section will address how and why GIS-modelling can be a helpful tool to identify the potential of geohazards, which in turn can be used as a guide to reduce the level of risk and lower the costs the hazards may afflict.

2.1.1 GIS-modelling of geohazards

Geographical Information Systems (GIS) is a collective term for the tools (computer hardware, software, applications and procedures) used to capture, store, analyze and present spatial data sets. GIS is used when one need to find answers to spatial challenges by evaluating the relationships between measurements from sensors in space and/or on the ground. It can also handle large data sets from various sources. Seeing that GIS have all of all of the abovementioned capabilities it is a very essential tool for modelling geohazards, – especially since GIS allows the spatial and temporal dimensions of hazards, such as floods, to be assessed and understood (Culshaw, 2018 & Kundu, 2017).

Two examples will followingly be given illustrating how GIS can be applied to map geohazards such as earthquakes and coastal storms.

Earthquakes, located in the category of geological hazard, have the possibility to afflict devastating damage to both infrastructure and people, and even entire cities can be destroyed in worst case scenario. By using GIS, it is possible to find areas prone to earthquakes and their susceptibility-rate. This can be done by e.g. combining remote sensing data from satellites containing information of the spatial distribution of the tectonic plates with ground data to assess the displacement-rate. One can also add other types of spatial data into the analysis to attain an even more updated risk-map. Some examples of these are; locations of earthquakes that has happened in the past, boundaries of the crust-plates, other secondary hazards that are

likely to be activated from an earthquake (e.g. landslide) and geological properties of the ground (Kundu, 2017).

Coastal hazards such as tsunamis, sea-level rise, and cyclones are another type of geohazards that also have the potential to afflict severe damage to humans and the built area, and they are especially critical to many of the world's cities since a great number of these are situated close to the coast. The coastal storm intensity and its reach can be modelled by using satellite observations of ocean surface wind vectors (e.g. ASCAT wind-data from the satellite METOP-A, run by EUMETSAT) combined with data showing the level of precipitation that has the same spatial coordinates and temporal resolution (Kundu, 2017).

2.2 Approaches to urban flood-modelling and relevant research in Norway

Due to the fact that much of the urban areas are impervious (i.e. that water cannot pass through the ground), they are prone to lower rates of infiltration and higher rates of runoff-water, causing pluvial or urban floods following extreme rainfall events (Chen, Hill & Urbano, 2009). The societal and economic consequences of this has turned out to be at a very critical level, claiming for an example 409 lives and a financial loss of 50 billion Indian rupees (RS) in Mumbai, India after a flash flood at 26th July 2005 (Kulkarni et al, 2014). Another example is in 2016 when 1192 towns in China were hit by urban floods, claiming 144 lives, causing a financial loss of 50.6 billion Chinese Yuan (RMB) and affecting 32.82 billion citizens (Liang, Lin & Wu, 2019).

Since urban floods can have severe impacts on society, methods and tools are needed in order to mitigate the harmful consequences they may have. This subchapter will first provide a deeper understanding of the characteristics of urban floods, and thereafter a review of some varying methods that are most common when utilizing GIS to model such events (section 2.2.1). An overview will also be given of some of the research of GIS-modelled urban flood that has previously been conducted in the more local context of Norway (section 2.2.2).

2.2.1 Characteristics of urban flood and the main methods of modelling them

According to Abede and Bulti (2020), the various methods of GIS-modelling urban flood can be categorized into the groups of; "*rapid flood spreading (RFS), overland flow (1D and 2D), and sewer-surface coupling approaches (1D-1D and 1D-2D)*," - leaving out the approach of

"*one-dimensional sewer (1D-S)*" since it only relates to drainage. The remaining of this section will provide an explanation of the categories above in order to facilitate for a better understanding of section 2.3 where the urban flood modelling tool used in this thesis, Itzï, will be explained.
However, first a description will be provided of some of the characteristics of urban flood. In addition, two key terms of the urban drainage system will be presented because the utilization (or not) of these have a large effect on the reliability of the outputs from the methods.

Flood inundation modelling (inundation referring to lands that are overflowed) are well suited for establishing the distribution and the range of the flood, as well as other characteristics such as e.g. how fast the runoff-water are moving on the surface. The latter is synonymous with flow velocity and is appropriate for risk assessing the potential damage to infrastructure. The former however, representing the actual water depth and range of the inundation can be used for e.g. mapping water resources or areas in need of better drainage capacity (Abede and Bulti, 2020).
Further on, although much of the rainfall in catchment-areas surrounding urban setting turns into runoff-water as illustrated in figure 1-1, some parts of the stormwater enter the processes of initial and continuing losses. Initial losses represent a smaller amount of the precipitation that are kept on rooftops, on vegetation, and in puddles on the ground etc. Continuing losses on the other hand are the amount of water that are being infiltrated through the ground or via evapotranspiration. This latter type of losses can occur as long as there is water on the surface, although the type of catchment, the rainfall-duration and the threshold-level of saturated soil will have an effect on the rate of loss, which subsequently will increase the rate of runoff-water (Abede and Bulti, 2020).

The two key terms mentioned above represent two different parts of the urban drainage system, where the first one, minor drainage system consists of manholes, inlets, ditches next to the road etc. (i.e. constructed drainage systems). This is where much of the runoff water would end up under normal precipitation events. The second type, the major drainage system, is the pathways that the runoff-water would take (on the surface) if and when the capacity of the minor drainage system is surpassed due to heavy precipitation (i.e. areas and channels that are not artificially made constructs to guide the runoff water). These pathways can be e.g. streets, depressed channels or depressed areas where the water is temporarily stored (Abede and Bulti, 2020).

The method of *rapid flood spreading (RFS)* is a more simplified method of modelling flood since it only acquires terrain data (DTM) as spatial input, and the output only illustrate the final state of a flooded area. It does not provide any flood velocity, nor does it take into account the pathway of the water and it is modelled within a duration of maximum 2 minutes – contrary to several hours. The method first finds the impact zones (areas prone to accumulation of water) using the terrain data and thereafter cells are established with the purpose to store the water. Secondly, the cells in each impact zone with the lowest height are identified, indicating where the water should start flooding. Finally, the flood can be computed, starting at the defined cells and moving on to the neighboring cells when these are filled up. It is completed when there is no more water left (Abede and Bulti, 2020).

The *one-dimensional (1D) overland flow modelling* method attempts to simulate the runoff water defined earlier as the major drainage system (i.e. only the water flowing on the surface, excluding the minor drainage system). Since the surface flow will be modelled in 1D, the route of the flow can only go in one direction, contrary to a 2D modelled overland flow where it is multidirectional (X-Y-Z coordinates). This implies that when for an instance a depressed area becomes overflooded and the water should be enabled to flow further, this method will not model such a feature.
The input-data requirements of the method are a DTM and a surface network dataset, and the modelling-duration is very short, – similar to the RFS-method (Abede and Bulti, 2020). The surface network can be created either manually or automatically by using the DEM combined with other tools. This is however a very time-consuming process and the water need to flow on the defined network in order to attain a viable result (Abede and Bulti, 2020). The 2D modelled overland flow method (which will be explained in the subsequent section) on the other hand does not need this type of data because the floodwater can automatically navigate on the surface of the DTM throughout the duration of the modelling (Djordjevic, 2010, pp. 116).
To conclude, the method can provide indications to areas of urban flood as long as the surface network dataset is of a good quality with well-defined channels for the waterflow to follow. But, seeing that it does not include the minor drainage system and it is in 1D, it will not be as accurate as the subsequent methods can be (Abede and Bulti, 2020).

The *two-dimensional (2D) overland flow modelling* method have, contrary to the 1D method, many more calculations at the cell-level since it represents a two-dimensional (multidirectional) waterflow. As a result, more dynamic outputs are given in the format of velocity, water depth-

level at each time step, and the maximum inundated level to mention some. Furthermore, as the accuracy of the model gets higher, requiring a more detailed DTM (i.e. higher resolution, preferable less than 5m) and topographic data as inputs, it can also provide a higher computational time than the beforementioned methods. This does however also require a longer run-time for processing the data. Another feature of this method is that it is more suitable for smaller scale modelling in urban areas due to the higher resolution and more nuanced cell-level calculations, but it still has limitations since it does not account for the minor drainage system in

Finally, the two remaining methods are the *coupling approaches of sewer-surface modelling in 1D-1D and 1D-2D* (where the sewer flow at the left side is always one-dimensional, while the surface flow at the right side can be either one-dimensional or two-dimensional). What distinguishes these two methods from beforementioned methods is that they include both the minor and major drainage systems, deeming them more accurate. The 1D and 2D surface flow methods are coupled to the 1D sewer flow (modelled below the ground) at defined points (manholes, inlets etc.) where the water can flow bi-directionally (i.e. entering the sewer if there is capacity for it, or spilling out if it is overflowing). The input-data of the 1D-1D method includes a DTM, surface network and a network of the stormwater drainage system. However, as explained earlier the waterflow of the 1D surface flow method must be confined within the defined surface network. If and when the drainage overflows, creating alternative pathways for the surface water to flow, it will not be modelled by the 1D surface flow. On the other side, remembering the capabilities of the 2D surface flow method (multidirectional modelling), the 1D-2D method has the ability to model the water from the overflowed drainage systems – deeming it the most accurate method explained here. It is however more suitable for smaller scaled, more complex systems since the data requirements (DTM, surface network, sewer network and topographical data) needs to be very detailed, which in turn creates a long computational run-time (Abede and Bulti, 2020).

2.2.2 GIS-modelled urban flood in Norway

This section will present some of the research that has been conducted in Norway where GIS has been applied to model urban flooding.

Between the years of 2011 and 2013, Meiforth (2013, pp. 3) conducted a research in the city of Trondheim, Norway where the aim was to map the flood streams that arrives after events of

heavy precipitation. To model the whole downtown area, tools from the spatial analyst and 3D analyst from ArcGIS were used to prepare the data's; height models (i.e. DTM) and 3D vector data (constructed from FKB-data which is the most accurate official topographical data that is accessible in Norway). The toolset was also used for the actual hydrological analysis. In order to get observable results by limiting the ducts/drainage, the analysis was performed during the winter when these were partially blocked by snow and ice. Subsequently, two different scenarios were modelled. One of them had all the ducts blocked, while the other one still had some of the larger ducts operational. To conclude, the primary result from this research was the ability to identify the locations and sizes of the flood stream as line features within the catchment area, which could further be used for municipal planning in Trondheim (Meiforth, 2013, pp. 3 & 43).

Another approach to flood-modelling was conducted by NVE (the Norwegian Water Resources and Energy Directorate) who in 2011 published a report where the aim was to assess the flood-risk susceptibility covering all of Norway. The method consisted of using GIS-analyses and hydrological parameters to map the spatial distribution of the areas susceptible to flood. However, due to the small scale of the outputted susceptibility map, being modelled on a national level where the DTM had a spatial resolution of 25x25m, it is only meant as an indication as to where one should perform more detailed flood-analyses as it only visualizes potentially hazardous areas prone to flood (NVE, 2011). Furthermore, the aim of the report was initially to include four significant flood-types in the Norwegian context to the analysis; fluvial floods (rivers), flash floods (flood-streams outside of the river networks), urban flood, and storm surge – and sea level rise. However, due to obstacles related to quantification, availability of data and information, the urban floods and sea level rise were not included in the GIS-modelling. The results from the analysis managed to identify 6777 unique areas throughout Norway that were susceptible to flood (NVE, 2011 pp. 8-9 & 21).

The final Norwegian research on GIS-modelled urban flood to be mentioned here is a report produced by Ramboll (a consulting engineering company) in 2015 on behalf of the Norwegian Environment Directorate (Miljødirektoratet). The aim of the report was to survey the methods and tools that could be used for modelling surface floods (Ramboll, 2015). Subsequently, the methods that were utilized were in fact very similar to the methods of GIS-modelled urban flood that Abede and Bulti (2020) categorized (as explained in section 2.2.1). Ramboll (2015) ordered the methods hierarchically into groups based on their application of tools, data, demand

of resources, their strength/weaknesses and their most important results. To sum these up in three categories (adhering to section 2.2.1), the lightest methods consisted of simple GIS-models to model surface floods. The next category that used more advanced tools, data, computational power and provided higher level of detail consisted of 1D/2D models to model either drainage or surface floods. Finally, the most advanced method was the coupled 1D (drainage) and 2D (surface flood) model. Two versions of this model were presented. One of these used the exact same methods as the 1D-2D model explained in section 2.2.1. The other model however also implemented the floods originating from rivers and creeks into the analysis, deeming it the most advanced method (Ramboll, 2015).

2.3 Itzï: Urban flood modelling

Itzï is an open source tool that enables a two-dimensional (2D) numerical modelling of the hydrologic and hydraulic processes of surface-floods. The tool is written in the Python programming language, and it is integrated with the open-source GIS-software of GRASS, enabling a utilization of various spatial and temporal resolutions of the datasets (s This integration also provides other positive factors such as:

- No need of changing spatial extent or resolution of every single input-data. This can be specified in GRASS' inherent computational region (e.g. if the DTM has a spatial resolution of 3m, and the rainfall data is at 100m, the simulation will nevertheless be executed at the defined resolution set in the computational region of GRASS).
- Space Time Raster Data Sets (STRDS) which are inherent to GRASS can be utilized. This facilitates for using e.g. rainfall-data that varies spatially and/or temporally, enabling the modelling of an entire extreme-precipitation event.
- One can also use absolute time when modelling the events (time and date), facilitating for modelling actual historical flood-events (Courty, Acuna and Bates, 2017).

Since the tool was developed by Courty (2018) as a part of his doctorate degree, an evaluation had to be performed to determine its validity. Hence, it was verified against three types of test cases where two of them were analytical test cases, while the third was a comparison against a similar model called LISFLOOD-FP, using the same numerical scheme (i.e. how the 2D water flow is calculated at the cell-level). The two former tests showed that Itzï is suitable to simulate "subcritical flow conditions" which was the aim of the test (Courty, Acuna and Bates, 2017).

For the third test, Itzï outputted almost identical results as the LISFLOOD-FP-model where they used the same parameters and ran for 83 minutes. A reproduction of an actual urban flood-event in Hull, UK from 25. June 2007 has also been used for validation where the results were compared against other sources containing information of the flood-extent. Here too the results were prominent and were able to locate the major flooded areas (Courty, Acuna and Bates, 2017).

For the modelling of the urban flood-event in Hull as explained above, Itzï was not coupled with a drainage model. The drainage was instead represented by using a raster-dataset with theoretical values representing the estimated hourly losses through drainage and infiltration in the urban (2.917mm/h) and rural (0.625mm/h) areas (Courty, Acuna and Bates, 2017). However, in a later version published by Courty (2018) the 2D surface flood model of Itzï was updated so that one had the option to couple the model to a 1D drainage model by the name of SWMM (Storm Water Management Model). SWMM is a frequent used and popular urban drainage modelling going all the way back to 1983, developed by the United States Environmental Protection Agency (EPA). Since this more advance method of coupling the 1D-2D is possible, the input-data should be of a high detail level and ought to include rainfall-data (preferably spatially distributed), DTM, landcover-dataset and sewer data (Courty, 2018).

3. Methodology

The aim of this chapter is to address the methods utilized in the thesis, including the decisions-makings in order to end up with the final outputs and supplementary theories supporting these decisions.

The first subchapter of data preparation will provide an overview of all the original data used as well as an explanation of the preparation of the precipitation-data. In the subsequent subchapter a detailed account will be given of the geospatial methods utilized in the GIS-software's of ArcGIS, GRASS and Itzï. ArcGIS was used for both preprocessing of input-data and for performing various network – and impact analyses on the flood-outputs generated from Itzï. GRASS was used for a continued preprocessing of the data originating from ArcGIS, as well as being the software of which Itzï is run through.

3.1 Data preparation

Prior to the GIS-analyses, several different datasets (both geographical and non-geographical) were collected from various sources and had to be preprocessed before being used in the GIS-software's Itzï, GRASS and ESRI ArcGIS Pro. A summary of these datasets can be seen in table 3-1 along with their names, data-sources, descriptions, datatypes, cell sizes (if applicable), date of acquirement and geographical coordinate-systems.

Table 3-1: Description of the input-datasets used in the analyses

Name	Description	Usage	Datatype	Coordinate System	Cell Size	Date of acquirement	Data source
DTM	**DTM_33_104_120.tif** (Digital Terrain Model)	Terrain-data to be used for flood-modelling	Raster	EUREF89 UTM sone 32N	1m	23.05.2019	Kartverket.no
Watershed-dataset	**Nedbørfelt Regine enhet** Polygon-dataset of rain catchment area	Used to create mask and watershed of AOI	Vector	ETRS89 UTM sone 32N	N/A	19.08.2019	NVE.no
Landcover-dataset	**FKB-AR5.** Landcover-dataset	Landcover dataset used to create friction - and infiltration/ losses-maps	Vector	EUREF89 UTM sone 32N	N/A	19.08.2019	Geovekst.no / Kartverket.no
Precipitation-statistics	Historical precipitation data from Bergen (Florida rain gauge) 14.09.19	Values used to create uniform and temporal precipitation-rasters and thereafter STRDS	Statistics	N/A	N/A	01.10.2019	Graf.itasdata.no
Water-dataset	**FKB-Vann.** Waterbody-dataset showing geographical locations of lakes, oceans, rivers, coastlines etc.	Generated outlet of domain for surface-water and a mask of lakes and ocean to crop DTM	Vector	EUREF89 UTM sone 32N	N/A	28.08.2019	Kartverket.no
Building-dataset	**FKB-Bygning.** Dataset containing detailed building-information	Used to add buildings in DTM for flood analysis and in post-analyses	Vector	EUREF89 UTM sone 32N	N/A	03.09.2019	Kartverket.no
Road-network dataset	**FKB-Veg.** Dataset containing geometry and attributes of roads	Used to calculate amount of urban flood on road-networks	Vector	EUREF89 UTM sone 32N	N/A	28.10.2019	Kartverket.no

3.1.1 Precipitation data and future forecasting

The aim of this subchapter is to locate a historical precipitation event in Bergen extensive enough that it may lead to surface-floods. Thereafter, a portion of that historical precipitation event will be assigned to an IDF-threshold (Intensity-Duration-Frequency) and accordingly the values will be aggregated to represent a similar precipitation event for year 2100.

3.1.1.1 Locating an extreme precipitation event

The weekend of 14-15.09.2019, NVE issued an orange cautionary level for precipitation-induced flood for the county of Hordaland (Opheim, 2019). This is the second highest cautionary level that can be issued, predicting comprehensive floods and expecting a return period for over 5 years, which will be explained further down (Varsom, n.d.) In hindsight, statistical precipitation data from Florida rain-gauge (located centrally in Bergen) showed that there had not been a precipitation event over the course of 24 hours at the same level since 26.09.2018, and one need to go back to 23.12.2017 to observe an event exceeding this level (Norsk Klimaservicesenter, n.d. B). Having located such a severe and up-to date event, the precipitation-data over 48 hours from 14-15.09.2019 was obtained from a web database (graf.itasdata.no) provided by the Water and Sewage department in Bergen municipality. The collected statistical data can be seen in the graph in figure 3-1, included a visual comparison of the average hourly precipitation levels of September 2019 (0.4mm), shown as linear, uniform values over 48 hours.

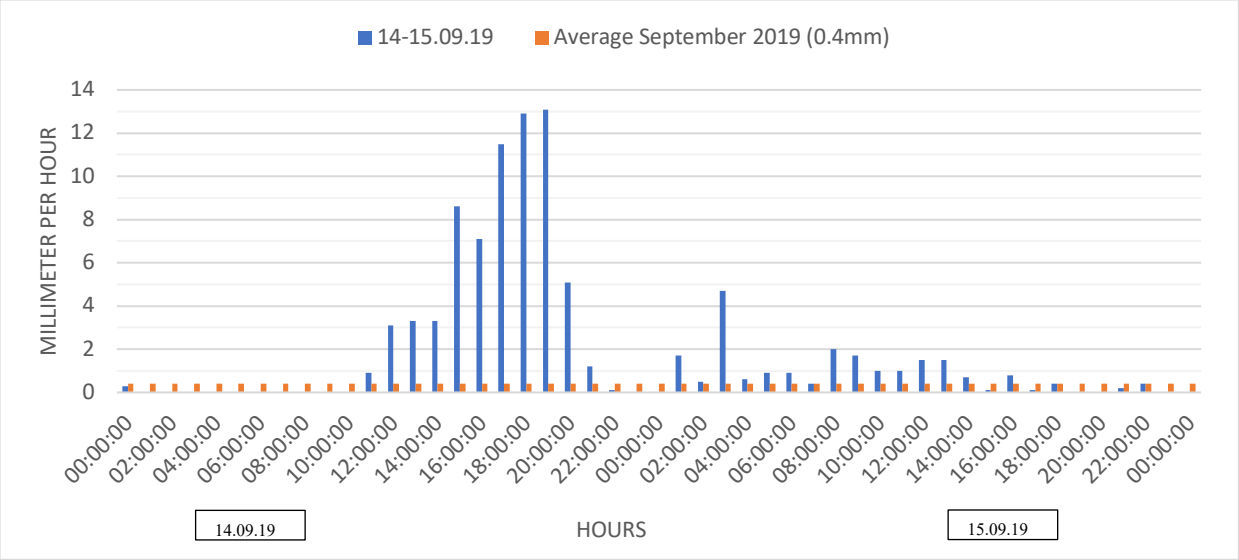

Figure 3-2: Precipitation-data in mm collected from Florida rain-gauge over a duration of 48 hours. Blue columns show precipitation values per hour from 14-15.09.2019. Orange line illustrate the average hourly precipitation-values derived from every hour in September 2019. Source: graf.itasdata.no

3.1.1.2 Estimation of Intensity-duration-frequency (IDF)-threshold for 2019

An IDF-threshold or curve is the probability that a given rainfall-event might occur at a location. It is composed of *Intensity*; the amount of precipitation (mm/h), *Duration*; the number of minutes/hours of precipitation with that intensity, and Frequency (return period); how often that given intensity and duration might repeat itself (The Climate Workspace, n.d.). In total, the amount of precipitation recorded at the selected event was 91,6 mm for all of the 48 hours. However, this is not within the limits of the IDF curve for short term heavy-precipitation recorded at Florida rain-gauge as presented in table 3-2 (Norsk Klimaservicesenter, n.d. A) By comparing the historical precipitation-event to the values of this table, there is a match for the 5-year return period over 6 hours (360 minutes). The threshold of this category is at or above 56,69mm in total precipitation, and in the 15th through the 21st hour, or from 15:00-21:00 the 14.09.2019 there was in total 58,3mm of precipitation.

Table 3-2. Intensity-duration-frequency (IDF) values for Florida rain-gauge, Bergen.

	Duration (Minutes)						
Return period (Year)	**60 min**	**90 min**	**120 min**	**180 min**	**360 min**	**720 min**	**1440 min**
2	17,21	20,63	23,83	30,02	43,63	63,94	88,13
5	19,94	23,33	28,15	36,94	**56,59**	85,97	119,23
10	21,78	25,11	30,96	41,47	65,23	100,66	139,97
20	23,51	26,78	33,70	45,90	73,44	114,48	159,84
25	24,05	27,32	34,56	47,20	76,03	119,23	165,89
50	25,78	29,00	37,22	51,52	84,24	132,62	184,90
100	27,47	30,67	39,89	55,73	92,23	146,45	203,90
200	29,12	32,29	42,48	59,94	100,22	159,84	223,78

Source: Norsk Klimaservicesenter (n.d. A).

3.1.1.3 Estimating extreme precipitation events for the year 2100

Having established that the historical 6-hour precipitation event with a total of 58,3mm of rain is within a 5-year return period at Florida rain-gauge, the next step is to find a way to aggregate these values in order to predict the values for the same scenario in the end of the 21st century.

Climate models predict a range of outcomes for precipitation at the end of the century, however a recent report by NCCS suggests a rough estimate can be obtained for short term heavy-precipitation at the west-coast region of Norway by taking the return period, duration of rainfall, locality, reference period, scenario period and climate models into account (Dyrrdal and Førland, 2019). The suggestions of the report can be seen in table 3-3, which is separated into the categories of duration (hours), 5-year (<M50) and 50-year (>M50) return periods, and dry

(Low M5) and wet (High M5) regions. Hence, a linear increase of 30% precipitation by the end of the century was opted for since the historical precipitation-data is within 4-6 hours, it is a 5-year return period and it is located in a wet region in Norway (circle in table 3-3).

Table 3-3. Recommended climate factor (percentage of increased precipitation) for the changes in short-term precipitation toward the years 2071-2100.
<M50 = 5-year return period. >M50 = 50-year return period. Low M5 = dry areas. High M5 = rain intensive areas.

	<M50		**>M50**	
Duration	Low M5	High M5	Low M5	High M5
<1 hour	**40**	**40**	**50**	**50**
2-3 hours	**40**	**30**	**40**	**30**
4-6 hours	**30**	**30**	**40**	**30**
7-24 hours	**30**	**20**	**30**	**30**

Source: Dyrrdal and Førland (2019).

To summarize, the values for the 6 hours of precipitation recorded 14.09.2019, and the estimated 2100-values calculated by adding a 30% increase from the 2019-values are presented in figure 3-2.

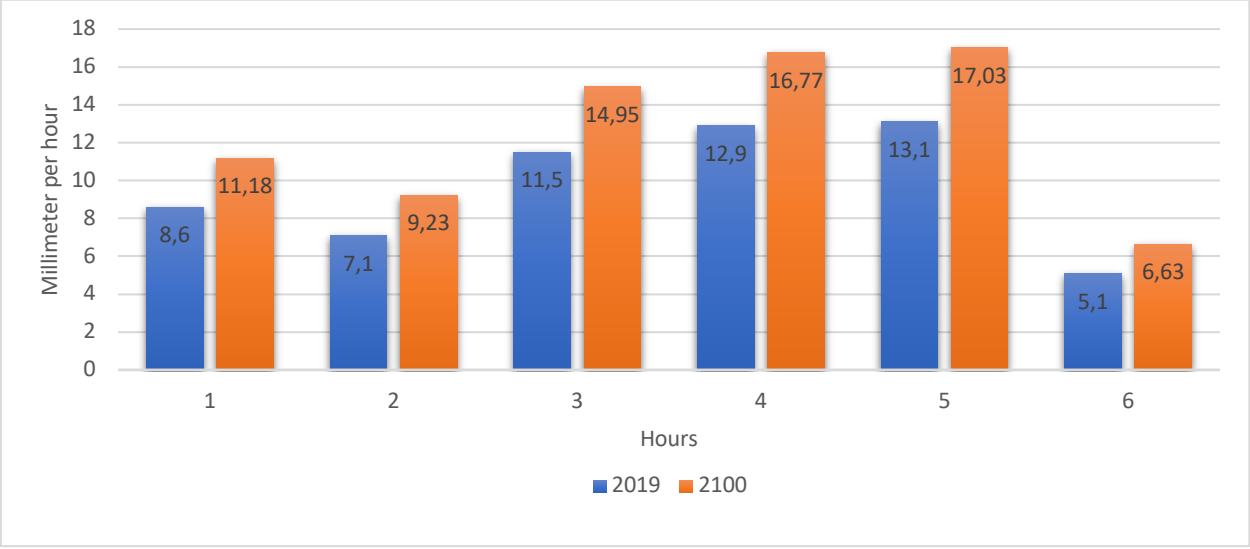

Figure 3-3. Graph of historical precipitation event in Bergen 14.09.19 (blue) and predicted climate factor for same event in year 2100 (orange). Return period = 5 years, duration = 6 hours, added climate factor = 1.3.

3.2 Geospatial analyses

The analyses performed can be separated into four major steps; the preprocessing in ArcGIS (3.2.1), the processing in GRASS (3.2.2), the flood simulation modelling in ITZÏ (3.3) and the network – and impact-analyses in ArcGIS (3.4). This section covers the ArcGIS and GRASS processing. The workflow followed is summarized in figure 3-3 and the data used is presented in table 1.

While the processing was performed locally, the flood simulation modelling was conducted on the Norwegian Research and Education Cloud (NREC) using a virtual machine with 16 CPUs and 64 GB of RAM. This had the advantage of allowing the model to run centrally.

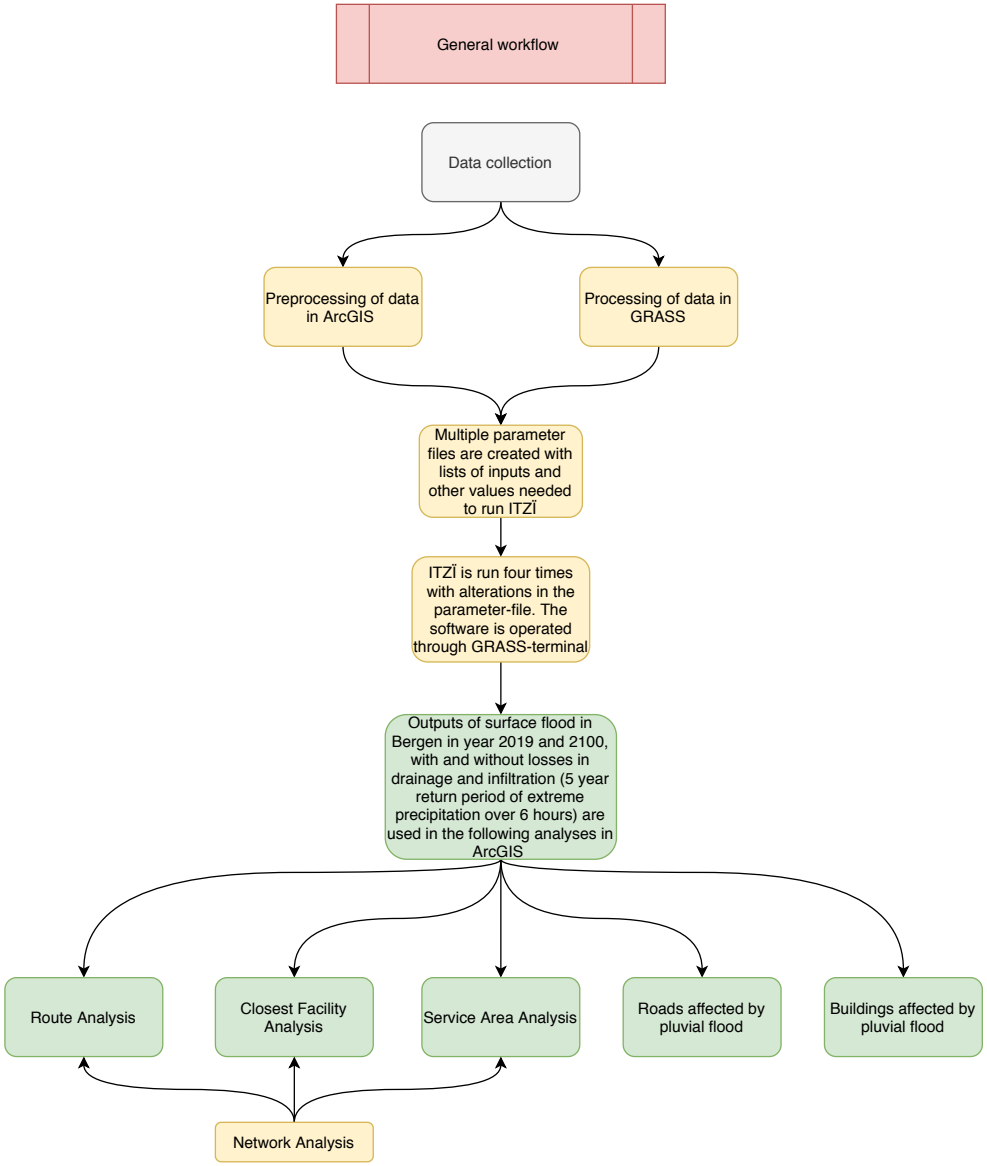

Figure 3-3. Flowchart illustrating the general workflow of all the different analyses and processes performed.

3.2.1 Preprocessing in ArcGIS

Prior to running the flood simulation, it was necessary to pre-process a selection of the GIS data in ArcGIS, presented in sections 3.2.1.1 - 3.2.1.6. The pre-processing steps are summarised in figure 3-4.

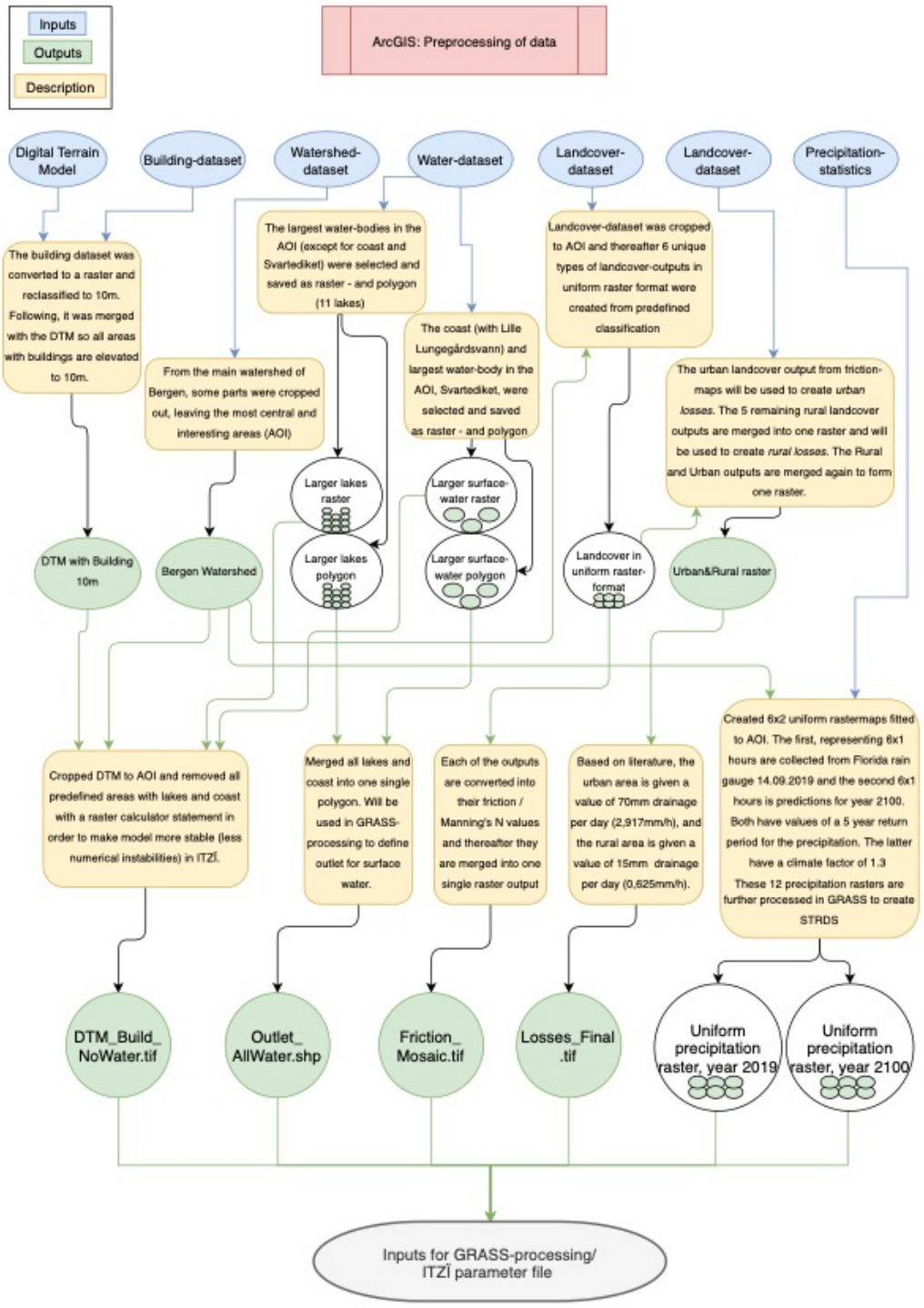

Figure 3-4: Flowchart outlining the preprocessing of the input-data

3.2.1.1 Delineating the Watershed

The border of the Bergen watershed was downloaded from NVE, however this initial size was deemed unsuitable as a study area for two reasons: Firstly, due to computational limitations it was unrealistic to study an area of 45km^2 in size (NVE, 2020). Secondly, since this study was focused on urban flooding in the centre of Bergen, it was not necessary to include some of the city's suburbs. As such, the analyses were restricted to the centre of Bergen and the immediate water catchment, as shown in figure 3.5. The new watershed is referred to as AOI (Area of Interest).

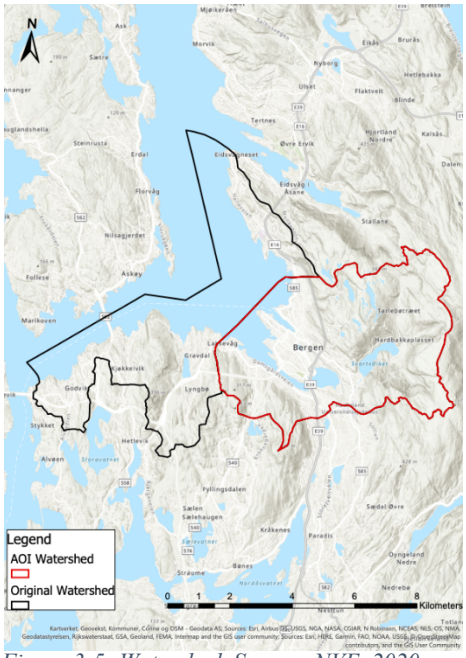

Figure 3-5: Watershed. Source: NVE, 2020

3.2.1.2 Defining the flow outlet

The outlet-data represents one out of three possible ways the surface-water can leave the model when run in Itzï, while the two others are infiltration-processes and drainage-systems. The purpose of the outlet when used in Itzï is to inform the model where the surface-water may leave the domain on the ground level. The outlet-data used the water-dataset as input.

After some initial tests in Itzï using the ocean (coastline), Lille Lungegårdsvann (a lake in the midst of Bergen connected to the ocean by an enclosed canal (Bergen Municipality, 2020) and Svartediket as outlets, an additional 11 of the larger lakes in the AOI were added to the dataset as the outlets, outlined in figure 3-6. This was done to better represent the coupling between the surface-water and the outlet-areas, and to avoid instabilities in the model relating to the storage of water in lakes and waterbodies.

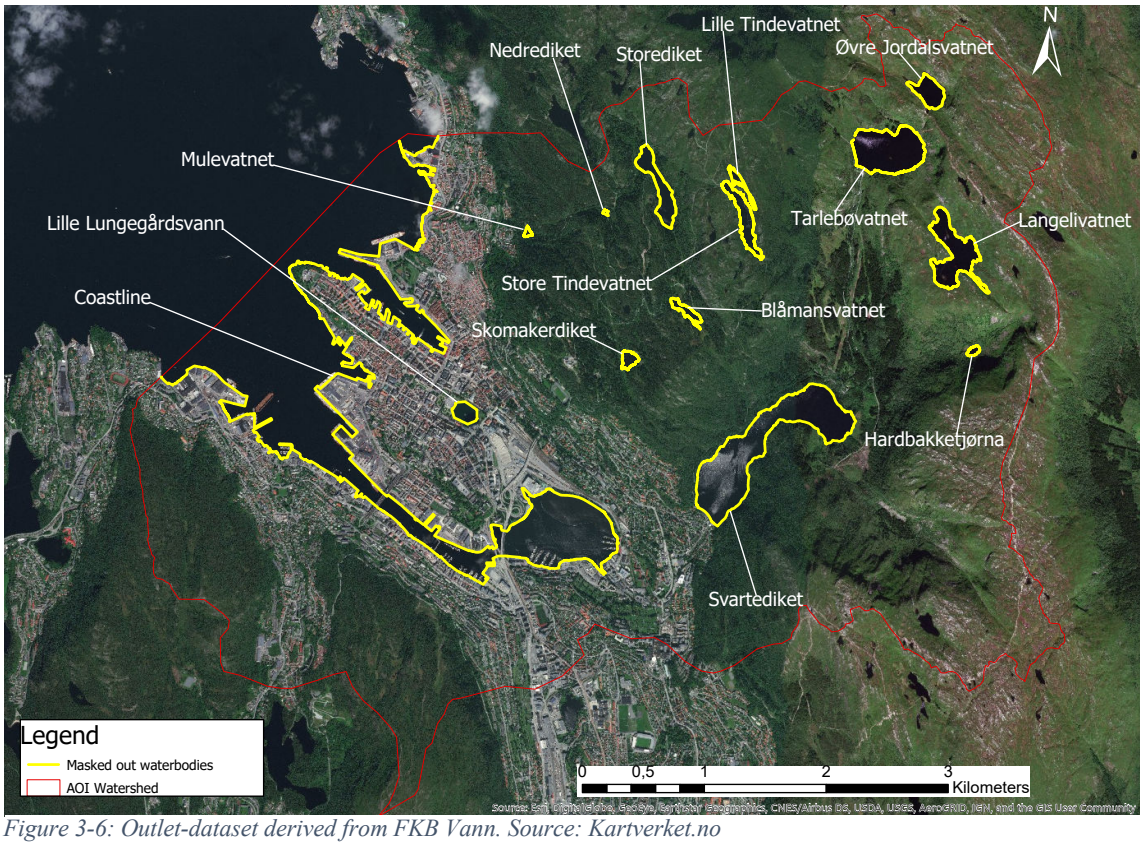

Figure 3-6: Outlet-dataset derived from FKB Vann. Source: Kartverket.no

3.2.1.3 Modification of the Digital Terrain Model

3.2.1.3.1 Defining DTM

In order for Itzï to model the direction water can flow for any given pixel (the flow direction), a digital terrain model (DTM) is required as an input. Seeing as there are several types of terrain models to choose from, there was a contemplation in the early stages as to which type of datatype to select. The choice fell on a DTM (Digital Terrain Model) instead of a DSM (Digital Surface Model) since it represents the true terrain and does not include the natural and built features of the landscape such as the DSM does. But, seeing that the AOI is within a largely urbanized area with numerous buildings acting as barriers for the water to flow through, a hybrid between a DTM and a DSM was created by adding building-data. To model flow direction – and accumulation, the other features of the DSM (e.g. trees and powerlines) is of less significance due to their limited size and was therefore not included (The Flood People, 2018).

3.2.1.3.2 Adding data to DTM

A DTM based on airborne LiDAR data from 2016 with a point density of 10 points per m^2 was downloaded at 1m resolution from the Norwegian Mapping Authority (Kartverket's) elevation data portal; Hoydedata.no. In addition, a detailed building-dataset was downloaded from Geonorge.no.

Subsequently, the building-dataset was converted to raster-format and thereafter reclassified in the raster calculator using a conditional statement (equation 1) so that all buildings received a value of 10 meters, ensuring that the water would flow around and not through these areas.

Finally, the pixel values from the DTM were added together to all the footprints of the buildings.

(Equation 1)

```
Con("BuildingRaster" == 1, 10 , "BuildingRaster")
```

3.2.1.3.3 Removing water bodies from the DTM

As will be explained in greater detail in the discussion-chapter, all of the waterbodies had to be removed from the DTM in the outlet-dataset to avoid instabilities in the Itzï-modelling relating to water storage.

Prior to the cropping, the outlet-polygons had to be decreased by approximately one cell-wide buffer, or in other words a one-meter line. This is to ensure that the surface-water leaving the domain does so within the lakes and ocean, but not before it passes through the outlet areas used as an input in Itzï.

The 14 polygons were first buffered one by one to create the 1m line, and thereafter the lines were used to erase all the data outside each polygon before they were converted to raster-formats. Since the aim was to use the lakes and ocean to erase parts of the DTM, the raster-calculator in ArcGIS had to be used. All of the 14 outputs were separately run through the calculator by the conditional statement below (equation 2), to finally end up with the DTM as illustrated in figure 3-7.

(Equation 2)

```
Con(isnull("Polygonraster"), "DTMraster")
```

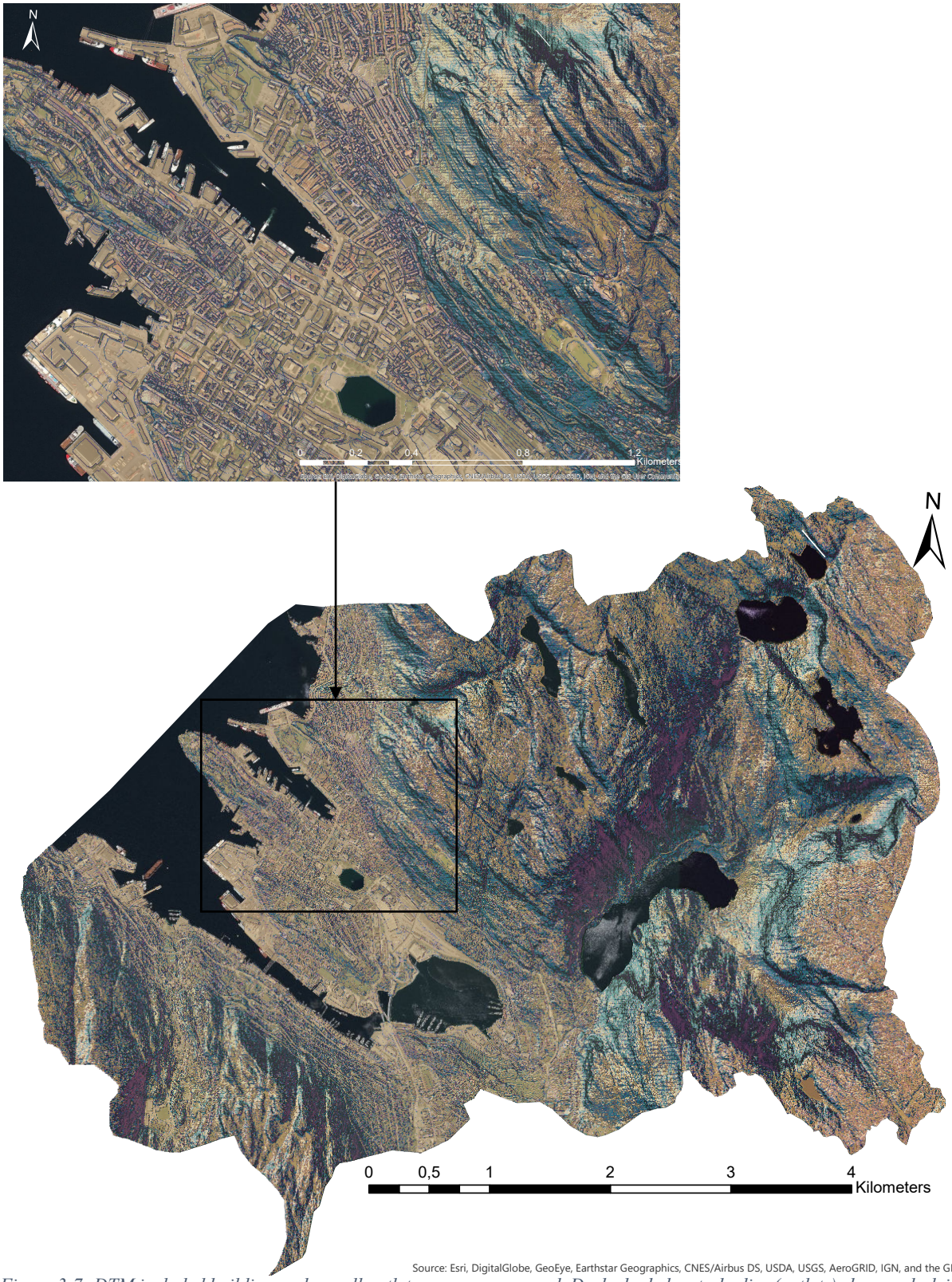

Source: Esri, DigitalGlobe, GeoEye, Earthstar Geographics, CNES/Airbus DS, USDA, USGS, AeroGRID, IGN, and the GIS User Community

Figure 3-7: DTM included buildings, where all outlet-areas are removed. Dark-shaded waterbodies (outlets) show underlying basemap. Layout consists of a basemap (imagery) with multiple hillshaded DTM-layers overlain for visual effects.

3.2.1.4 Assigning Manning's N coefficient to friction-map

3.2.1.4.1 Establishing landcover-classes

Another important element to include in the Itzï-modelling is a dataset representing the friction-values, or in other words the resistance that the hydraulic processes receives by the various landcover-types (Courty, Acuna and Bates, 2017, pp. 1842). These friction-values are usually represented by using Manning's n friction coefficient (i.e. higher value equals higher friction and vice versa), where in this instance 5 out of the 6 selected landcover-classes in the AOI are given a unique value based on Chow's (1959, pp. 109-113) propositions. The last landcover class, Marsh, received its values from a United Stated Geological Survey-report (Arcement and Schneider, 1989, pp. 9) since it did not exist in Chow's (1959) propositions.

Three of the landcover classes were created by the suggestions from Courty, Acuna and Bates (2017) since they were also covering large parts of this AOI (i.e. artificial surface, cultivated land and forest). The remaining three landcover classes were chosen based on a visual interpretation of the different categories in the landcover dataset in comparison in to the AOI (i.e. earth, marsh and waterbodies). So, by now there are established 6 unique landcover classes, each with its own Manning's n friction coefficient. Subsequently, the next step was to extract and merge the various landcover-categories from the dataset in order to generate the landcover-classes, and thereafter crop them to the borders of the AOI and convert them into 6 separate uniform raster-datasets. All of the data's and values explained here is summarized in table 3-4.

Table 3-4. Landcover categories – and classes with Manning's n coefficient-values. Higher manning's n values = higher friction.

Landcover category	**Landcover class**	**Manning's n friction coefficient**
Built up area	Artificial surface	0.019
Transport (roads)		
Fully cultivated land	Cultivated land	0.040
Cultivated pasture		
Forest	Forest	0.060
Open land (bare rock)	Earth (bare rock)	0.020
Marsh	Marsh	0.045
Fresh water	Waterbodies	0.030
Ocean		

3.2.1.4.2 Creating friction-map

The 6 datasets were eventually assigned their corresponding Manning's n values through the raster calculator by using equation 3. They were thereafter combined to create the final output, as illustrated in figure 3-8. Since the majority of waterbodies had already been masked out (see section 3.2.1.3.2), the effect of choosing a friction coefficient was limited to the small waterbodies remaining.

(Equation 3)

```
"Rastermap" -1 +float(coefficient-value)
```

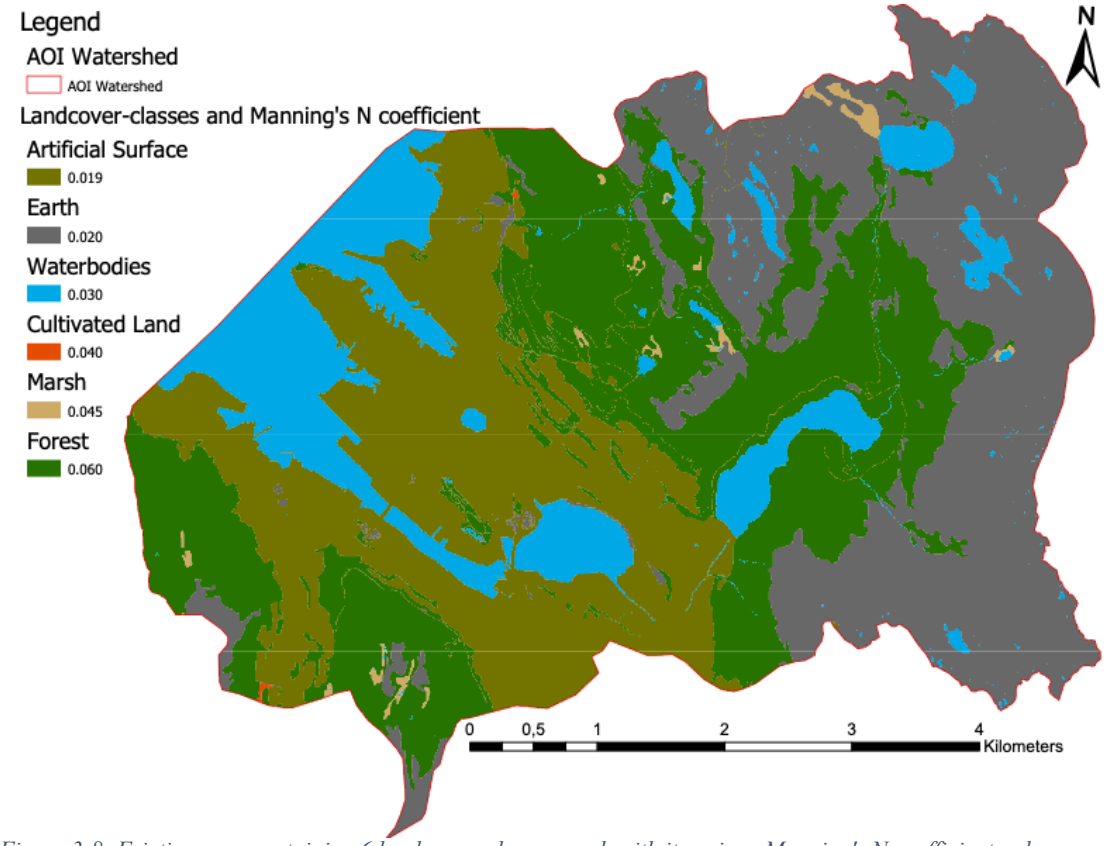

Figure 3-8: Friction-map containing 6 land cover classes, each with its unique Manning's N coefficient-values.

3.2.1.5 Infiltration and drainage represented by Losses-map

Following the suggestions by Courty, Acuna and Bates (2017) as to which data should be used as input to the Itzï-analysis, it was early on decided that the drainage should be represented by coupling the surface model (Itzï) to a drainage model called SWMM (Storm Water Management Model). Likewise, it was decided that the infiltration-data should be generated by the different types of soil-textures in the AOI, which would thereafter be given values based on their matching hydraulic conductivity-levels as proposed by Rawls, Brakensiek and Miller (1983).

3.2.1.5.1 Infiltration

By following the recommendation from Courty (2018), the global soil database SoilGrids250m was used to download three datasets, one for *clay*, one for *silt* and one for *sand* - having a spatial resolution of 250m (Soilgrids, n.d.). These all showed their specific content in percentage in the top 60cm layer of the soil. In order to figure out the soil textures by combining the percentages of the three different soil-types, several calculations were required. Figure 3-9 show how the different soil-percentages defines the type of soil texture.

The calculations were performed by the help of the USDA's (United States Department of Agriculture) own calculations, (USDA, n.d.). 12 different calculations were needed in order to create each type of texture. An example of one of the calculations can be seen in equation 4 below, representing the texture loam. All the numbers are in percentages:

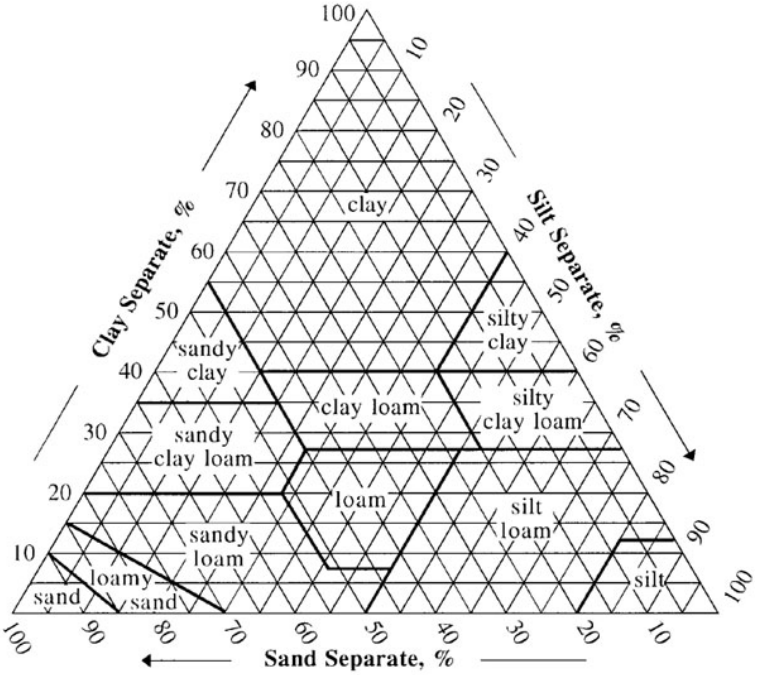

Figure 3-9: Triangle showing relation between percentages of soil (clay, sand and silt) and soil-textures. Source: USDA (n.d.)

(Equation 4)

```
((clay >= 7 && clay < 27) && (silt >= 28 && silt < 50) &&
(sand <= 52))
```

As a means to shorten down the processing time, a python script was written which both calculated all the soil textures and simultaneously gave them their corresponding hydraulic conductivity-value as suggested by Rawls, Brakensiek and Miller (1983). However, seeing that the raster output of *"sandy loam"* covered all but 9 cells in the AOI, and *"loam"* covered 8 out of the remaining 9 cells, the infiltration-data was rendered too general and were set aside. This also applied for the coupling of the drainage through SWMM – part since it relied on the usage of infiltration-data to be performed.

3.2.1.5.2 Theoretical approach to represent losses

Luckily, another option was feasible where both drainage and infiltration-processes would be represented in the Itzï modelling. Yu and Coulthard (2015, in Courty, Acuna and Bates, 2017) presents two default drainage and infiltration capacity values for the lower rainfall areas in the UK. These default values are 70mm/day for the urban area, and 15mm/day for the rural area. Since there has been no breakthrough in finding other approaches to illustrate infiltration and/or drainage, or other theoretical values more adapt to the rain intensive AOI in Western Norway, these values were used as input for the analysis, hereby called "Losses". The urban and rural losses can be broken down into hourly values. For the urban area the losses are 70mm/24 hours = 2.917mm/h, and the losses for the rural area are 15mm/24 = 0.625mm/h. This means that for each predefined hour the Itzï-analysis is processing, a net sum of surface-water is derived from the urban and rural areas.

Having established the values, they need to be assigned to a raster-map representing the urban and rural areas. These already exist from the creating of the friction-map. Hence, the "Artificial surface"-raster is used for the urban area, and the remaining 5 landcover classes were combined to form the rural dataset.

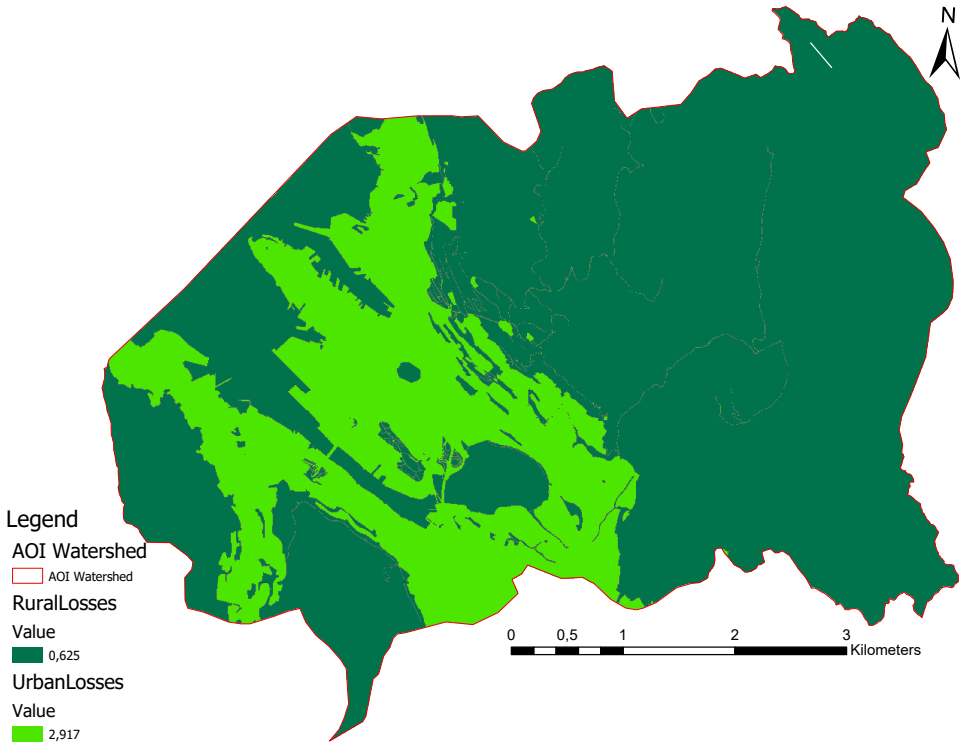

Figure 3-10: Losses-map with drainage and infiltration values for urban and rural areas in AOI

Finally, the two datasets were merged together and subsequently run through the raster calculator by using equation 5 in order to receive its losses-values. The resultant map can be seen in figure 3-10 above.

(Equation 5)

```
float( con("losses" ==1, 0.625, con("losses" ==3, 2.917,
0.0)))
```

3.2.1.6 Precipitation Raster

Figure 3-2 (in section 3.1.1.2) illustrates the 6-hour, 5-year return period precipitation values in mm for both the historical event in 2019 and the predicted values for 2100 based on the climate factor of 1.3. Since these data are to be used in the Itzï analyses, the precipitation values need to be converted into a gridded raster dataset. Due to the fact that within the AOI there was only one rain-gauge to collect data from (Florida), each raster-dataset will therefore contain uniform values (i.e. one value). A total of 12 uniform raster datasets were created and cropped to the AOI, 6 of them with the 2019 values and the remaining 6 with the 2100 values. A list of the precipitation values from figure 3-2 can be seen in table 3-5 below.

Table 3-5: precipitation values in mm for year 2019 and 2100

Year	**Hours**					
	1	**2**	**3**	**4**	**5**	**6**
2019	8,6 mm	7,1 mm	11,5 mm	12,9 mm	13,1 mm	5,1 mm
2100	11,8 mm	9,23 mm	14,95 mm	16,77 mm	17,03 mm	6,63 mm

3.2.2 Processing in GRASS

This section will cover all the processing of data to be used as input into the Itzï modelling which needed to be performed in GRASS as opposed to ArcGIS. This entails the manipulating of the DTM, the outlet and the two groups of precipitation-rasters previously created in ArcGIS. A visual overview of the workflow can be seen in figure 3-11.

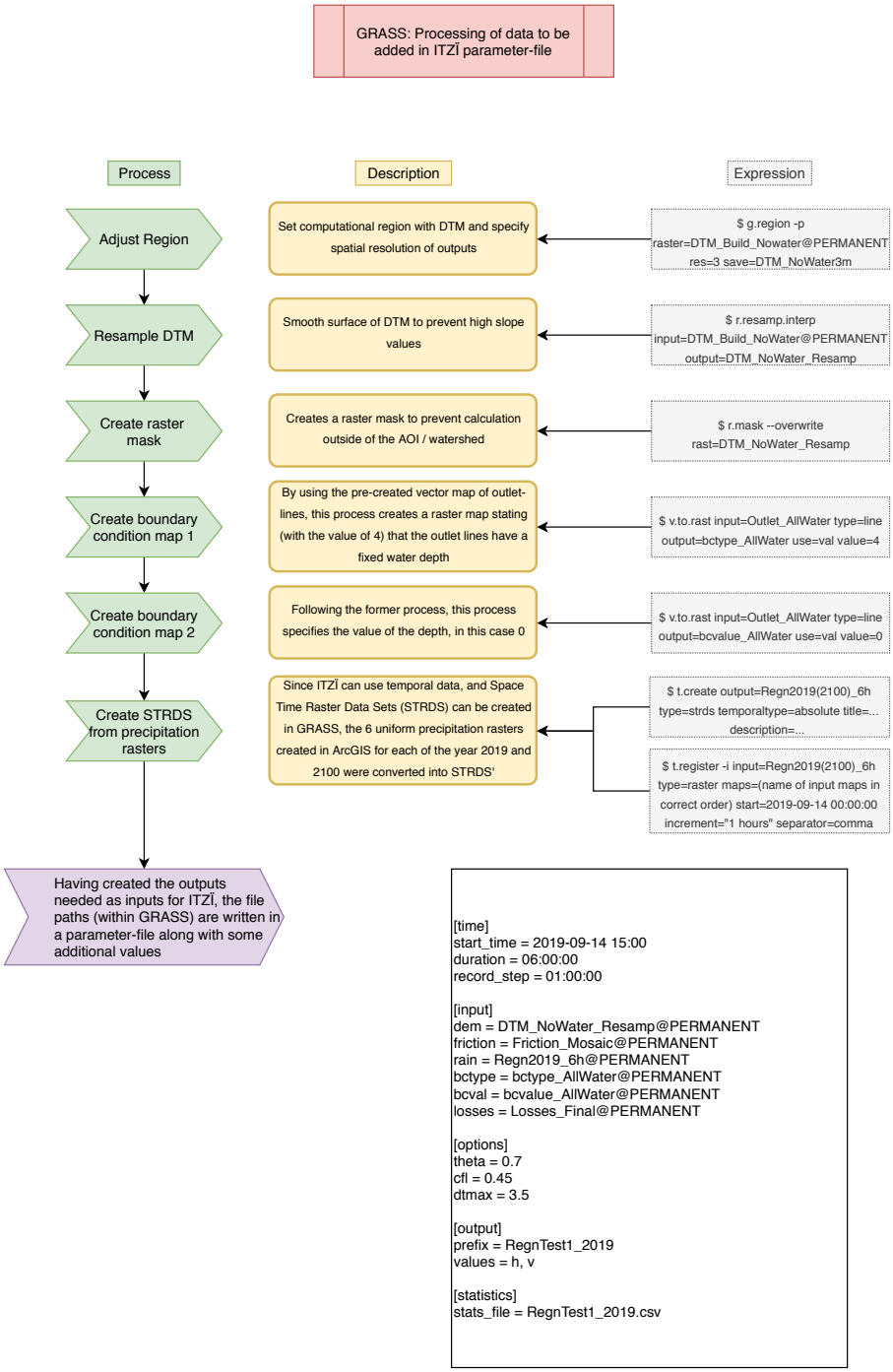

Figure 3-11: Flowchart showing the processing of data in GRASS to be added in Itzï parameter-file

3.2.2.1 Modification of DTM

First and foremost, the DTM was used to set the region in GRASS to perform all analyses within the borders of the AOI. Subsequently it was resampled from 1m to 3m in order to save computational power, and simultaneously a bilinear interpolation (i.e. average of 4 by 4 cells) was executed to smoothen the surface of the new output in order to avoid large variations of pixel-values caused by the resolution of the DTM (GRASS, n.d. A). The DTM was also used to create a raster-mask to prevent calculations outside of the AOI/watershed when creating the boundary condition maps (appendix 1a-c (GRASS, n.d. B)).

3.2.2.2 Boundary condition set up

To account for the part of the surface-water that is leaving the AOI, being via the border of the watershed or by entering a lake, a raster map of the boundary condition type (bctype) and a rastermap of the boundary condition value (bcval) must be present to serve as inputs into the parameter-files. The dataset to be edited to represent bcval and bctype is the polygon outlet-dataset created in ArcGIS as explained in section 3.2.1.2.

3.2.2.2.1 Boundary condition type

For the bctype, the condition is set to value 4, representing "user-defined water depth inside the domain," or in other words the boundaries are given a fixed water depth (appendix 1d). By doing so, the water depth may be edited as well (Itzï, n.d. A). All four conditions are listed in table 3-6.

Table 3-6: Boundary condition types.

Value	Description
0 or 1	Closed boundary
2	Open boundary
3	Not implemented yet
4	User defined water depth inside domain

Source: Itzï (n.d. A)

3.2.2.1.2 Boundary condition value

The bcval is coupled with the bctype by stating the water-depth value wanted. In this case, the value or water depth was set to 0, allowing the surface-water to enter the ocean and lakes defined in the outlet-file (appendix 1e).

3.2.2.3 Creation of Space Time Raster Datasets (STRDS)

The aim of the Itzï-analysis was to create two sets of surface-flood outputs, each applying a 6-hour group of precipitation (both 2019 and 2100 values). Hence, a datatype capable of storing temporally varying precipitation-data were needed. Rather than calculating the mean value and applying it to one raster, a STRDS (Space Time Raster Data Set) can contain multiple rasters with differing values that are indexed by time, which is the preferable datatype for managing time series-analyses in GRASS (GRASS, n.d. C).
Consequently, two STRDSs were created in GRASS, one for the 2019 raster-maps and one for the 2100 raster-maps. Thereafter both groups of precipitation-data were loaded into each their STRDS (appendix 1f & 1g).

In addition to the manipulation of the three output-data as mentioned above, the remaining data from section 3.2.1 (friction and losses) had to be uploaded into a database in GRASS (in this case, called "permanent"). Thenceforth, two Itzï-compatible parameter-files were created, each with one precipitation STRDS, containing all the input-data as listed in table 3-7.
The usage of the parameter-files will accordingly be explained in section 3.3.

Table 3-7: Inputs to the Itzï parameter-files. Data-name is the names used when added to the parameter-files. Note that the@PERMANENT refers to the database that the files were stored in within GRASS

Datatype	**Data-name and GRASS-path**
DEM (DTM)	DTM_NoWater_Resamp@PERMANENT
Friction	Friction_Mosaic@PERMANENT
Rain (precipitation-STRDS)	Regn2019(2100)_6h@PERMANENT
Bctype (Boundary condition type – Outlet)	bctype_AllWater@PERMANENT
Bcval (Boundary condition value – Outlet)	bcvalue_AllWater@PERMANENT
Losses	Losses_Final@PERMANENT

3.3 ITZÏ Modelling

Following the data-preparation of section 3.2, Itzï was run through the GRASS-terminal. Hence, when the parameter-files were ready to be executed, the statement of equation 6 was entered into the terminal to start the analyses.

(Equation 6)

```
Itzi run <parameter_file_name>
```

However, before the final outputs generated from running the statement above can be created, an explanation of the parameter-file and some of its content must be accounted for, as well as a brief summary of the main outputs in order to facilitate for better understanding of section 3.4, where these will be used as inputs.

3.3.1 Itzï parameter-file

As the parameter-file in figure 3-12 illustrates, there are 5 main categories (in brackets) where inputs, specifications and parameters can be added and altered. These are accordingly; time, input, options, output, and statistics. Since much of this is straightforward, only parts of it will be explained here.

The options that are altered in this analysis due to numerical instabilities is "theta" (intertia weighting coefficient), "clf" (coefficient applied to calculate time-step) and "dtmax" (maximum surface flow time-step in seconds). These will be further addressed in the discussion chapter (Itzï, n.d. A).

The model gave outputs of water depth (h) and flow speed velocity (v) along with a statistics CSV. The "h" and "v" outputs were of the datatype STRDS, where four STRDS' of 6 hours were created for both "h" and "v". One each for year 2019 and 2100 where the input "losses" was included, and one each for year 2019 and 2100 where the same input was excluded. The reason to this was to evaluate the difference with and without drainage and infiltration. It is however only the water depth (h) outputs which will be used as inputs in the network – and impact analyses in the post-analyses in section 3.4

```
[time]
start_time = 2019-09-14 15:00
duration = 06:00:00
record_step = 01:00:00

[input]
dem = DTM_NoWater_Resamp@PERMANENT
friction = Friction_Mosaic@PERMANENT
rain = Regn2019_6h@PERMANENT
bctype = bctype_AllWater@PERMANENT
bcval = bcvalue_AllWater@PERMANENT
losses = Losses_Final@PERMANENT

[options]
theta = 0.7
cfl = 0.45
dtmax = 3.5

[output]
prefix = RegnTest1_2019
values = h, v

[statistics]
stats_file = RegnTest1_2019.csv
```

Figure 3-12: Itzï Parameter-file

3.4 Network analyses

The surface-flood maps outputted from Itzï were subsequently used for a route analysis, a closest-facility analysis and a service-area analysis, which are all a part of the network analysis tool in ArcGIS. In addition, two different impact analyses were also performed by using the flood-maps as input-parameter. One of these measured the extent of roads within the AOI flooded by surface-water, and the other measured the extent of buildings within the AOI that are in contact with the surface-water. Figure 3-13 presents an overview of the workflow in a flowchart.

Out of the 6 individual hours of water depth-outputs (h) in each time-series rasters (STRDS) from Itzï, the fifth hour from each time-series were used as input to the analyses mentioned above. This is because the fifth hour produced the most amount of water in the domain and had the least amount of errors by studying the statistics CSV.

Due to the car's ability to travel through flooded areas, 30 cm was chosen as a classification threshold for the flood-maps since the average height of air inlets of cars ranges between 25-35 cm (Yin, et al, 2016, pp. 141). Everything below the threshold of 30 cm grants the car free passage, and everything above indicates a barrier (i.e. flooded road-segment). Following the classification, the flood-maps were converted to vector (polygon) format.
Another task to complete before initiating the analyses was to scale the polygons in each dataset from 11 000-13 000 down to a number below 2000 in order to be able to run the various tools. Hence, the tool "simplify polygon" was used with the method "retain weighted effective areas" to remove the polygons below 1m in size, since it is the larger flooded areas that are of interest in this analysis. The new simplified flood-barrier maps have an average of 1650 polygons and will be used for all the following analyses.

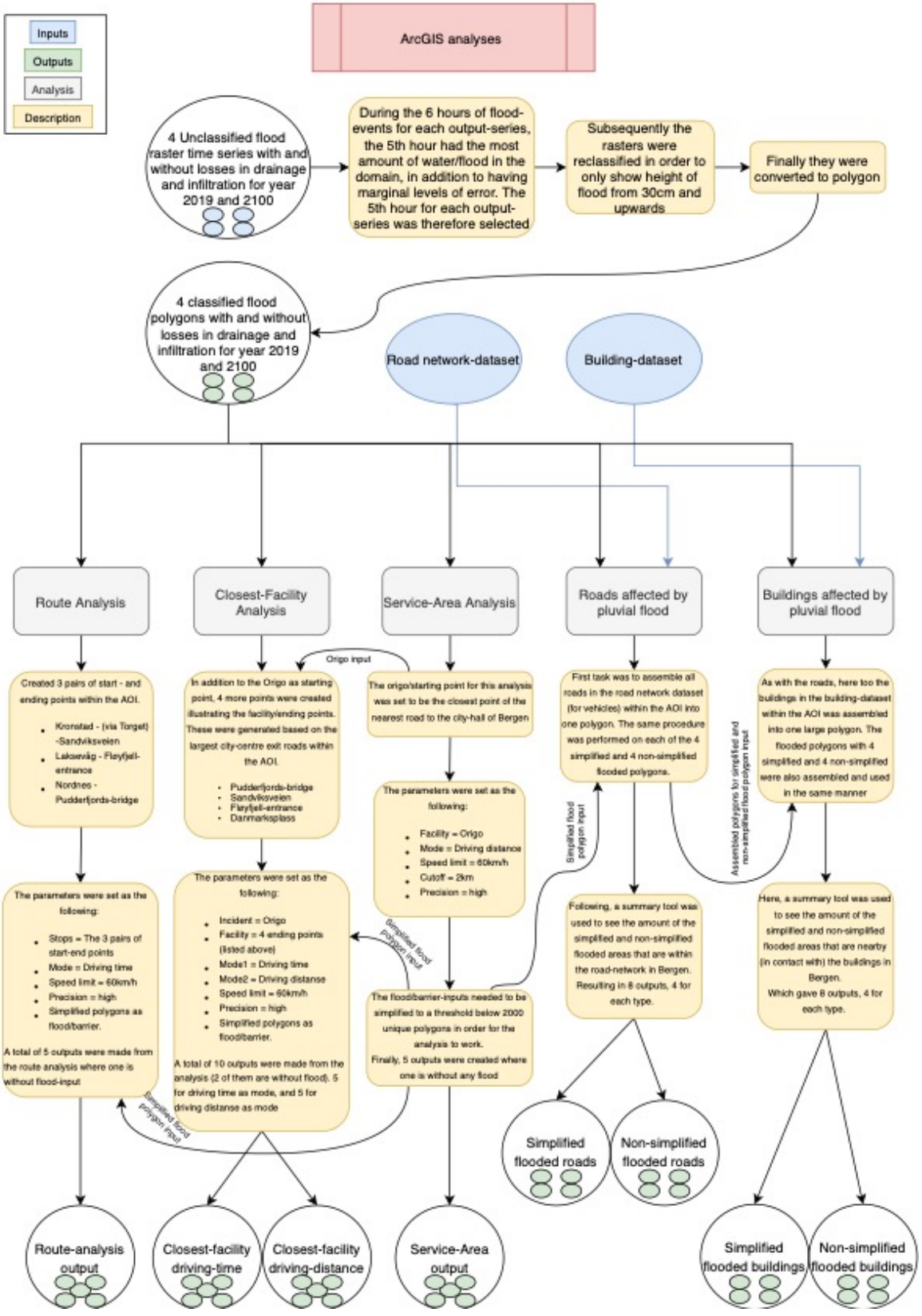

Figure 3-13: Flowchart illustrating the network – and impact-analyses

3.4.1 Service Area Analysis

Service area analysis provides a buffer around a defined center showing reachable areas based on the criteria added (ArcGIS Pro, n.d. B). Hence, this analysis will use a pre-defined starting point (origo), accurately placed in the AOI in order to calculate the areas reachable by a car within a 2-kilometer wide buffer surrounding the origo, with a speed limit of 60km/h. Seeing as it is a network analysis, the service area buffers provided will follow the road network provided from the network analysis tool, contrary to simply creating outputs of aerially reachable areas. Since there is no need for an external source of road-network data as this is implemented in the network analysis tool, the inputs to this analysis are the origo and the vectorized flood-barrier maps. The origo is a point located at the nearest road-segment to the city hall of Bergen (figure 3-14) since there are (usually) a large number of employees in this building, and simultaneously it is a very central location in downtown Bergen where a multitude of people, both from within and outside of the municipality commute daily.

There were 5 different outputs wanted from this analysis, which were acquired by using the parameters and inputs as mentioned above and only variating the flood-barrier inputs. The first output is supposed to illustrate the areas that may be reached on a day without any precipitation (i.e. a dry day) and did therefore not have any barrier-inputs. The subsequent four outputs each used one of the four unique vectorized flood-barrier inputs to illustrate the variation of the service area with varying amounts of surface-flood.

3.4.2 Closest Facility Analysis

Unlike the service area analysis which measures areas within range from a defined point, the closest facility analysis measures the cost of travelling between one (or several) incidents and one (or several) facilities (ArcGIS Pro, n.d. A). In this case the incident refers to the starting point, i.e. where the route starts. The origo used in the previous subchapter were also be used here as the starting point. The facilities on the other hand is the end-stop of the route. As known, the flood-polygons are only present within the AOI. This means that the facilities or end-stops need to be within the AOI as well. Based on this, four major roads in the northern, eastern, western and southern parts of Bergen city-center were defined as the facilities as illustrated in figure 3-17. These road-segments are located at the entrance of Fløyfjellet, at Danmarksplass, on the Pudderfjord-bridge and in Sandviken, and are meant to represent some of the main commuting routes by car in Bergen.

The aim of this analysis was to locate the fastest routes from the origo (incident) to the facilities, and subsequently examine the added costs by using the different flood-barrier datasets as inputs (i.e. added driving-length or time due to rerouting to avoid increasingly flooded areas). There were in total 10 different outputs generated from this analysis, 5 of them had driving time as parameter and the other 5 had the parameter of driving distance. The speed limit of 60km/h is was as default for all of them. One of the five analyses from each of the two groups were run without any flood-barrier, and the remaining four analyses from both groups were coupled with one each of the four simplified flood-barriers.

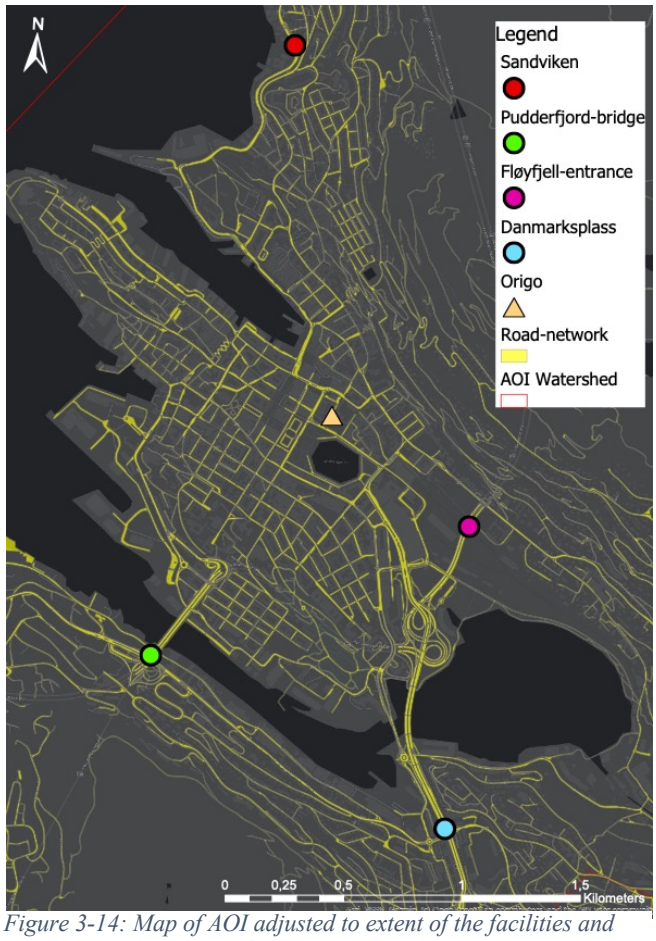

Figure 3-14: Map of AOI adjusted to extent of the facilities and incidents used in closest facility analysis

3.4.3 Route Analysis Layer

Finally, an account will be given on the how the outputs from the route analysis were generated, which is the last of the network-analyses. The aim of this analysis was to see how various routes throughout the city are affected by different levels of flood-barriers. To begin with, this route analysis does not use a single incident (starting point), but rather a set of connected start – and ending points which represents different travel-routes. In order to receive as much as data as possible when adding the flood-barriers, the points representing the start and end of the routes were placed far away from each other at the borders of the AOI or at a canalized area such as the outermost area of Nordnes. This will intensify the effects of flooding and ensure that some sort of rerouting will be needed. Three different routes were specified as can be seen in figure 3-15. The first route extends from a point at Laksevåg to the entrance of Fløyfjellet. The second route have a point at Nordnes and the other one is placed on the Pudderfjord-bridge. The third route however have three points in order to make sure that the road travelled lies within the AOI and not outside. One of the border-points is located south at Kronstad, the second border-point is placed due north in Sandviken, the last point is placed between these two locations at Torget.

By having the three routes established, traversing throughout the road-network in the AOI, the analyses were ready to be run. As with the parameter in the two former analyses, the speed limit is also 60 km/h here. A total of 5 outputs were generated by using the same procedure as with the service area analysis, only swapping the driving distance parameter with driving time.

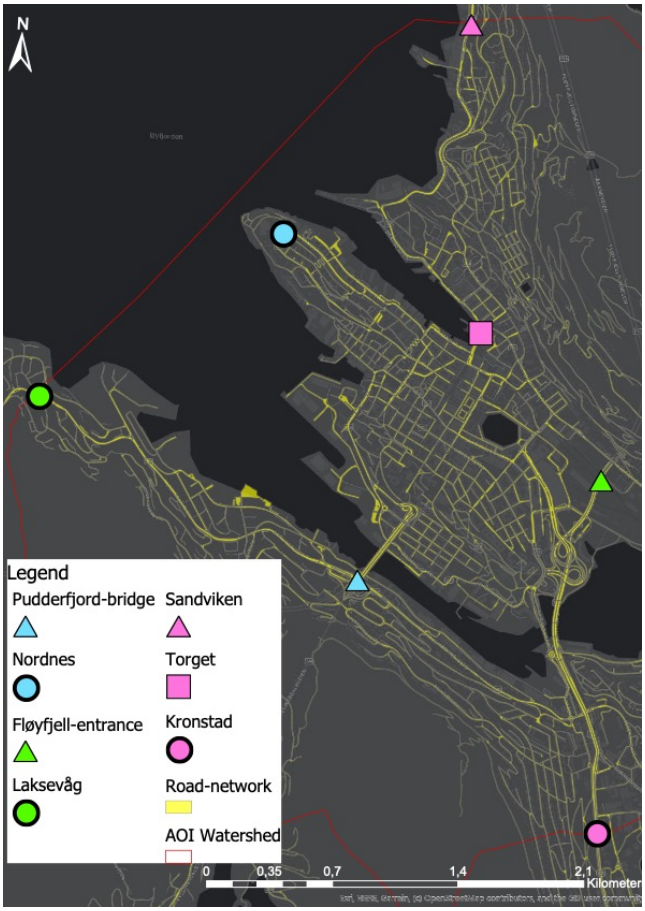

Figure 3-15: The points representing the start and end (and checkpoint) of the three routes used in the route-analyses

3.4.4 Impact of flooding on road network

Since there has been performed several network analyses, it is also important to have information of the total affectedness of flood to the road-network. This section will provide an explanation of how the areas of flooded roads (≥ 30cm) were calculated. As known, there has been produced 4 classified flood-polygon datasets, both with and without losses-input of the precipitation events in 2019 and 2100, and subsequently 4 simplified versions of these flood polygon datasets. Since the former were classified from the original outputs from Itzï and the latter were used in the network-analyses, both of these groups will be used to calculate the flood impact on the road-network.

Both a road-network dataset (FKB-Veg) and the flood-polygon datasets as mentioned above was used as inputs and "summarize within" was used as the tool to process the data. However, in order for the tool to provide the desired outputs, some editing needed to be done. The road-network dataset and had to be turned in to one polygon (a precondition of the tool). In addition, seeing as the road-network dataset contained not only roadways for cars, but also roads for pedestrian and other types, the roadways for cars needed to be extracted into a new dataset. Following the completion of the extraction, the dataset was dissolved into one polygon and subsequently run through the tool where the road-network polygon was used as input and the various flood-polygons as summary features. The processing returned 8 different results as statistics in total square meters.

3.4.5 Impact of flooding on buildings

This section builds on the same principles as the previous one, but rather than summarizing the area of flood impacting (within) the road-network, a calculating of the flooded areas nearby the buildings in the AOI will be explained here. The same 8 flood-datasets will be used here as well, while the road-network dataset is replaced with a building-dataset. The tool used to calculate the amount of flood in contact with the buildings within the AOI is called "summarize nearest." This tool summarizes the total sum of square meter of flood that are at or within a specified distance of the buildings. The distance representing "nearby" in this analysis was set to be at or within 2 meters of each building. For the processing, the building-dataset first had to be dissolved into one single polygon, and thereafter the 8 separate analyses were run, resulting in statistics showing nearby flooded areas as total square meter.

4. Results

The results obtained from the modelling in Itzï (section 3.3) and the network – and impact analyses in ArcGIS (section 3.4) will be presented in this section.
However, as there are a multitude of various results to be presented in the subsequent sections, the main findings are briefly outlined below in order to assist the reader to easier grasp the essence from each subchapter.

Section 4.1 presents the flood-results from the four STRDS-outputs modelled in Itzï in the following subchapters:

- **Water-depth (4.1.1)** – Presents where the modelled water (from the 5th hour) is distributed throughout the AOI and visualizes that large amounts of the water is actually of a very low water-depth.

- **Velocity's magnitude (4.1.2)** – Presents how the velocity of the flood (meter per second) increases hierarchically from the output of 2019 (with losses) to the output of 2100 (no losses). The areas with the highest discharge were generally located within the vicinity of where water could accumulate. The section also displays the accuracy of the runoff-water in the AOI by comparing it to a dataset attained by Bergen Municipality.

- **Flood simulation statistics (4.1.3)** – The statistics from all the timeseries modelled in Itzï are presented here. It is justified that the 5th hour was chosen due to having the highest flood-volume of all the timesteps, while still having low levels of numerical errors. The relation of the water that are entering and exiting the modelled timeseries are also presented here, showing that there is a net sum of increase of flood-volume.

- **Converting and comparing the water-depth maps (4.1.4)**
    - *Vectorization and classification of the flood maps (4.1.4.1)* – This section describes the converting of the flood-maps to polygons and classifying it to a threshold of ≥ 30cm, representing the height of flooded roads that are no longer passable for cars. The resulting flood polygons are illustrated in a map.

- *Simplification of the flood maps (4.1.4.2)* – It is here explained that the polygons had to be downscaled (simplified) from a number of 11 233 – 13 123 to 1170 – 1859 due to requirements from the software used. The new polygons are also here presented in a map.

- *Validation of the flood maps (4.1.4.3)* – Polygons from the 2100 output (no losses-input), having a threshold of ≥ 10cm are in this section compared to two other map-layers (flood-zones by Bergen Municipality and flood-susceptibility areas by NVE) showing areas prone to flood in the AOI. This comparison illustrates that the 2100 flood polygons do correlate especially inland in the urban area, but in the rural areas there is a lower correlation due to the NVE-map showing flooded waterbodies, whilst the 2100 flood polygons do not (since these areas were cropped out, explained in section 3.2.1.3).

Sequentially, section 4.2 presents the results from the network-analyses in the following subchapters:

- **Impact of flood on road-network and buildings (4.2.1)**
  - *Measuring impact of flood on road-network (4.2.1.1)* – Here it is established that even though the road-network merely covers 3,86% of the total area of the AOI, between 7,45-11,5% of the total area of the flood-polygons are located on the roads, indicating that many of the road-segments are fairly depressed compared to its surroundings and are thus prone to be flooded.

  - *Measuring impact of flood on buildings (4.2.1.2)* – The same trends as for the previous section are observable here, indicating that the buildings within the AOI are also more prone to receive a larger share of the accumulated water than its surrounding areas.

- **Areas of mobility with increasing flood-levels (4.2.2)** – This section show the decrease of reachable areas within 2 km when the higher flood-levels are inserted as barriers, affecting the road-network. However, even though all four levels of barriers reduce the serviceable area, there is a significant gap between the 2019 (with losses) polygons compared to the other three barrier-polygons. This increase is mostly due to a

large flood-polygon appearing on Bryggen (highlighted in the figures), having a substantial effect.

- **Fastest and shortest routes from origo to the outskirts with increasing flood-levels (4.2.3)** – As the title explain, routes are mapped from a predefined point (Origo) to several other points on the outskirts of the urban are in the AOI, and by applying the various levels of the flood (barriers), these routes are rerouted to a longer path, or in worst case the model did not find an alternative path. This occurred to the stop at the Pudderfjord-bridge since a flood at the northern end blocked the road. The other routes were also affected by the various flood-polygons, but the model was able to find alternative (albeit slower) routes for these. The major flood-barriers blocking the routes are highlighted in white circles in the figures.

- **Fastest routes from one outskirt to another with increasing flood-levels (4.2.4)** – This section is similar to section 4.2.3, but rather than locating the fastest and shortest routes from the predefined point, the aim is instead to measure the fastest routes from locations at one end of the urban area within the AOI to another. Many of the same barriers from the previous section blocks the routes here as well, while some new are introduced seeing that there are different routes taken. The main barriers influencing the routes are highlighted in white circles in figure 4-32, showing that some of the routes (especially those using the 2100 flood-barriers) had to take reroutes into smaller and narrower streets.

4.1 Itzï-modelling results

It is only the outputs from the fifth hour from each timeseries that will be presented as figures here, since it is within this hour the highest magnitude of flood within the domain (AOI) are observed. The statistical data section (4.1.3) will on the other hand include all of the outputs.

4.1.1 Water-depth results from Itzï (5th hour)

Following the completion of the Itzï-modelling, raw, unedited versions of the water-depth rasters were outputted. These outputs provide the height and location of the surface-water in the AOI. But, seeing that the initial outputs were displayed in a continuous format where 0m

was the lowest and ≈ 10m was the highest value, and most of the pixels represents water-heights ranging between 0-1 meters, the values were classified into 7 different groups to easier differentiate between the levels (0,01m, 0,05m, 0,1m, 0,5m, 1m, 5, and the highest value at ≈ 10m).

Figures 4-1 – 4-4 display the distribution of the surface-water of the four different outputs from the fifth hour of the modelling. As these maps illustrate, the majority of the AOI is covered in water (blue/green/purple), while some mountainous areas, buildings and the outlet areas are completely dry (gray/black, i.e. basemap). Variation in water-heights in some of the areas can be observed by comparing the figures.

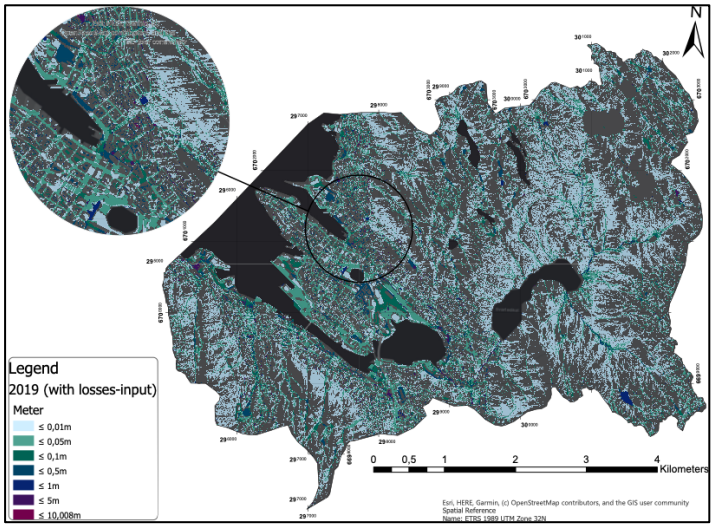

Figure 4-1: Water-depth output from Itzï. Classified raster-map from 5th hour in 2019 with losses-input

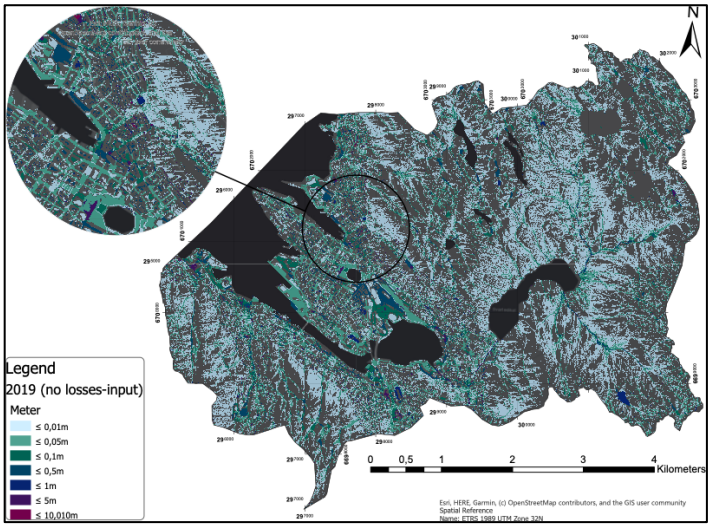

Figure 4-2: Water-depth output from Itzï. Classified raster-map from 5th hour in 2019 with no losses-input

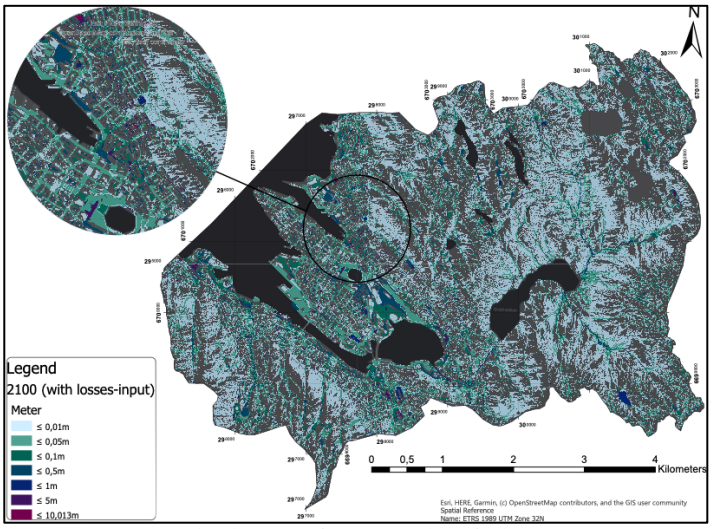

Figure 4-3: Water-depth output from Itzï. Classified raster-map map from 5th hour in 2100 with losses-input

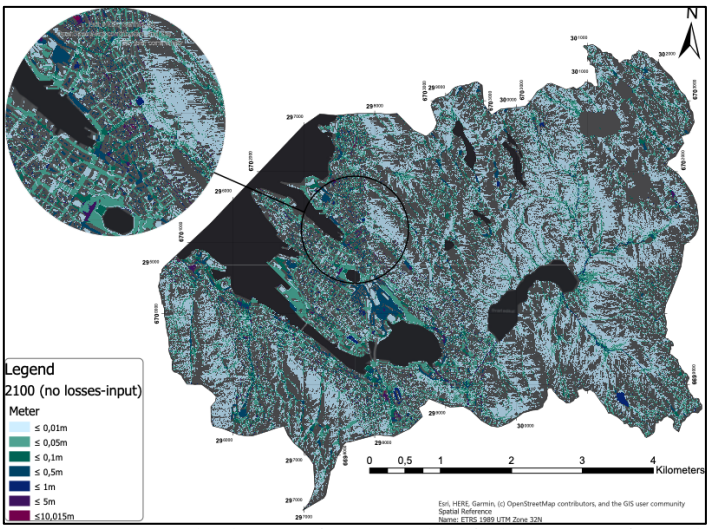

Figure 4-4: Water-depth output from Itzï. Classified raster-map from 5th hour in 2100 with no losses-input

Figures 4-5 – 4-8 show the same results where the road-network is included, and the basemap-layer is removed to get another perspective of the flood-maps and how the water is distributed on the road-segments (larger versions of figures 4-1 – 4-8 can be seen in appendix 2).

Finally, even though the flooded areas seem to be very extensive, much of the water-depths in these areas are in fact of a very insignificant level as will be explained in section 4.1.4.

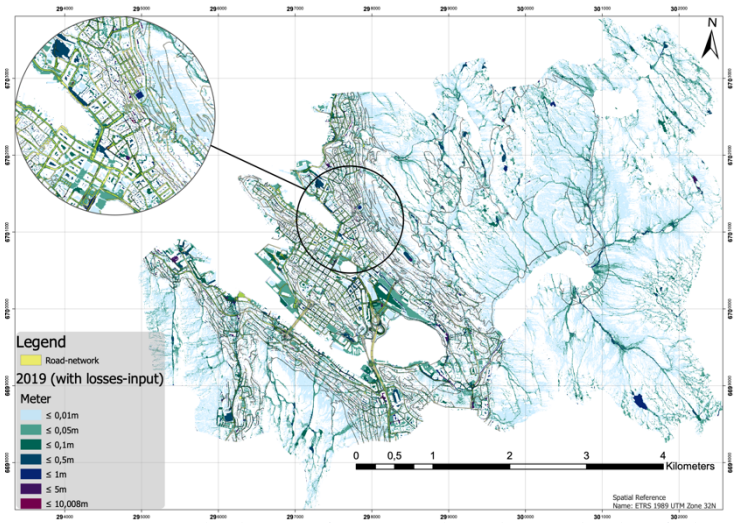

Figure 4-5: Water-depth output from Itzï with road-network. Classified raster-map from 5th hour in 2019 with losses-input

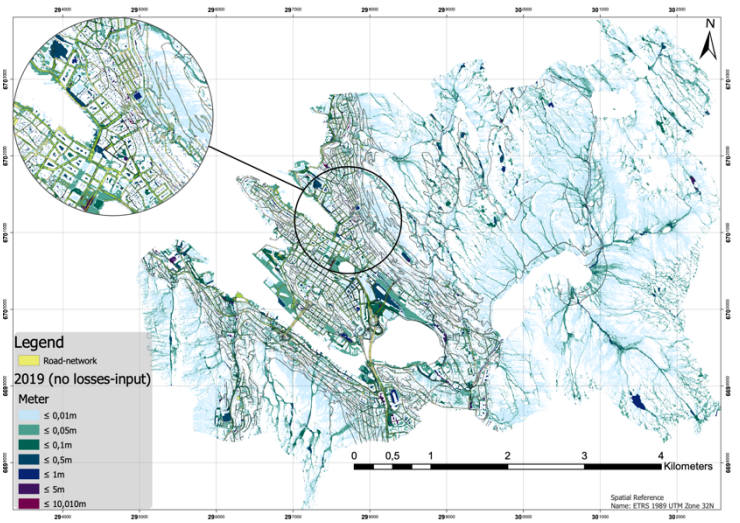

Figure 4-6: Water-depth output from Itzï with road-network. Classified raster-map from 5th hour in 2019 with no losses-input

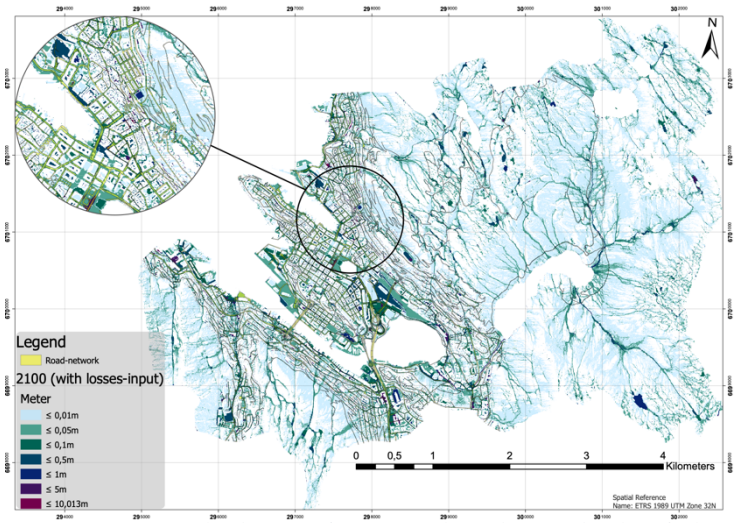

Figure 4-7: Water-depth output from Itzï with road-network. Classified raster-map from 5th hour in 2100 with losses-input

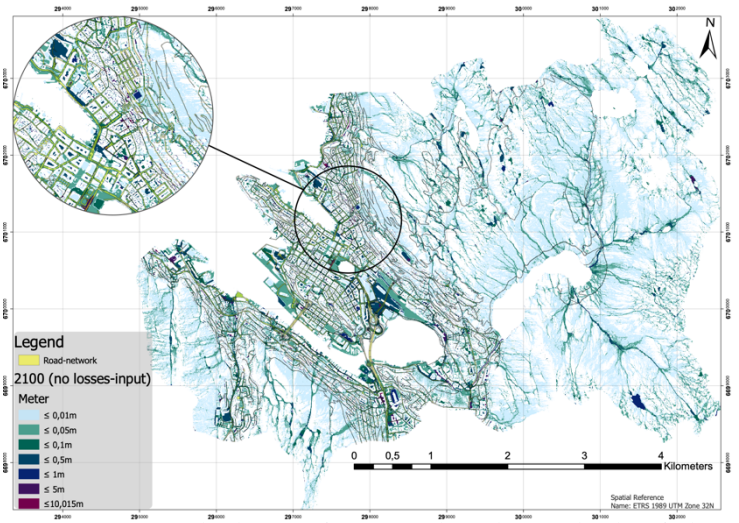

Figure 4-8: Water-depth output from Itzï with road-network. Classified raster-map from 5th hour in 2100 with no losses-input

4.1.2 Magnitude of velocity results from Itzï (5th hour)

In addition to the water-depth outputs, the magnitude of velocity (i.e. the intensity and distribution of the runoff-water) was the other map-type predefined in the parameter-file to be outputted from Itzï. By looking at figures 4-9 – 4-12 (larger versions are added in appendix 3-1), these maps illustrate the intensity of the water in meter per second within the catchment area. The original continuous data has been classified into 7 groups for visual purposes, where the classes represents the natural grouping (breaks) of the distribution of the data, as seen in the legends (ArcGIS Pro, n.d. C). The maps display where the water is channeled down the mountainside (as the higher values represents), while the hierarchical relation between the figures show that the maps increases in both intensity (brighter colors) and in their highest value.

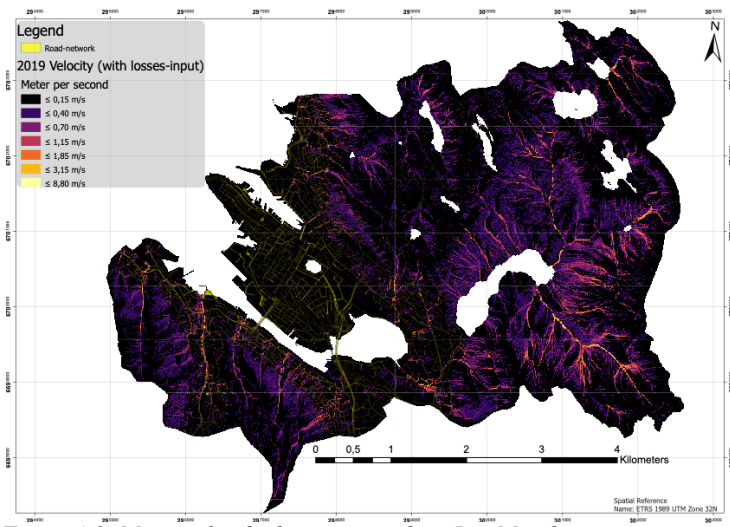

Figure 4-9: Magnitude of velocity output from Itzï. Map from 5th hour in 2019 with losses-input.

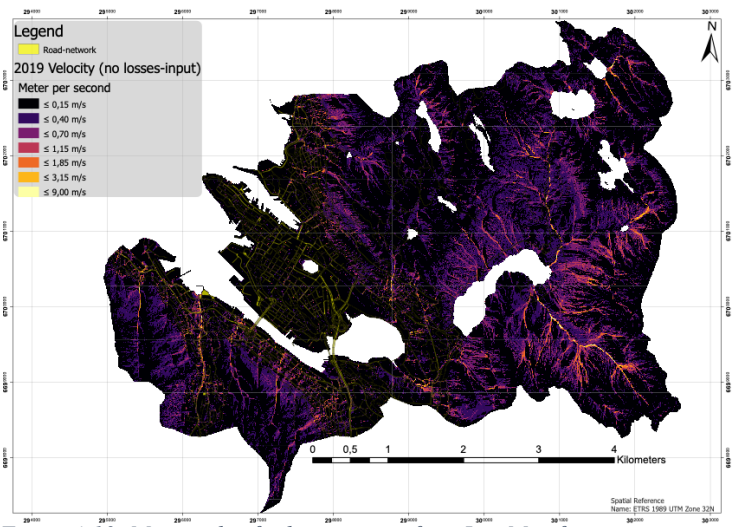

Figure 4-10: Magnitude of velocity output from Itzï. Map from 5th hour in 2019 with no losses-input.

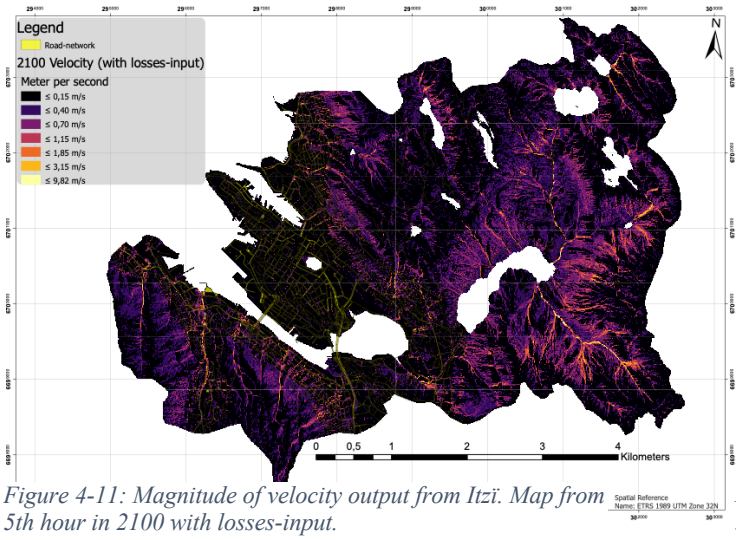

Figure 4-11: Magnitude of velocity output from Itzï. Map from 5th hour in 2100 with losses-input.

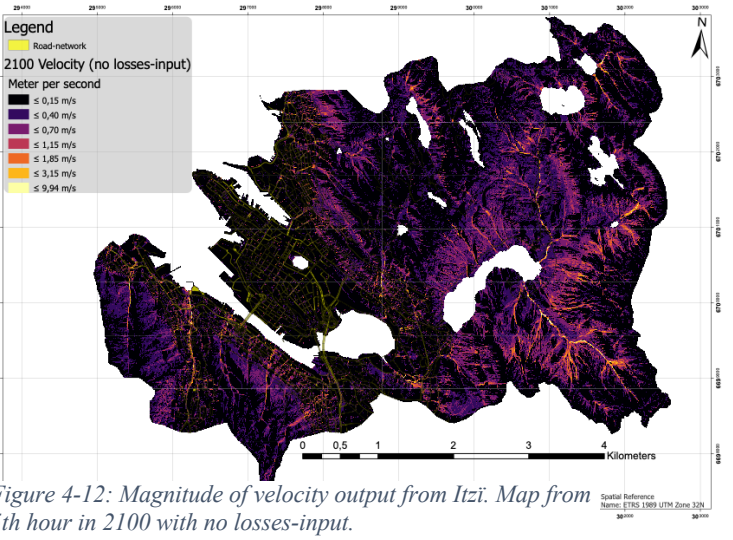

Figure 4-12: Magnitude of velocity output from Itzï. Map from 5th hour in 2100 with no losses-input.

Figure 4-13 is the same layout as figure 4-12, albeit where a map-layer from Bergen Municipality is included, representing the extent and distribution of the runoff water within the catchment area. As observable, there is a large correlation between these two data-layers, i.e. that the runoff waterlines are drawn towards the higher values of the velocity. (Larger version is added in appendix 3-2).

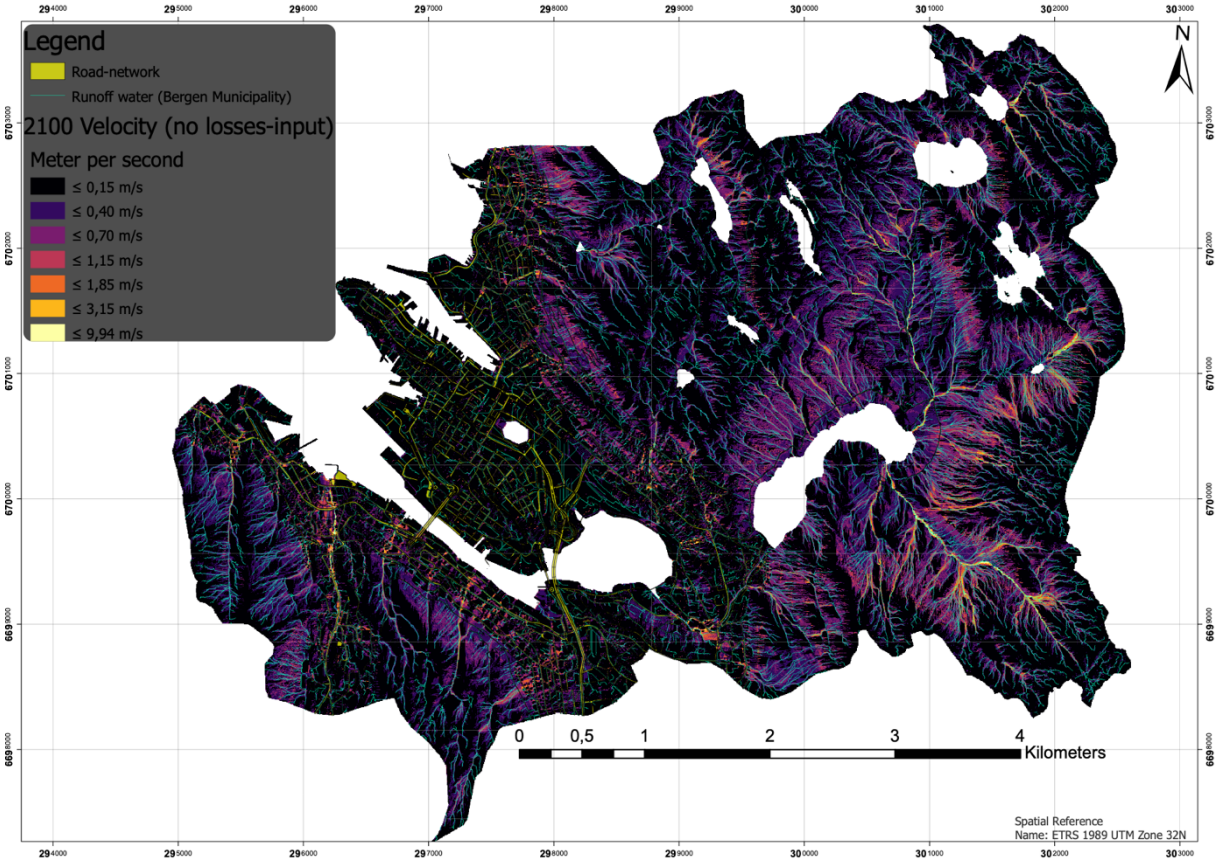

Figure 4-13: Magnitude of velocity output from 5th hour in 2100 with no losses-input compared to runoff water-dataset from Bergen Municipality. Source: Bergen Municipality (n.d.).

4.1.3 Flood simulation statistics

The CVS-file is where all the statistics from the Itzï-modelling was stored and can be seen in table 4-1. The table presents the statistics of all six hours from each of the four timeseries outputted from Itzï.

Highlighted in green is the fifth timestep from each timeseries used to represent the four categories of outputs since they have the highest amount of water within the domain (AOI), as the domain volume column shows. The table also display the amount of total added water through precipitation (rain volume), and the amount of water that exited the domain, both through boundary volume (the boundaries set in the outlet-files) and losses volume (drainage and infiltration). In these columns the fifth hour also had the highest number within each timeseries.

At the right side of the table, the created volume column represents the certainty of the modelled flood for each timestep, i.e. if the variation of the new water depths calculated in each cell from the previous timestep is low, the created volume will be to a minimum, indicating that the numerical errors will be low as well. The opposite would indicate high numerical errors (Courty, Acuna and Bates, 2017, pp. 1838). Lastly, the %error column shows the percentage of the variation in domain volume due to numerical errors (calculated by; created volume / (domain volume – old domain volume) *100 (Itzï, n.d. A)). The numerical instabilities/errors encountered in the model will be further addressed in chapter 5. However, the low amount of variation as seen in each of the 5th hours serves as a further justification of choosing this hour to represent the four categories of outputs.

Table 4-1: CVS-statistics for all outputs of the Itzï-modelling. Volumes are in m^3.

CATEGORIES OF OUTPUTS	SIM TIME	BOUNDARY VOL (M^3)	RAIN VOL (M^3)	LOSSES VOL (M^3)	DOMAIN VOL (M^3)	CREATED VOL (M^3)	%ERROR
2019							
WITH LOSSES-*INPUT*	14.09.2019 16:00	-12661455.931	230129.205	-33858.759	172343.034	12633686.679	7330.55%
	14.09.2019 17:00	-83857.281	190215.212	-33672.886	245348.803	18.847	0.03%
	14.09.2019 18:00	-137958.398	308096.139	-34143.294	381848.653	3.021	0.00%
	14.09.2019 19:00	-206955.946	346778.436	-34240.816	486800.974	3.228	0.00%
	14.09.2019 20:00	-247539.455	352137.237	-34254.870	556540.644	9.599	0.01%
	14.09.2019 21:00	-166587.090	137246.304	-33189.401	491692.434	1.108	-
2019							
NO LOSSES-INPUT	14.09.2019 16:00	-28507443.344	230129.223	-0.000	200398.666	28474536.888	14208.95%
	14.09.2019 17:00	-97312.933	190215.212	-0.000	293664.378	15.538	0.02%
	14.09.2019 18:00	-162258.215	308096.139	-0.000	439996.816	0.835	0.00%
	14.09.2019 19:00	-240229.087	346778.436	-0.000	546026.184	6.544	0.01%
	14.09.2019 20:00	-278890.187	352137.237	-0.000	618713.919	0.086	0.00%
	14.09.2019 21:00	-194811.890	137246.304	-0.000	558205.849	0.824	-
2100							
WITH LOSSES-*INPUT*	14.09.2100 16:00	-21847086.139	300752.641	-34106.431	221867.949	21799768.063	9825.56%
	14.09.2100 17:00	-119923.643	248238.815	-33960.584	315690.164	16.185	0.02%
	14.09.2100 18:00	-203737.248	400283.626	-34335.850	478802.495	2.809	0.00%
	14.09.2100 19:00	-302655.892	450295.339	-34423.980	591811.296	0.000	0.00%
	14.09.2100 20:00	-344076.081	458168.679	-34435.947	670291.111	0.000	0.00%
	14.09.2100 21:00	-225574.604	177710.412	-33619.328	586263.520	0.340	-
2100							
NO LOSSES-INPUT	14.09.2100 16:00	-16922798.160	300752.641	-0.000	249374.091	16867917.696	6764.10%
	14.09.2100 17:00	-136710.918	248238.797	-0.000	360372.287	13.116	0.01%
	14.09.2100 18:00	-231978.675	400283.626	-0.000	529672.330	1.326	0.00%
	14.09.2100 19:00	-335583.369	450295.374	-0.000	644178.838	0.000	0.00%
	14.09.2100 20:00	-377854.651	458168.644	-0.000	723275.143	0.000	0.00%
	14.09.2100 21:00	-253361.186	177710.412	-0.000	644584.066	0.331	-

The following two paragraphs will present the relation between the amounts of water that are entering and exiting the model for each of the timeseries in order to better understand how and why the flood is increasing in size.

Figures 4-14 – 4-17 display a comparison between the input data of the modelling (rain volume) and the amount of simulated water accumulated in the domain (domain volume) for all six hours of each timeseries. The first hour show that the simulated water in the domain is lower than the precipitation (input data) since all the models starts at 0. Consequently, since the boundary volume and losses volume, being the negative factor, are less than the positive factor of the domain volume, the domain volume increases more for each passing hour than what it receives from the precipitation.

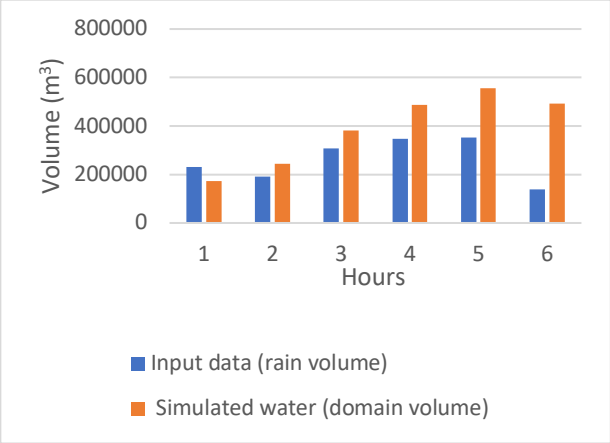

Figure 4-14: 2019 timeseries (with losses-input). Correlation between input data and simulated water within domain

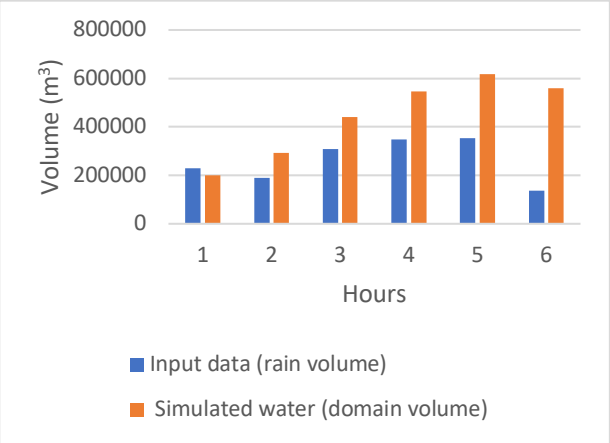

Figure 4-15: 2019 timeseries (with no losses-input). Correlation between input data and simulated water within domain

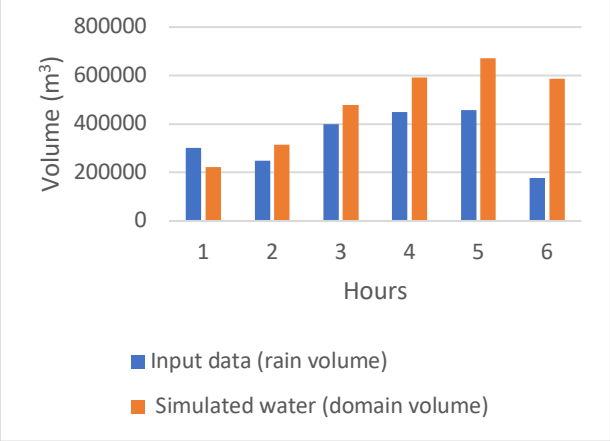

Figure 4-16: 2100 timeseries (with losses-input). Correlation between input data and simulated water within domain

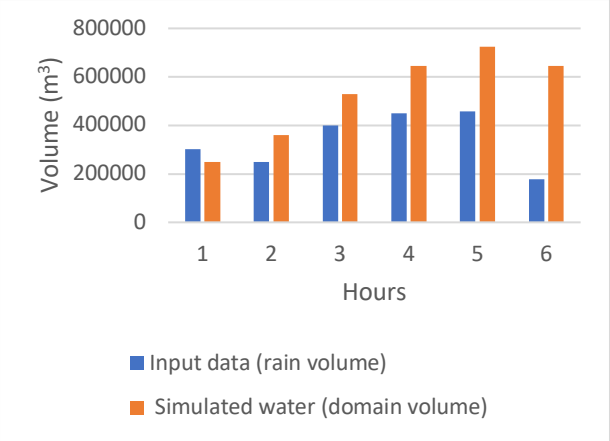

Figure 4-17: 2100 timeseries (with no losses-input). Correlation between input data and simulated water within domain

The negative factor mentioned above can be seen in figures 4-18 – 4-21, representing the four timeseries. Here the relationship between the simulated water (domain volume) and the amount of water that exited the domain for each timestep (boundary and losses volume) is compared. The first hour from each timeseries was removed because of its inaccurate representation due to high numerical errors creating large amounts of volume. As the figures show, the removed volume is larger in figures 4-18 (compared to 4-19) and 4-20 (compared to 4-21) since the modelling of these two timeseries removed water via the defined losses-data and by the boundary conditions. For the modelling of the timeseries in figures 4-19 and 4-21, they solely had the boundary conditions as a parameter for extracting the water, resulting in an even higher volume of simulated water (domain volume) since none of it is being infiltrated (through the ground) nor by entering the drainage.

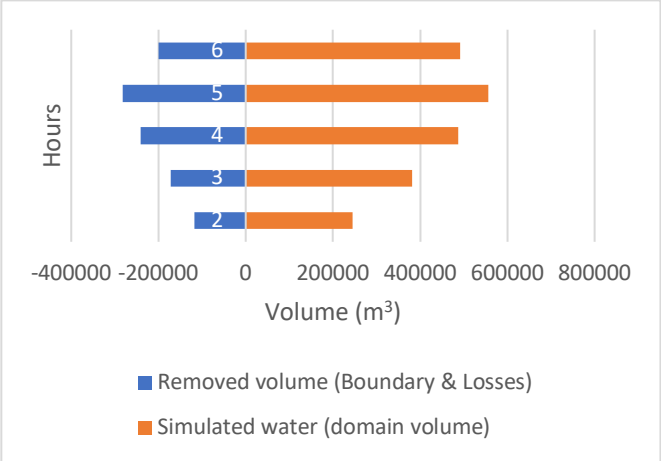

Figure 4-18: 2019 timeseries (with losses-input). Relation between simulated water in domain and volume that leaves the domain (by boundary and losses) for each timestep

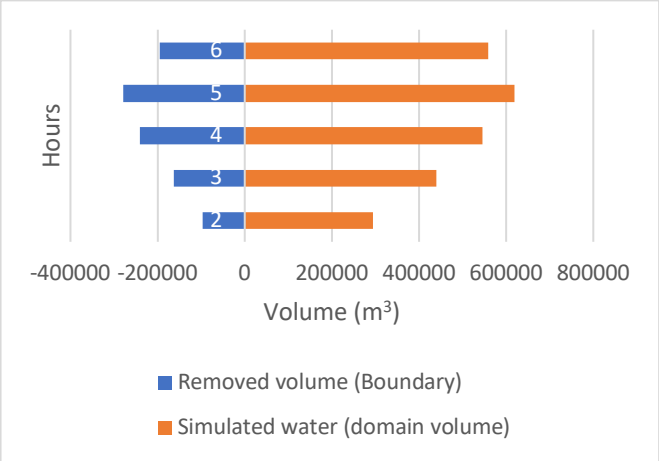

Figure 4-19: 2019 timeseries (with no losses-input). Relation between simulated water in domain and volume that leaves the domain (by boundary) for each timestep

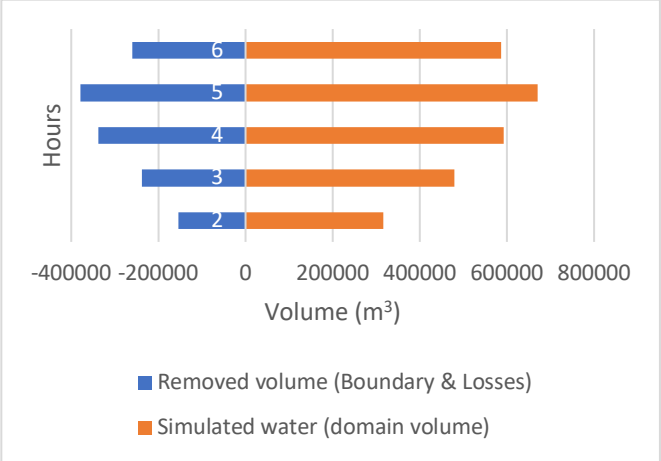

Figure 4-20: 2100 timeseries (with losses-input). Relation between simulated water in domain and volume that leaves the domain (by boundary and losses) for each timestep

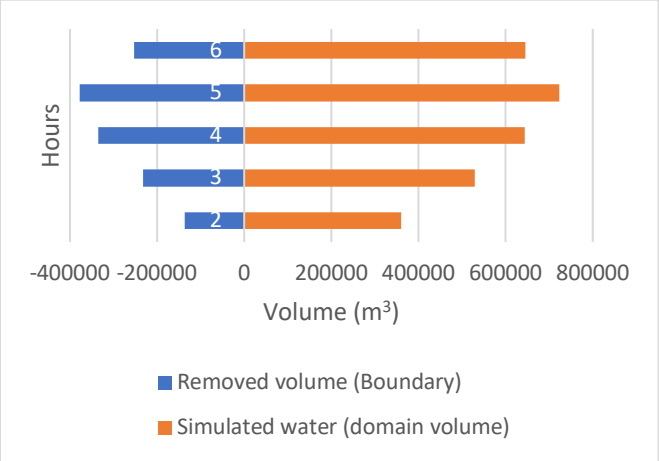

Figure 4-21: 2100 timeseries (with no losses-input). Relation between simulated water in domain and volume that leaves the domain (by boundary) for each timestep

4.1.4 Converting and comparing the water-depth maps

4.1.4.1 Vectorization and classification of the flood maps

To use the flood-results for the network-analyses, they had to be converted into a threshold that could be used for illustrating blocked and open road-segments (i.e. barriers) for cars. Both figure 4-22 and the zoomed in version of figure 4-23 show the four different 5th hour outputs presented in section 4.1.1 (figures 4-1 – 4-8) which has now been vectorized and classified into the threshold of wiw(i.e. at or above 30 cm). The first layer representing the dataset 2019 with losses-input (red) is placed at the top. This means that the areas covered in blue polygons (2019 with no losses-input) does not contain any of the red polygons. The same applies for the yellow (2100 with losses-input) – and green polygons (2100 with no losses-input), where the areas of i.e. green (farthest down in hierarchy) will not cover any of the yellow, blue or red polygons since it is already present there. Also, by comparing the classified flood-maps to the unclassified water-depth maps of figures 4-1 – 4-8, it is apparent that large parts of the unclassified maps contained water-depths below 30 cm.

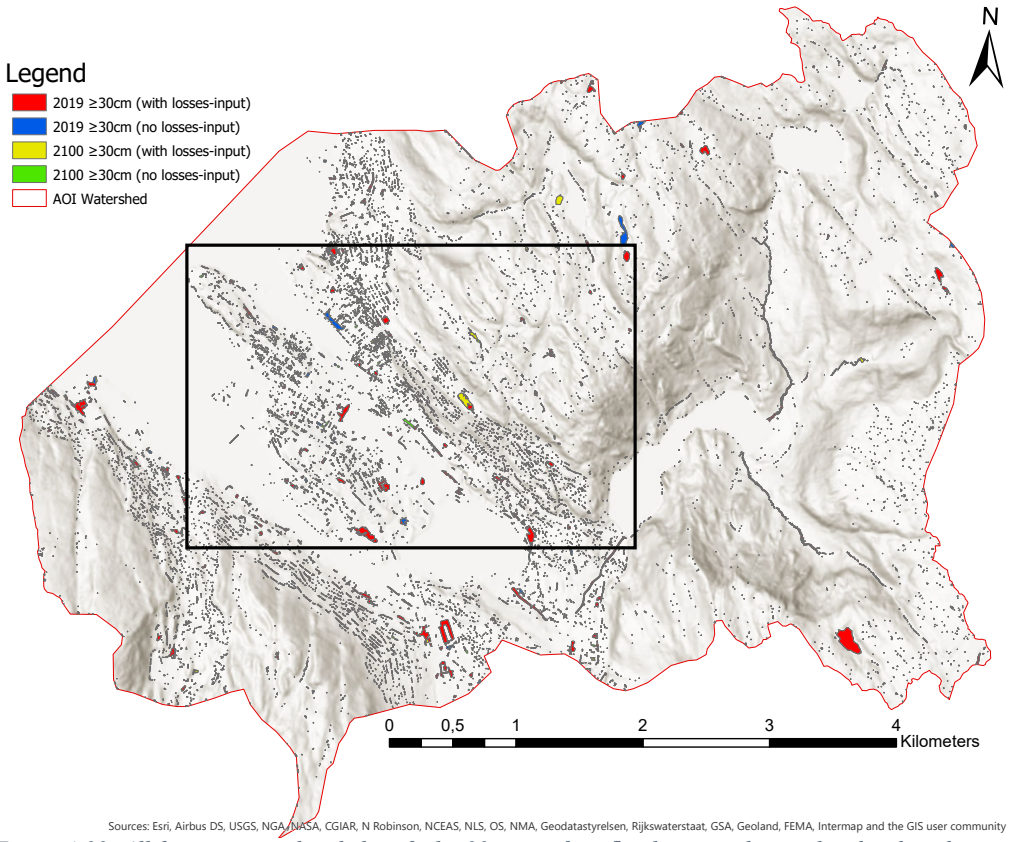

Figure 4-22: All four vectorized and classified ≥ 30 cm surface-flood maps in hierarchical order where areas in blue, yellow or green show areas not flood-covered by the lower ranked maps. (Box is extent of figure 4-23 & 4-24)

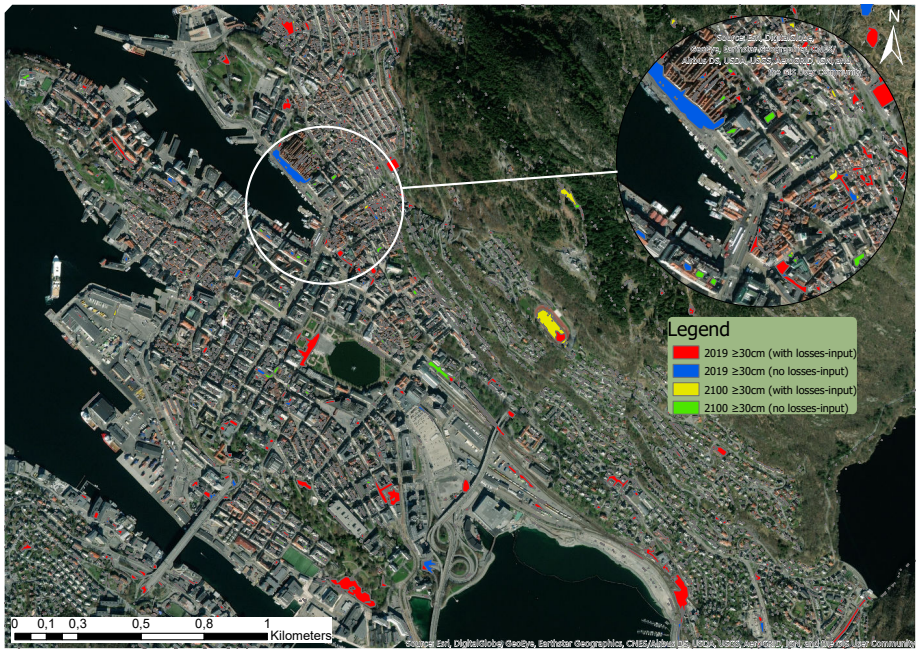

Figure 4-23: A more focused version of figure 4-15, included imagery basemap.

4.1.4.2 Simplification of the flood maps

To successfully run the flood-polygons in the network-analyses they had to be reduced to a threshold below 2000 polygons per dataset. Figure 4-24, having the same scale as figure 4-23, presents these new simplified datasets (referred to as barrier 1, 2, 3 and 4 in the network analyses). There is not too much visual difference between the polygons in figure 4-23 and figure 4-24 since the downscaling of the original 11 233 – 13 123 polygons down to 1170 – 1859 affected mostly the smaller polygons while preserving the size and characteristics of the larger ones. This relation will be further addressed in section 4.2.

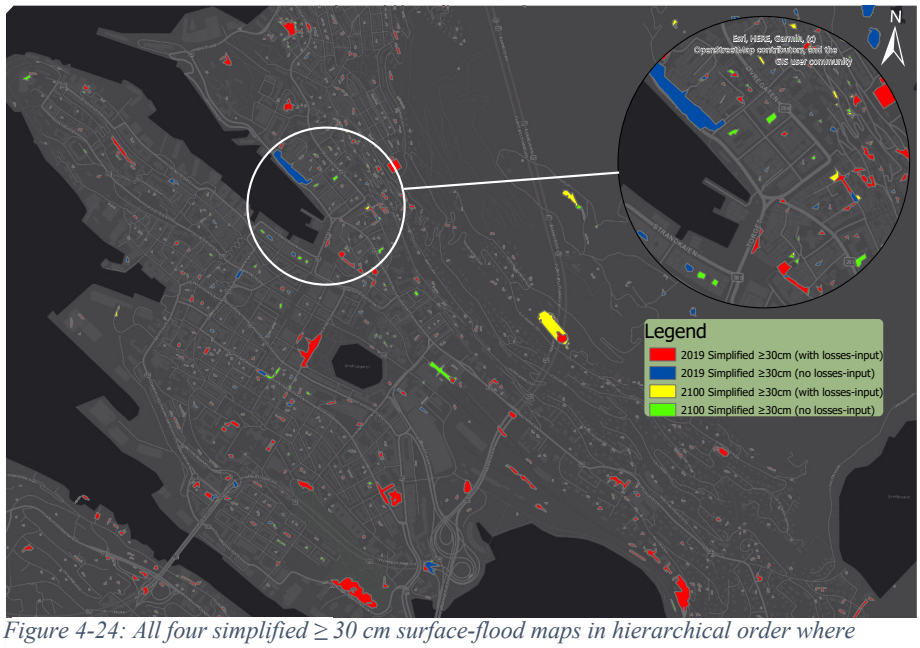

Figure 4-24: All four simplified ≥ 30 cm surface-flood maps in hierarchical order where areas in blue, yellow or green show areas not flood-covered by the lower ranked layers.

4.1.4.3 Validation of the flood maps

Before turning to the network-analyses, a surface-flood map from Itzï will be compared to two other available sources of flood-zones maps. The first of these map-layers, the regulated flood-zones, is an excerpt (from 2018) of flood-zones requiring special consideration from all the zoning (regulated) plans in Bergen Municipality. It is composed of flood trails, zones with risks of flood or flood-prone zones mapped by hydraulic analyses (Bergen Municipality, 2019). As figure 4-25 show, the regulated flood-zones seems to be a minor excerpt as it for the most part covers the outlet originating from Svartediket and the surrounding shoreline of the ocean. The data-basis of the regulated flood-zones was however not published along with the data-layer. It is therefore not possible to compare the water-height nor the preconditions of how the zones were established to the Itzï-results.
The second source of flood-zones, the flood susceptibility-areas, is collected from NVE and is far more extensive than the regulated flood-zones as seen in figure 4-25. This map-layer is produced on a national scale and is meant to serve as guidance for municipalities. It does not state any probability of flood, but merely provide indications as to where one should perform more detailed flood-analyses (NVE, 2011).

Since these two map-layers do not include any information of the probability of flood nor the water-depths, the Itzï flood-polygons were classified to ≥10 cm from the output; 2100 no losses-input in order to create a binary flood polygon that can be compared to the Bergen municipality and the NVE flood maps.

Hence, as seen in figure 4-25, the 2100 flood-polygons (no losses-input) stretches throughout the landscape and are noticeably more extensive than the other map-layers. Many of these polygons are also (partly) covered by one or both of the other two layers.
The NVE-map indicates flood-risks along much of the shoreline of the AOI, as well as the major waterbodies at the higher elevations (which does not correlate with the 2100 flood-polygons since these lakes were cropped out, described in section 3.2.1.3). The water-streams from these waterbodies does however greatly cover, and thus correlate with the 2100 flood-polygons as they both indicates higher river-floods. Lastly, The NVE-map also show a larger flood-risk area more inland in the urban zone, which is also partly covered by both the 2100 flood-polygons and the Bergen Municipality flood-zone map-layer. However, despite observing both areas of correlations and non-correlations, the two comparison-maps (NVE and

Bergen Municipality) are of a more generalized format, informing that the actual comparison to the 2100 flood-polygons should not be given too much weight.

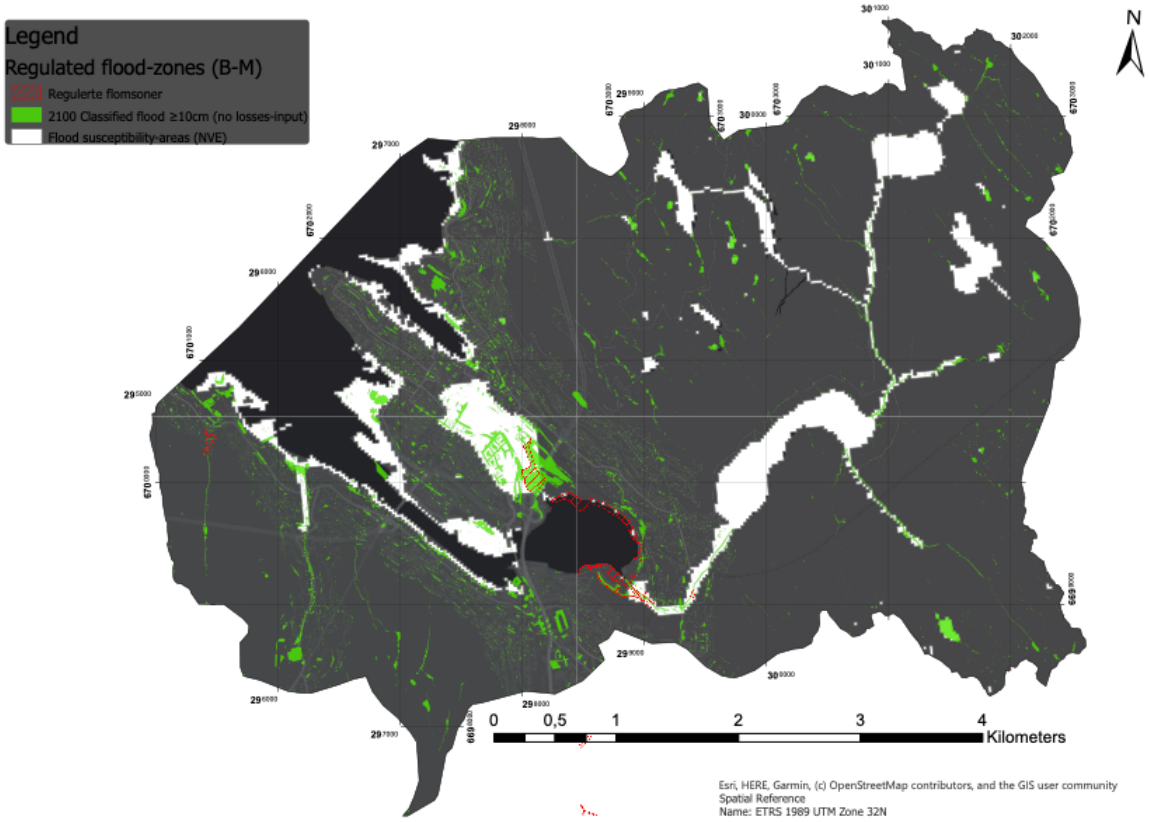

Figure 4-25: Comparison of the classified ≥10 cm (2100 no losses-input) flood-polygons to the two map layers; regulated flood zones (regulerte flomsoner) (Bergen Municipality, n.d.) and flood susceptibility-areas (NVE, 2011). B-M = Bergen Municipality.

4.2 Network-analysis results

The four simplified ≥30 cm flood-polygons from the fifth hour of each modelled timeseries in Itzï are in this section used as input-barriers into the processing of the various network analyses performed. This is done in order to assess the costs added to the level of mobility (by car) on the road-network, induced by the different extreme precipitation-scenarios. The results will be presented both in the forms of figures and tables.

4.2.1 Impact of flood on road-network and buildings

In order to see how much of a difference there actually is between the generated flood-polygons, both the four simplified polygons representing the barriers and the four original (non-simplified) polygons were used as input when analyzing the impact of flood on the road-network (4.2.1.1) and the total amount of buildings (4.2.1.2) within the AOI. The aim is to get an understanding of the dimensions of the flood-polygons when compared to these other physical elements. Also, the measure units for both sections are provided in km^2 since it is the total area of the roads and buildings being occupied by the flooded polygons that was set at the objective. However, for the sake of providing adequate and accurate information of the magnitude of the road-network within the AOI, the total length should also be specified, which is 398km.

4.2.1.1 Measuring impact of flood on road-network

The statistics from this analysis can be seen in table 4-2. The four rows at the top represents the simplified flood-polygons (B1, B2, B3 & B4 is the abbreviations of the barrier-names), while the four at the bottom is the original flood-polygons.

The percentage of flooded roads compared to the total area of the road-network (1,18 km^2) ranges between 1,48% – 2,19% for the simplified polygons and 1,85% - 2,67% for the original polygons. However, even though this does not seem as an expansive flood for any of the groups, the amount of flood occurring on the road-network compared to the total amount of flood in each group is substantially higher, ranging between 8,81% – 11,5% for the former and 7,45% - 8,22% for the latter. This may be an effect of roads being more depressed than its surrounding areas, causing the surface-water to accumulate in these areas. This large percentage of flooded roads will also be observable in the figures in the remaining sections of this chapter. In many of these figures there are several white circles added, showing some of the areas where the flood is acting as barriers to the road network, affecting both the smaller and larger roads. The northern end of the Pudderfjord-bridge is a larger road segment prone to flood, to mention one. By looking at the flooded roads compared to the area of the AOI (30,79 km^2), the percentage is as expected, hierarchically ordered from the 2019 with losses data – to 2100 no losses data. The total area of the road-network covers 3,86% of the area in the AOI.

Table 4-2: Road-network compared to the four simplified (barriers) and four original ≥30cm flood-polygon layers

Flood-layer	Layer-type	Number of flood-polygons	Flood polygon (km²)	Total area of roads (km²)	Flooded road-area (km²)	Flooded roads compared to all roads (%)	Flooded roads compared to total flood (%)	Flooded roads compared to AOI (%)
2019 (with losses) **B1**	Simplified	1170	0,153	1,18	0,017	1,48	11,50	0,05
2019 (no losses) **B2**	Simplified	1650	0,244	1,18	0,022	1,89	9,21	0,07
2100 (with losses) **B3**	Simplified	1722	0,267	1,18	0,023	1,98	8,81	0,07
2100 (no losses) **B4**	Simplified	1859	0,284	1,18	0,026	2,19	9,17	0,08
2019 (with losses)	Original	11233	0,295	1,18	0,022	1,85	7,45	0,07
2019 (no losses)	Original	12173	0,336	1,18	0,027	2,33	8,22	0,09
2100 (with losses)	Original	12510	0,363	1,18	0,028	2,43	7,94	0,09
2100 (no losses)	Original	13123	0,386	1,18	0,031	2,67	8,20	0,10

4.2.1.2 Measuring impact of flood on buildings

As explained in section 3.4.5, the summarize nearby tool was used for this analysis with a buffer of 2-meters, contrary to the summarize within tool used for the road-impact. This mean that it is not the flood inside the actual buildings that has been located, but rather the flood within a proximity of 2-meters of each building – seeing that there should be no water inside the buildings as defined in section 3.2.1.3.

By looking at table 4-3, the simplified flood-polygons ranges between 15,8% - 22,15%, while the original flood-polygons ranges between 24,99% - 26,35% of the flood that is covered by the 2-meter buffer around each building. These two groups show a large increase compared to the amount of flood covering the roads from the previous section. However, this is justifiable when comparing the difference in total area of the roads and buildings (1,18 km^2 vs 3,24 km^2). For the percentage of flood (2-meter buffer) nearby buildings compared to the AOI it is the same as for the previous section, a hierarchical increase from the 2019 with losses data to the 2100 with no losses data. The total area of the buildings covers 10,53% of the AOI

Table 4-3: Buildings compared to the four simplified (barriers) and four original ≥30cm flood-polygon layers

Flood-layer	Layer-type	Number of flood-polygons	Flood polygon (km²)	Total area of buildings (km²)	Flood nearby buildings (2m buffer) (km²)	Flood nearby buildings (2m buffer) compared to total flood (%)	Flood nearby buildings compared to AOI (%)
2019 (with losses) **B1**	Simplified	1170	0,153	3,24	0,033	22,15	0,11
2019 (no losses) **B2**	Simplified	1650	0,244	3,24	0,040	16,38	0,12
2100 (with losses) **B3**	Simplified	1722	0,267	3,24	0,042	15,80	0,13
2100 (no losses) **B4**	Simplified	1859	0,284	3,24	0,048	17,01	0,15
2019 (with losses)	Original	11233	0,295	3,24	0,074	25,28	0,24
2019 (no losses)	Original	12173	0,336	3,24	0,087	25,89	0,28
2100 (with losses)	Original	12510	0,363	3,24	0,090	24,99	0,29
2100 (no losses)	Original	13123	0,386	3,24	0,101	26,35	0,33

4.2.2 Areas of mobility with increasing flood-levels

The aim of this service areas analysis was to find all areas reachable within 2 kilometers (via the road-network) from the defined origo, where one of the barriers was applied for each service area analysis and the speed limit was set to 60 km/h (the speed limit is same for section 4.2.3 and 4.2.4). The results from the analysis are visually presented in figure 4-26 (service area 2 using barrier 1), figure 4-27 (service area 3 using barrier 2) figure 4-28 (service area 4 using barrier 3) and figure 4-29 (service area 5 using barrier 4), while the statistics is presented in table 4-4.

Common for all these figures is that they have the service area 1 layer in the background. This is an output where no barriers were applied, representing the default mode of reachable areas (i.e. all areas within range of 2 km from the origo on a dry day with no flood). The areas of mobility from this layer is 10.67m^2 (table 4-4) and is far more reaching in certain areas than any of the other service-areas.

Turning to figure 4-26 where service area 2 with barrier 1 is displayed, this layer covers an area of 8,41km^2 which is approximately 2 km^2 smaller than service area 1. The large reduction is due to the emergence of the barriers covering an area of 0,15km^2. It is possible to see the various road-segments that are cut off due to flood, affecting the total serviceable area.
The same trend applies for figure 4-27 with service area 3 (using barrier 2), which is reduced to 7,14km^2 while the barrier has increased to 0,24km^2. One noticeable difference between these two figures is the large barrier that has emerged within the highlighted area, affecting the service area northwards.

Figure 4-28 and 4-29 with service area 4 (barrier 3) with an area of 6,99km^2, and service area 5 (barrier 5) with an area of 6,94km^2 is very identical in shape and size. Their barrier-sizes are 0,26km^2 for the former and 0,28km^2 for the latter. This can also be observed in figure 4-24 (section 4.1.4.2) as presented earlier.
Consequently, there seems to be a larger gap between the barriers blocking the roads in the two outputs of 2019 (with and without losses-input), contrary to the barriers blocking the roads from the two outputs of 2100 (with and without losses-input) – even though there is a significant variation of the barrier-sizes and number of polygons (table 4-4).

Figure 4-26: Service area 1 (no barrier) and service area 2 (barrier 1 as input)

Figure 4-27: Service area 1 (no barrier) and service area 3 (barrier 2 as input)

Figure 4-28: Service area 1 (no barrier) and service area 4 (barrier 3 as input)

Figure 4-29: Service area 1 (no barrier) and service area 5 (barrier 4 as input)

Table 4-4: Service areas (km^2) with area (km^2) and number of polygons for each barrier

Service area analysis (included what barriers used)	Service area (km^2)	Barrier (km^2)	Number of polygons
Service Area 1 (No barrier)	10,67	0	0
Service Area 2 (Barrier 1)	8,41	0.15	1170
Service Area 3 (Barrier 2)	7,14	0.24	1650
Service Area 4 (Barrier 3)	6,99	0.26	1722
Service Area 5 (Barrier 4)	6,94	0.28	1859

4.2.3 Fastest and shortest routes from origo to the outskirts with increasing flood-levels

The aim of this analysis was to calculate the fastest and shortest routes from the Origo to an end destination (where 5 of them were run with driving time and the other 5 were run with driving distance as parameter) using the flood barriers as inputs. The visual results are presented in figures 4-30 and 4-31, while the statistics can be seen in table 4-5.

The default modes here (the outputs that did not have flood as input) are the two layers in figure 4-30; shortest driving distance (no barrier) and shortest driving time (no barrier). These were also the only results that managed to separate routes based on driving time and distance, while the rest of the routes gave the same path for both modes. The white circles show significant barriers that blocked some of the routes as seen in figure 4-31, while the two groups of blue-shaded polygons in the same figure illustrates the flood-barriers. The reason as to why there are only two barriers and two differing routes in figure 4-31 is because the outputs from the layer shortest driving time & distance (using barrier 1) gave one set of route, while the remaining routes using barrier 2, 3 and 4 gave the exact same routes, visualized in the figure by the name shortest driving time & distance (visualized by barrier 4).

Hence, the layer shortest driving time & distance (using barrier 1) in figure 4-31 managed to generate routes for all stops but the Pudderfjord-bridge, seeing that it was blocked by several flood-barriers as indicated in the white circles. It did however manage to match one out of the two default mode routes (figure 4-30 and table 4-5) for every other end-stop, indicating that even though the flood was immense, it is possible to find acceptable alternative routes.

It is the exact same result for the layer shortest driving time & distance (using barrier 4), except for a smaller reroute due to flood in the zoomed in circle (heading towards Sandviken), resulting in a slightly longer route (in terms of both time and distance).

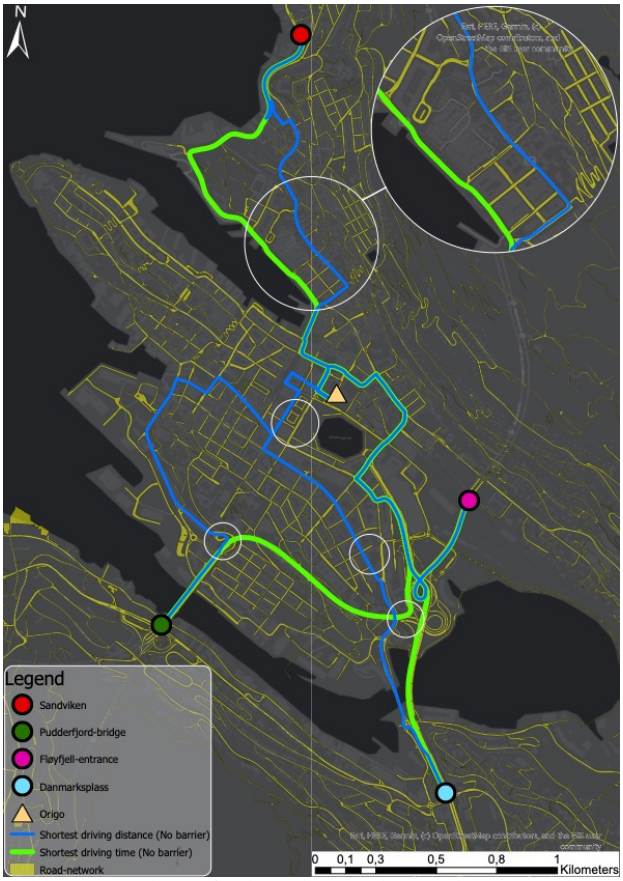

Figure 4-30: Closest facility. Shortest driving distance and time using no barriers as input

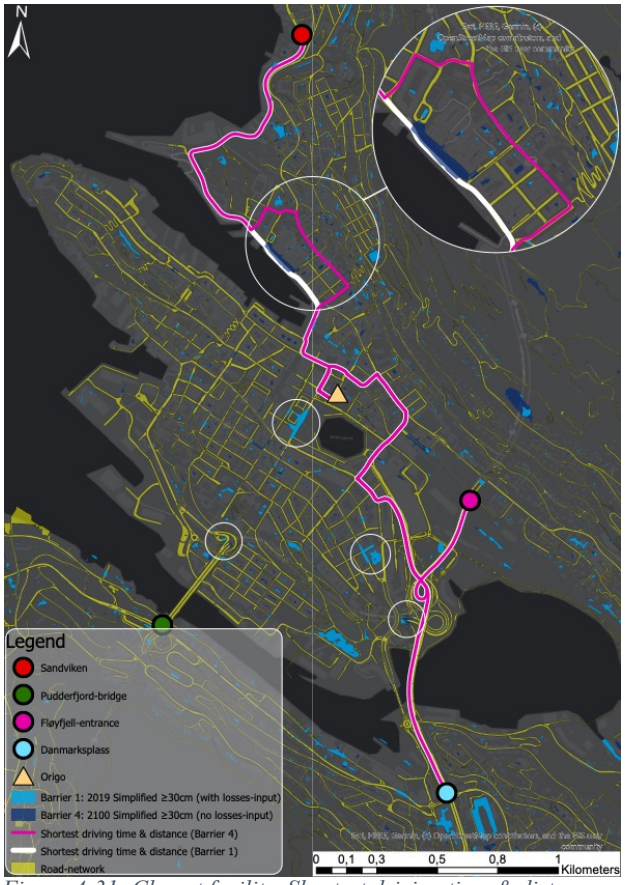

Figure 4-31: Closest facility. Shortest driving time & distance combined using barrier 1, and shortest driving time & distance using barrier 2, 3 and 4 (illustrated here by barrier 4)

Table 4-5: Closest facility analyses with routes (origin-destination), driving time in minutes and driving distance in km

Closest Facility analyses (included what barriers used)	*Origin - Destination*	*Driving time (minutes)*	*Driving distance (km)*
Shortest driving distance (No barrier)	Origo - Sandviken	5,54	2,28
Shortest driving time (No barrier)	Origo - Sandviken	5,21	2,33
Shortest driving time & distance (Barrier 1)	Origo - Sandviken	5,21	2,33
Shortest driving time & distance (Barrier 2-4)	Origo - Sandviken	6,79	2,72
Shortest driving distance (No barrier)	Origo - Pudderfjord-bridge	6,96	2,54
Shortest driving time (No barrier)	Origo - Pudderfjord-bridge	6,18	3,14
Shortest driving distance (No barrier)	Origo - Fløyfjell-entrance	5,31	2,24
Shortest driving time (No barrier)	Origo - Fløyfjell-entrance	5,31	2,24
Shortest driving time & distance (Barrier 1)	Origo - Fløyfjell-entrance	5,31	2,24
Shortest driving time & distance (Barrier 2-4)	Origo - Fløyfjell-entrance	5,31	2,24
Shortest driving distance (No barrier)	Origo - Danmarksplass	7,74	2,52
Shortest driving time (No barrier)	Origo - Danmarksplass	5,78	2,61
Shortest driving time & distance (Barrier 1)	Origo - Danmarksplass	5,78	2,61
Shortest driving time & distance (Barrier 2-4)	Origo - Danmarksplass	5,78	2,61

4.2.4 Fastest routes from one outskirt to another with increasing flood-levels

In this analysis the aim was to calculate the fastest routes between stops from one end to the other in the urban landscape of the AOI (as indicated by the shared colors of the various points in figure 4-32) using driving time as mode. The results had some similarities with the previous section seeing that it too only gave different route-outputs for the default mode of route 1 (having no barrier), route 2 (using barrier 1), while the rest of the routes using barrier 2, 3 and 4 were alike and thus assembled into the layer called route 3-5 (visualized by barrier 4).

Table 4-6 show the statistical outputs while figure 4-32 display the different paths taken for these three routes where the white circles illustrates some of the areas where the flood-barriers hindered the routes from taking the fastest paths in terms of time.

The figure display that the route from Nordnes to the Pudderfjord-bridge was hindered by all of the barriers to create an efficient route for all but Route 1 (having no barrier) seeing that it was not obstructed by any flood. As expected, table 4-6 show that route 1 (no barrier) is shortest both in terms of time and distance while route 3-5 (barrier 4) comes last, closely followed by route 2 (barrier 1) due to smaller reroutes as seen in the figure.

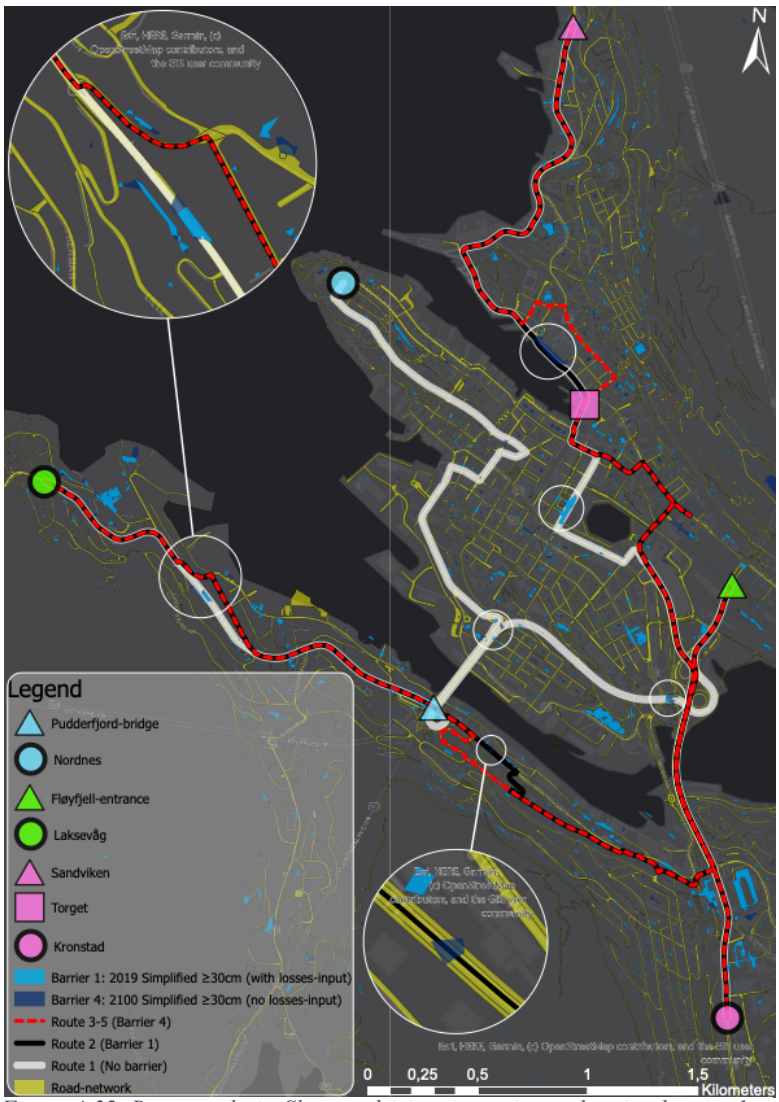

Figure 4-32: Route analysis. Shortest driving time using no barrier, barrier 1, and barrier 2, 3 and 4 (illustrated here by barrier 4)

Table 4-6: Route analyses with routes (origin-destination), driving time in minutes and distance in km

Route analyses (included what barrier used)	*Origin - Destination*	*Driving time (minutes)*	*Driving distance (km)*
Route 1 (No barrier)	Nordnes - Pudderfjord-bridge	6,73	3,02
Route 1 (No barrier)	Laksevåg - Fløyfjell-entrance	6,83	4,68
Route 2 (Barrier 1)	Laksevåg - Fløyfjell-entrance	11,81	5,45
Route 3-5 (Barrier 2-4)	Laksevåg - Fløyfjell-entrance	11,92	5,58
Route 1 (No barrier)	Kronstad - Torget - Sandviken	10,85	5,69
Route 2 (Barrier 1)	Kronstad - Torget - Sandviken	11,40	5,82
Route 3-5 (Barrier 2-4)	Kronstad - Torget - Sandviken	12,98	6,21

5. Discussion

The main focus of this thesis has been to present a method of modelling a historical urban flood-event occurring in Bergen the 14th. September 2019 and thereafter compare the flood-impacts to aggregated precipitation estimates of the same event that could take place by the end of the century. The purpose has been to identify the distribution and depth of the surface-water, and thereafter identify vulnerable road network segments that are prone to flooding and evaluate how the mobility is affected.

This chapter will hence address and discuss the results and the limitations and uncertainties that could have affected the results by answering the research questions in sections 5.1 – 5.3.

5.1 *How well can a major flood event be replicated using hydrological modelling based on high-resolution LIDAR data?*

5.1.1 Representation of a coupled surface flood and drainage model

Itzï is a hydraulic and hydrological too integrated with GRASS with the objective of modelling the processes of urban flood using a two-dimensional numerical overland flow method (Courty, Acuna and Bates, 2017). This method was evaluated and deemed suitable for modelling urban floods as explained in chapter 2. Furthermore, the method (2D) is more suitable for a detailed urban scale contrary to using a one-dimensional method as defined by Abede and Bulti (2020). However, to attain an even more accurate modelling, it should also include the minor drainage system (manholes, inlets etc.). This has in a later version been implemented to Itzï by coupling it to SWMM (Courty, 2018) which, by applying SWMM and thus becoming a 1D-2D model, would categorize Itzï as the most accurate method of urban flood GIS-modelling (Abede and Bulti, 2020).

This coupling was howbeit unsuccessfully implemented in this project (section 3.2.1.5) first and foremost due to the poor and general quality of the outputs that were meant to represent the infiltration-data (as "continuing losses" defined in section 2.2.1, - evapotranspiration can however not be represented in Itzï). Another approach to represent the infiltration was therefore needed. The utilization of the coupling with SWMM was also forfeited due to a limited time for the technical implementation, the large size of the AOI, the acquirement of large amounts of data, the editing of the input data to SWMM, and since both of these drainage-processes

would nevertheless be represented by the dataset called losses. This however affected the accuracy of the model in multiple ways:

- First of all, the method was no longer using the highest accuracy method of the 1D (drainage model) – 2D (surface flood model) – approach, but rather a 2D (surface flood model) approach with a user-defined value for the amount of water to be remover via the losses-dataset (sewers and infiltration). As a consequence, the dynamics of the coupled model is non-existent.
- Secondly, the theoretical values to represent the losses-dataset are derived from lower rainfall areas in the UK, which is not necessarily applicable for Bergen. These were used because no other sources of such data were located. The city with the highest amount of precipitation annually in the UK is Cardiff, being at respectively 1152mm in average (Lock, 2019). Bergen however has annually 2500mm of precipitation in average, far surpassing Cardiff. Also, the geology and topography of Norway and the UK have their own characteristics in each country (Arwyn et al, 2012 & Mapscaping, 2018).
- Third and last, the flood-results outputted from Itzï showed multiple areas that were inundated above 30cm, and the losses-dataset is a uniform map with drainage-values for the rural and urban areas. Consequently, some of these locally inundated areas might in fact have a much larger drainage capacity system set in place to remove some of the surplus water, in which the losses-dataset would not account for.

The utilization of four different flood scenarios, two in 2019 with and without losses and two in 2100 with and without losses were meant to illustrate how the impacts from the precipitation varies whether there is or is not a source of drainage and infiltration. These four scenarios are further addressed in the remaining of this chapter.

5.1.2 Possibilities of SWMM and other implementations to enhance the results

Had SWMM been fully implemented, it would have been possible to represent green infrastructure in the model (e.g. vegetation on rooftops that could store some of the water from the precipitation) in order to lower the intensity of the runoff-water in the urban areas. This could have the benefit of reducing the extent of the flood. Also, despite a full implementation of SWMM, there can be malfunctions in the drainage system which would be realistic to present such as inlets or manholes being clogging up by leaves. Furthermore, modelling seasonal

impacts such as snow smelting in the spring (which is a typical feature in Norway) would deem the results more realistic.

5.1.3 Numerical instabilities and deficiencies of outlets

One major implication that arose during the modelling in Itzï was large numbers of numerical instabilities/errors. These were visible in the early stages of the outputted maps from Itzï by showing an abundance of areas exceeding 1 meter in water-depth and surge-like waves that flowed down the mountainside into the waterbodies. How it was concluded as numerical errors was due to high numbers in the created volume and %error – columns in the statistical file. One of the early outputs can be seen in figures 5-1 (water-depth) and 5-2 (velocity) where the surge-like waves are highlighted by red circles.

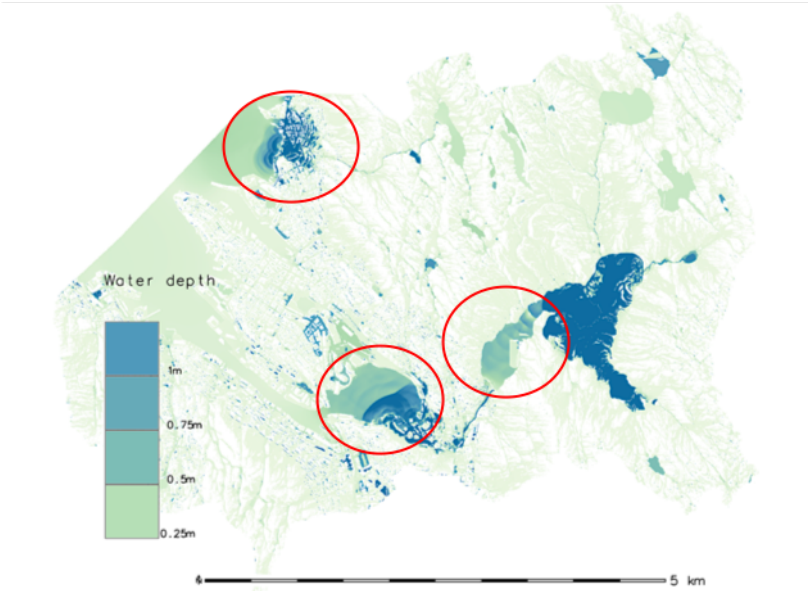

Figure 5-1: Early phase Itzï-output (water depth) from 5th hour in 2019, containing high domain volume and numerical instabilities as illustrated in red circles.

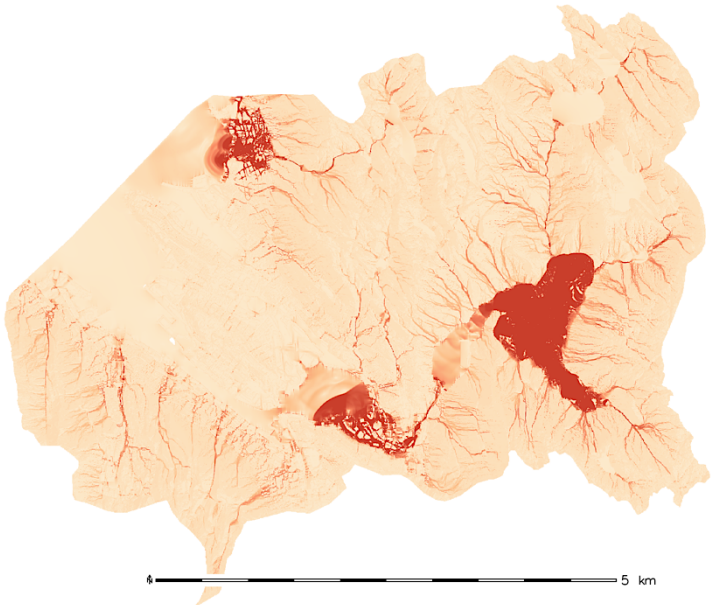

Figure 5-2: Early phase Itzï-output (magnitude of velocity) from 5th hour in 2019, containing high domain volume and numerical instabilities.

The abundance of areas exceeding 1 meter in water depth appeared to be a result of deficiencies of outlets in the analysis, which was later on resolved by adding more lakes to the outlet-dataset (section 3.2.1.2) and removing these same lakes from the DTM (section 3.2.1.3.3).

The wave-like surface flows on the other hand were a result of high numbers of created volume and %error (which is errors that appear by unstable calculations on the cell level when running the model). There are two ways of trying to control these numerical instabilities in the parameters-file; the first is to reduce the time-step by altering the values of "cfl" and "dtmax," and the other option is to alter the value in "theta" (Source 20). Hence, a total of 28 tests were run where the three options were continuously altered until a prominent result with the least amount of numerical errors as possible was given, using the following parameters: : theta – 0.7, cfl – 0.45 and dtmax – 3.5. Seeing that these values had to be altered from the default in order to output the final flood-maps, it might also have had an effect on the accuracy of the results.

5.1.4 Instability from 1st modelled hour of each flood-scenario

One more possible limitation from the Itzï processing were the first hour (at 16:00) simulated for all of the four timeseries (section 4.1.3). Here one can see an abnormal high number in almost every column, and especially high in the created volume and % error – columns. This occurs because the processing of the hour prior to this (at 15:00) starts at 0 in every column. However, by studying figure 3-1 (section 3.1.1.1) this is not representative of the actual event since it did have water in the domain in the prior hours. The high amount of precipitation

occurring in the intersection between these two hours seem to have a large effect on Itzï's capability to process it, creating unstable results for the first hour. Nevertheless, since the presented results were not from the first hour, and all of the following hours that were modelled were close to 0 in the abovementioned two columns, these should be much more stable.

5.1.5 Maximum water-depth instability

A last notion of the accuracy of the model affected by the numerical instabilities involves the outputted water-depth maps (section 4.1.1). As the figures 4-1 – 4-8 showed, the maximum water depths calculated in each output were at approximately 10 meters. Luckily, areas having this level of water-depth were greatly limited seeing that it is a very unrealistic result. A possible reason as to why such a high number was outputted can be due to smaller amount of numerical errors, but it can also be due to e.g. areas of high depression where the water could accumulate.

5.1.6 Strength and weaknesses of DTM

Another possible factor that could have affected the replication of the flood event is the data that was and was not added to the DTM (section 3.2.1.3.2). As known, all of the building was added to the DTM with a height of 10 meters in order to prevent the water flowing through, but rather around these areas (since the buildings are large physical objects capable of blocking the flow-path). Although this would provide a more accurate representation of how the water navigates through the urban environment, there are still other features capable of affecting the route of the surface water that were not included in the DTM. Examples of these are larger vegetation and temporary (or permanent if recent enough) installments that were not present at the time when the LIDAR-data was recorded. In addition, an even higher resolution of the DTM would provide more detailed outputs, but this would be at the expense of the computational time. In the early stages of the modelling it was attempted to run Itzï using a DTM of 1m resolution, but, seeing that the run-time was estimated to be 500 days, the 3m DTM was used instead. This latter approach had a run time of approximately 4-6 hours to output each timeseries of flood-results.

5.1.7 Uniform precipitation data

The utilization of the precipitation-data is another factor that had consequences to the accuracy of the results (sections 3.2.1.6 & 3.2.2.3). The total amount of rain per hour modelled was derived from the only rain gauge within the AOI (Florida rain-gauge). Consequently, the model does not take into account the spatially distributed precipitation that may differentiate locally

throughout the AOI, but rather uses a uniform, standard value for each passing hour that is sampled from one unique location.

5.1.8 Validation of flood-results

Having accounted for the major factors that could affect the accuracy of the modelled flood event that occurred in Bergen the 14.09.19, there were unfortunately no available records (per the authors knowledge) that could be used to validate the flood-results. However, the runoff water from Bergen Municipality correlates to a great extent to the velocity's direction as seen in figure 4-13 (section 4.1.2). This indicates that even though the water-height could have been even more accurate if some of the abovementioned factors were resolved, the flow and distribution of the water appears to be very accurate.

5.2 *What are the potential impacts of a flood based on end of century precipitation estimates?*

5.2.1 Aggregation of precipitation

To start at the beginning, it was estimated that the selected 6 hours of precipitation data with a total amount of 58,3mm rain from the historical flood-event of 14.09.19 were within the threshold of a 5-year return period based on the IDF-values for the Florida rain-gauge (section 3.1.1). Furthermore, it was "roughly" estimated that the amount of rain from this short-term heavy precipitation event could represent the same scenario by the end of the century (when it is expected far worse events of precipitation) by adding a linear increase of 30% to the number of 58,3mm. It is however acknowledged that this way of representing the futuristic increase of rainfall is merely a simplification and was only done to get a first estimate of the end of century precipitation. Furthermore, a linear increase to represent the amount of rain in the future is also rather questionable, but it is the most up-to-date and local source of prediction that were available.

Thus, already here it is established that the end of century, short term precipitation will amount to a 30% increase in Bergen, which by definition is one potential impact. This precipitation will also have major impacts on the surface of Bergen, which will be addressed below.

5.2.2 Identifying areas susceptible to flood

By comparing the two flood results from 2019 (with and without losses) in figures 4-1, 4-2, and 4-5, 4-6, to the two flood result from 2100 (with and without losses) in figures 4-3, 4-4 and 4-7, 4-8, it is possible to distinguish some more general areas that becomes more flooded in 2100 (section 4.1.1). One example is in the highlighted circle where several areas gradually turns into darker colors, indicating a higher water-depth. However, as these maps may be suited as overview maps showing a broad assessment of the distribution and water depth of the outputs, is harder to interpret the more detailed layout of the flood from these maps. One reason to this is due to the small scale of the map, while another reason is due to the large range of the water-depths (as explained above).

Subsequently, this latter obstacle was solved by further classifying the results, setting the threshold to ≥ 30cm which represented an extensive surface flood that is capable of acting as a barrier to a cars movement (section 4.1.4). By examining the maps in figures 4-22 – 4-23 (original polygons) and 4-24 (simplified polygons), containing these new, classified flood extents (with and without losses), the impacts of a flood occurring in Bergen in 2100 contrary to 2019 are much more evident here. The red and blue colors represent tentatively the 2019 with losses, and the 2019 with no losses – results, while the yellow and green colors represents the 2100 with losses and 2100 with no losses – results. The areas of the green polygons does not have any of the yellow, blue or red polygons underneath, indicating that these floods are only occurring when there is no drainage capacity and by using the precipitation estimates of the end of the century. Similarly, the yellow polygons (using the precipitation levels for 2100 and also accounts for drainage) represents areas of flood that are not reached by any of the two 2019-polygons, but the green polygons (since it is higher up in the hierarchy) is present underneath.

5.2.2.1 Four large flood-areas in proximity to the city-centre to occur in 2100

Hence, by referring to the larger scaled map in figure 4-24, the larger impacts of the flood occurring in 2100 that are bypassing the impacts of the historic event of 2019 are represented by the yellow and green colors. There are still a multiple of smaller inundated areas that are hard to identify. Nevertheless, two larger and distinctive flood-polygons representing the 2100 with losses flood (yellow) can be observed on the mountainside at the right side of the map (Mountain of Fløyen), while two smaller polygons (but yet of a significant size) representing the 2100 flood with no losses (green) can be detected in the urban area on the western and eastern side of Lille Lungegårdsvann. These are all areas to be cautious of in the future. A final

notion is to remember that these new areas representing the magnitude of the 2100-flood does also contains the flooded areas from the 2019-flood.

5.2.3 Relocation of flood in end of century scenario

To round of this section, table 4-3 showed the amount of flood that occurred nearby buildings from all the above-mentioned flood-polygons (section 4.2.1). An interesting result observed here was that even though the total area of flood nearby buildings increased exponentially by the higher ordered flood-polygons (2019 to 2100 flood), there were indications to a negative trend when the flood nearby buildings was compared to the total amount of total flood (the original and simplified flood-polygons gave slightly varying results). This indicates that even though the flood is expected to increase in the future by adding a linear increase of 30% to the amount of short-term precipitation observed at present day, the increase of flood nearby buildings (buildings that existed in 2019) compared to the total flood is much more limited, almost decreasing. Some of the same trends, albeit to a less extent can be seen in table 4-2 where the amount of flood occurring on the road-network was examined. A possible explanation to this phenomenon may be that the depressed areas on the roads and areas nearby buildings where the flood can culminate are already inundated, forcing the water to flow elsewhere.

Another interesting finding from these two tables was that much of the flood distributed throughout the AOI actually seems to be concentrated on the road network and around the buildings. This was proved by first establishing that the area of the road-network covers 3,86% of the AOI. Secondly, between 7,45-11,5% of the total area of the flood-polygons were found to be located on the road network. The same trends were also observed for the flood around the buildings. At first though this should be treated as a critical risk that could bring forth large economic impacts to the infrastructure in Bergen. However, per the explanation further up stating that the futuristic flood does not seem to accumulate at the same level in these same areas, it indicates that the expected high risk-level of high economic costs can be lowered.

5.2.3.1 Limitation of impact analyses

There was however one major limitation from this abovementioned analysis that hindered the measuring of more nuanced impacts. This was the impossibility by the use of the summarize within tool (used to measure flood-impact on road-network) and the summarize nearby tool (used to measure flood-impact nearby buildings) in ArcGIS to pinpoint critical infrastructures

(or other interesting features) that was flooded because the results were outputted as total area in the format of statistics, not as a visual map.

5.3 *Which parts of the Bergen road network are most vulnerable to flooding; and what are the implications for the whole road network?*

Having applied the three different network tools of service area analysis (section 4.2.2), closest facility analysis (section 4.2.3) and route analysis (section 4.2.4) to measure the vulnerability of the road-network to flood, the identified road-segments prone to flood and its significance for the car's mobility in Bergen will subsequently be presented and discussed here.

5.3.1 Reduced mobility in the neighborhoods of Møhlenpris and Sydnes

First and foremost, the service area analysis showed how the potential mobility is with no flood, which was calculated within a distance of 2km from the city hall in Bergen (origo) and with a speed limit of 60km/h. One of the first and largest areas that becomes blocked due flood (by any of the flood-barriers) is the entire neighborhood of Møhlenpris (the area stretching from the right side of the Pudderfjord-bridge and all the way to the bridge on the bottom-right side of the maps) as seen in figures 4-26 – 4-29. Furthermore, on the upper-left side of the Pudderfjord-bridge, another area called Sydnes also becomes gradually boxed in as the different flood-barriers are applied. One difference here is that the first example of Møhlenpris became cut off already by the first flood-barrier of 2019 (with losses), the latter example of Sydnes were actually partly open when the 2019 (with losses) barrier was applied, while the three remaining barriers had more or less a larger and similar impact. Therefore, in theory, when the actual urban flood-event occurred the 14th. September 2019 in Bergen, the roads leading into Sydnes should have been more accessible by car than the roads leading into Møhlenpris as long as the drainage still functioned.

5.3.2 Bryggen: A world cultural heritage area prone to be flooded

One large flood-barrier that kept affecting all of the analyses was the one located on Bryggen (highlighted in the zoomed inn circle). While the first flood-barrier (2019 with losses) was not affecting this area, all of the remaining three flood-barriers did, however. The appearance of surface-water here is critical by several reasons. First of all, this is a major trafficked road, leading vehicles in and out of Bergen northwards, and affecting especially many of the

commuters that are travelling by bus. Secondly, Bryggen, with its characteristic wooden houses is on the UNESCO list (United Nations Educational, Scientific and Cultural Organization) for World Cultural Heritage due to its importance for the trading empire of the Hanseatic League during the 14th to the 16th century (UNESCO, n.d.). Third, as seen in the results from the two other analyses (figures 4-30 – 4-32), when the flood appears on Bryggen, the routes are redirected onto a smaller road on the upside instead. This affect both the cost of time and distance, but also stretches the capacity of the alternative road since it is much narrower and its surface is overlaid by bricks, not asphalt. And fourth but not least, the new route of the local light rail train in Bergen (Bybanen) is planned to be developed over Bryggen going northwards (Miljøløftet, n.d.).

Hence, all of these abovementioned factors act as justifications as to why the flood over Bryggen is perhaps one of the more critical areas of the road network that are prone to flooding.

5.3.3 Blockade of major trafficked roads

By adhering to the figures 4-30 – 4.32 again, other considerable flood-barriers that blocked the major trafficked roads and thus deeming these areas especially vulnerable were all of the floods encapsulated by the white circles. These flood-barriers also illustrate the implications for the whole road network since they are, in best case, rerouting the traffic to smaller roads which is longer both in terms of distance and time. Worst case scenario, as seen by the Origo – Pudderfjord-bridge route in figures 4-30 and 4-31, and the Nordnes – Pudderfjord-bridge route in figure 4-32, there are no other alternative routes to take due to the layout of the road-network and the distribution of the flood-barriers.

5.3.4 Cross-examination of identified vulnerable areas

Furthermore, by comparing these abovementioned results to figure 4-25 where the 2100 (no losses) flood-results with a water depth of ≥ 10cm was validated against the identified flood-zones by NVE and Bergen Municipality, one can see that especially the areas around and below (south of) Lille Lungegårdsvann, but also Møhlenpris are matching areas defined as susceptible to flood (section 4.1.4.3). However, taking the vulnerability of the road network into account, and by applying the water depth threshold of ≥ 30cm instead of the ≥ 10cm threshold, it is mostly the area on the upper side of Lille Lungegårdsvann and Møhlenpris where the roads are affected by flood.

5.3.4.1 Limitation of cross-examination

However, as explained in the theory chapter, the NVE-flood map does not take urban flood into account, but rather fluvial floods (rivers), flash floods (flood-streams outside of the river networks) and storm surges. It is also produced on a national scale where the DTM had a resolution of 25x25. Also, the regulated flood-zones from Bergen Municipality is only a minor excerpt from various regulated zoning plans in Bergen, deeming it more generalized. This suggest that the outputs from Itzï are more suited for representing the actual urban floods in Bergen since it can provide more detailed and extensive flood-information on a street level resolution.

5.3.5 Limitations and assumptions of road network analyses

Finally, as with the Itzï model, there are also limitations and uncertainties to the network-analysis result. First of all, the speed limit of 60km/h may have slowed down and therefore altered some of the routes that were supposed to find the quickest way from A to B. However, seeing that most of the routes were modelled within the dense and urbanized area of Bergen, the speed limits here are in fact mainly at or below 60km/h.

Furthermore, since the utilized road network dataset was provided from the network analysis tool in ArcGIS, it is first of all unknown if it followed all the local speed limits. Secondly, it is also unsure if all the routes taken are actually drivable. By studying the routes more in detail, there was one segment that appeared to be plotted wrong. In figure 4-30 the "shortest driving distance (no barrier)" route in blue going from Origo to the Pudderfjord-bride, is actually taking a small detour close to the Origo onto the pedestrian zone of Torgalmenningen.

In addition, the street network has shown to take narrow and erratic shortcuts, one of which was identified in figure 4-30 by the same blue route as above. At the northern end towards Sandviken it took a path that navigated through multiple turns, and it is, by the authors own experience, not a road suited for heavy traffic.

Another limitation regards the appliance of the flood-barriers. While some of these were of a great magnitude, such as the one on Bryggen, others were in fact of a very small size. This was not represented in the model, resulting in blocked roads whether the flood-polygon had a size of 1^{m2} or 10^{m2}. It is safe to say that the cars would have been able to bypass the former size.

Lastly, by looking more in detail at the entrance of the Fløyfjell-entrance in the figures, there is a flood-polygon present there. This was deliberately not accounted for in the network-

analyses since when the flood was modelled in Itzï, it was not specified that this depression right in front of the tunnel was actually leading straight into an opening in the mountain.

6. Conclusion

This thesis can be divided into two different sections. The first part aimed at implementing the new hydraulic and hydrological GIS-tool of Itzï which is integrated with the GIS-software GRASS and utilize this to replicate an urban flood event with precipitation levels of a 5-year return period over 6 hours that occurred in Bergen the 14th. September of 2019. Furthermore, another important task was to establish the estimates of a similar scenario that used projections of precipitation expected by of the end of the century and hence measure the increase of the flood extent between these two events. These two scenarios were consequently modelled both with and without any drainage and infiltration in order to evaluate the value of having a fully operational drainage system and unsaturated soils prior to and during extreme precipitation events.

One of the major limitations of these processes was the unsuccessful incorporating of a fully integrated one-dimensional drainage model and two-dimensional surface-flood model. This was due to the unsatisfactory output of the infiltration-dataset and not being able to utilize the drainage model of SWMM (Storm Water Management Model) because of the limited time of implementing and understanding the technical software. Instead, a theoretical solution of drainage was implemented where the values representing the losses-dataset was based on a study in the UK of the lower rainfall areas.

The results however were able to produce stable outputs of the extent of the floods for each scenario where a gradual increase of surface flood was experienced from the 2019 event with the losses data, to the 2019 event with no losses, and further to the 2100 event with losses data, culminating with the 2100 event with no losses data. Furthermore, one key finding was that the road network and areas around the buildings in Bergen received a large share of the total surface flood compared to the whole modelled area, but the increased amount of flood in these same areas by the end of the century had a much lower growth than the estimated 30% that was added to the amount of precipitation.

The second part of this thesis aimed at assessing how vulnerable the road network in Bergen is to the different scenarios of flood in order to understand how the level of mobility is affected. This was performed by utilizing three different network analyses where areas of flood at or above 30cm acted as barriers for the continued movement of vehicles, forcing them to take reroutes if possible. The results showed that many of the major roads leading in and out of Bergen were blocked by either the 2019 flood with losses-data, or the three remaining ones.

Thus, a distinction related to the impact on the road network could be made between these two groups of flood scenarios.
Furthermore, other important findings illustrated that the roads leading into the neighborhood of Møhlenpris were completely blocked by all the flood-scenarios, while the roads leading into another district called Sydnes became gradually more blocked as the different scenarios were compared, but still remaining fairly open by the 2019 flood included drainage and infiltration (using the losses data).
Perhaps the most vulnerable road prone to flooding was Bryggen in Bergen, which is in an area among other factors that is on the UNESCO list (United Nations Educational, Scientific and Cultural Organization) for World Cultural Heritage. In addition, it is a very trafficked road directed northward from Bergen city centre. Hence, even though there might be local drainage systems set in place that the theoretical losses dataset did not account for, the results showed that it was only during the 2019 flood when the losses-data was applied that the flood did not occur.

To conclude, this thesis has shown that the city-planners of Bergen should take areas such as Bryggen and Møhlenpris into account when planning for more intensified precipitation events in the future. Furthermore, the results presented here should not be interpreted as a blueprint as there are multiple limitations and uncertainties to the outputs, but rather serve as guidelines as to where one should be more cautious of flood, both today and in the future.

6.1 Further research

There are several different approaches which would advance the results from this thesis by creating more detailed and accurate outputs that informs of the urban flood and its vulnerability to the infrastructure in Bergen. Most of the limitations mentioned in the previous chapter is not included in this lineup. The suggestions are:

- A complete coupling of the SWMM and Itzï. This would also acquire another approach to represent the spatial variation of the infiltration-data than what has been attempted in this thesis. Furthermore, in GRASS it is possible to implement green infrastructure (i.e. vegetation on roofs etc. that can contribute to hold an amount of the precipitation so that the intensity of the surface flood is reduced), which would be interesting to observe the effects of.

- Identify the different categories of buildings and see how these are affected by the flood in order to assess the economic impacts. In addition, finding methods that can visually display the results would be more practical than merely statistical outputs.

- Include other types of commuters than motorists who uses the roads, such as bicyclists or pedestrians, and see how vulnerable these groups are to a flood event.

- Use a finer resolution of the DTM for higher accuracy of the distribution of flood.

- Include other types data to Itzï, such as spatially varied rainfall, porosity of soil or hydraulic conductivity of soil.

- Couple the urban surface flood model of Itzï to a river flood model.

- Couple the network analyses to annual average daily traffic data in order to see how much traffic has to be redirected due to blocked roads. This was intended to do in this thesis, but due to time constraints it was not implemented.

- Find high-resolution LiDAR-data of other areas in Norway and model the flood in order to evaluate and compare the results to the findings from this thesis.

- Last (and perhaps most difficult to accomplish) is to couple the data from the Norwegian Meteorological Institute (Yr) with Itzï to allow for short term flood modelling.

7. References

- Abede, B.G. and Bulti, D.T. (2020) A review of flood modeling methods for urban pluvial flood application, *Modelling Earth Systems and Environment.* DOI: 10.1007/s40808-020-00803-z

- Arcement, G.J. and Schneider, V.R. (1989) *Guide for selecting Manning's roughness coefficients for natural channels and flood plains.* 2339. Denver: USGS. DOI: 10.3133/wsp2339

- ArcGIS Pro (n.d. A) *Closest facility analysis layer.* Available from: <https://pro.arcgis.com/en/pro-app/help/analysis/networks/closest-facility-analysis-layer.htm> [Read 17. Desember. 2019].

- ArcGIS Pro (n.d. B) *Service area analysis layer.* Available from: <https://pro.arcgis.com/en/pro-app/help/analysis/networks/service-area-analysis-layer.htm> [Read 19. Desember. 2019].

- ArcGIS Pro (n.d. C) *Data classification methods.* Available from: <https://pro.arcgis.com/en/pro-app/help/mapping/layer-properties/data-classification-methods.htm> [Read 10. May. 2020].

- Arwyn, J. et al. (2012) *The state of soil in Europe: A contribution of the JRC to the European Environment Agency's Environment State and Outlook Report.* SOER 2010. Publications Office of the European Union. DOI: 10.2788/77361

- Ballas, D., Clarke, G., Franklin, R.S. and Newing, A. (2018) *GIS and the Social Sciences: Theory and Applications.* London, New York: Routledge

- Bergen Municipality (n.d.) *Kommunedelplan for Overvann* – Webapp. Available from: <https://kart.bergen.kommune.no/portal/apps/webappviewer/index.html?id=04ae4415f33c431e9810327c18a263a1> [Read 05. March. 2020].

- Bergen Municipality (2014) *Bergen ROS 2014: Overordnet risiko- og sårbarhetsanalyse for Bergen* [Internet]. Bergen: Bergen municipality. Available from: <https://www.bergen.kommune.no/omkommunen/avdelinger/seksjon-for-samfunnssikkerhet-og-beredskap/10471/article-126944> [Read 29. August. 2018].

- Bergen Municipality (2017) *Hvordan kan vi håndtere enda mer nedbør?* [Internet]. Bergen: Bergen municipality. Available from: <https://www.bergen.kommune.no/omkommunen/avdelinger/vannog-avlopsetaten/9330/9333/article-111420> [Read 27. November. 2018].

- Bergen Municipality (2019) *Kommunedelplan for Overvann 2019-2029.* Available from: <https://www.bergen.kommune.no/publisering/api/filer/T536941663> [Read 05. March. 2020].

- Bergen Municipality (2020) *Byparken.* Available from: <https://www.bergen.kommune.no/innbyggerhjelpen/natur-klima-miljo/natur/park/byparken> [Read 15. February. 2020].

- Brandon Mississippi (2018) *Stormwater*. Brandon. Available from: <https://www.brandonms.org/departments/public-works/stormwater/> [Read 27. November. 2018].

- Bulkeley, H. (2013) *Cities and Climate Change.* USA, Canada: Routledge.

- Chen, J., Hill, A.A. and Urbano, L,D. (2009) A GIS-based model for urban flood inundation, *Journal of Hydrology,* 373(1-2), pp. 184-192. DOI: 10.1016/j.jhydrol.2009.04.021

- Chow, V.T. (1959) *Open-Channel Hydraulics.* New York: McGraw-Hill.

- Courty, L.G. (2018) *Integrated modelling of overland flows and drainage networks in a urban environment.* Doctoral thesis. Mexico: National Autonomous University of Mexico. DOI: 10.31237/osf.io/38w4t

- Courty, L.G., Acuna, A.P. and Bates, P.B. (2017) Itzî (version 17.1): an open-source, distributed GIS model for dynamic flood simulation, *Geoscientific Model Development,* 10(4), pp. 1835-1847. DOI: 10.5194/gmd-10-1835-2017

- Culshaw, M. (2018) Geohazards, in *Encyclopedia of Engineering Geology*. Available from: <https://link.springer.com/referenceworkentry/10.1007/978-3-319-73568-9_134> [Read 25. May. 2020].

- Demuzere, M., Bhave, A.H., Faehnle, M., Feliu, E., Geneletti, D., Heidrich, O., Mittal, N., Olazabel, E., Orru, H. and Orru, K. (2014) Mitigating and adapting to climate change: Multi-functional and multi-scale assessment of green urban infrastructure. *Journal of Environmental Management* [Internet]. 146, pp. 107-115. DOI: <https://doi.org/10.1016/j.jenvman.2014.07.025> [Read 28. November. 2018].

- Derkzen, M.L., van Teeffelen, A.J.A. and Verburg, P.H. (2017) Green infrastructure for urban climate adaptation: How do residents' views on climate impacts and green infrastructure shape adaptation preferences? *Landscape and Urban Planning* [Internet]. 157, pp. 106-130. DOI: <https://doi.org/10.1016/j.landurbplan.2016.05.027> [Read 29. November. 2018].

- Djordjevic, S. (2010) Coupled models. In: Ashley, R., Cashman, A., Evelpidou, N., Garvin, S., Pasche, E. and Zevenbergen, C. (eds) *Urban Flood Management.* Florida: Taylor & Francis Group, pp. 115.

- Dyrrdal, A.V. and Førland, E.J. (2019) *Klimapåslag for kortidsnedbør – Anbefalte verdier for Norge.* 5/2019. NCCS.

- European Commission (2016) *Green Infrastructure* [Internet]. 12. September. European Commission. Available from: <http://ec.europa.eu2/environment/nature/ecosystems/index_en.htm> [Read 28. November. 2018].

- Fredriksen, I. & Oldeide, A.A. (2018) Jeg kan ikke hugse at det har vært så vilt, vått og ekstremt noen gang. *Bergens Tidende* [Internet]. 27. September. Available from:

<https://www.bt.no/nyheter/lokalt/i/zLJjGr/--Jeg-kan-ikke-huske-at-det-har-vart-sa-vilt_-vatt-og-ekstremt-noen-gang?spid_rel=2> [Read 27. November. 2018].

- Gill, S.E., Ennos, A.R., Handley, J.F. and Pauleit, S. (2007) Adapting Cities for Climate Change: The Role of the Green Infrastructure. *Built Environment* [Internet]. 33 (1), pp. 115-133. DOI: <https://doi.org/10.2148/benv.33.1.115> [Read 29. November. 2018].

- GRASS (n.d. A) *r.resamp.interp.* Available from: <https://grass.osgeo.org/grass76/manuals/r.resamp.interp.html> [Read 29. October. 2019].

- GRASS (n.d. B) *r.mask.* Available from: <https://grass.osgeo.org/grass76/manuals/r.mask.html> [Read 29. October. 2019].

- GRASS (n.d. C) *Temporal data processing in GRASS GIS.* Available from: <https://grass.osgeo.org/grass76/manuals/temporalintro.html> [Read 30. October. 2019].

- Hansen, E.E. (2018) Nedbørsrekord i Bergen i september. *Aftenposten* [Internet]. 29. September. Available from: <https://www.aftenposten.no/norge/i/rLR7el/Nedborsrekord-i-Bergen-i-september> [Read 27. November. 2018].

- Hordaland Fylkeskommune (2014) *Klimaplan for Hordaland 2014-2030, Regional klima- og energiplan* [Internet]. Bergen, Hordaland Fylkeskommune. Available from: <https://www.hordaland.no/globalassets/for-hfk/plan-og-planarbeid/regionale-planar/a4_klimaplan14-30_web-bokmerke-og-navigasjon.pdf> [Read 16. November. 2018].

- IPCC (2014) *Climate Change 2014: Synthesis Report. Contribution of Working Groups I, II and III to the Fifth Assessment Report of the Intergovernmental Panel on Climate Change* [Internett]. IPCC: Geneva, Switzerland, 151 pp. Available from: <http://www.ipcc.ch/report/ar5/syr/> [Read 28. August. 2018].

- Itzï (n.d. A) *Configuration file.* Available from: < https://itzi.readthedocs.io/en/latest/conf_file.html> [Read 28. March. 2019].

- Itzï (n.d. B) *Controlling numerical errors.* Available from: <https://itzi.readthedocs.io/en/latest/faq.html#controlling-numerical-instabilities> [Read 05 January. 2020].

- Johansen, E.N. & Krantz, A. (2018) Nedbørskaos på Vestlandet: Vi har ikke opplevd liknende. *NRK* [Internet]. 26. September. Available from: <https://www.nrk.no/hordaland/nedborskaos-pa-vestlandet_-_-vi-har-ikke-opplevd-lignende-1.14223142> [Read 28. November. 2018].

- Kulkarni, A.T., Eldho, T.I., Mohan, B.K., Mohanty, J. and Rao, E.P. (2014) A web GIS based integrated flood assessment modelling tool for coastal urban watersheds, *Computers & Geosciences,* 64 (march), pp. 7-14. DOI: 10.1016/j.cageo.2013.11.002

- Kundu S.N. (2017) Geohazard Modeling Using Remote Sensing and GIS. In: Sengupta D., Agrahari S. (eds) *Modelling Trends in Solid and Hazardous Waste Management.* Singapore: Springer, pp. 127-139.

- Liang, Q., Lin, L. and Wu, Z. (2019) Urban flood susceptibility analysis using a GIS-based multi-criteria analysis framework, *Natural Hazards,* 97, pp. 455-475. DOI: 10.1007/s11069-019-03615-2

- Lock, H. (2019) Where is the world's rainiest city, *The Guardian,* 07.June. Available from: < https://www.theguardian.com/cities/2019/jun/07/where-is-the-worlds-rainiest-city> [Read 09. June. 2020].

- Mapscaping (2018) *The topography of Europe.* Available from: <https://mapscaping.com/blogs/geo-candy/the-topography-of-europe> [Read 10. June. 2020].

- Meiforth, J.J. (2013) *Modelling flood streams for urban planning in Trondheim, Norway.* Professional project. Salzburg: UniGIS Professional University of Salzburg. Available from: < https://www.trondheim.kommune.no/globalassets/10-bilder-og-filer/10-byutvikling/kommunalteknikk/vann-og-avlop/meiforth2013_flood_streams_trondheim_v3.pdf> [Read 02. June. 2020].

- Miljøløftet (n.d.) *Bybanen til Åsane.* Available from: <https://xn--miljlftet-o8ab.no/prosjektliste/kollektiv/bybanen-til-asane/> [Read 12. June. 2020].

- NCCS (2015) *Klima I Norge 2100,* Kunnskapsgrunnlag for klimatilpasning oppdatert I 2015 [Internet]. NCCS report no. 2/2015. Available from: <https://cms.met.no/site/2/klimaservicesenteret/rapporter-og-publikasjoner/_attachment/6616?_ts=14ff3d4eeb8> [Read 15. November. 2018].

- Norsk Klimaservicesenter (n.d. A) *Nedbørintensitet.* Available from: <https://klimaservicesenter.no/faces/desktop/idf.xhtml> [Read 15. Desember. 2019].

- Norsk Klimaservicesenter (n.d. B) *Observasjoner og værstatistikk.* Available from: <https://klimaservicesenter.no/observations/> [Read 19. Desember. 2019].

- NVE (2011) *Preliminary flood risk assessment in Norway: An example of a methodology based on a GIS-approach.* 7/2011. Oslo: Norwegian Water Resources and Energy Directorate. Available from: <http://publikasjoner.nve.no/report/2011/report2011_07.pdf> [Read 02. June. 2020].

- NVE (2020) *Nedbørfelt (REGINE).* Available from: <https://www.nve.no/karttjenester/kartdata/vassdragsdata/nedborfelt-regine/> [Read 10. May. 2019].

- O'Brien K. and Selboe, E. (2015). Climate change as an Adaptive Challenge. In: O'Brien K. and Selboe, E. ed. *The Adaptive Challenge of Climate Change*. London: Cambridge, pp. 1-23.

- Opheim, T. (2019) Her fosser vannet ned trappene, *Bergens Tidende,* 14. September. Available from: <https://www.bt.no/nyheter/lokalt/i/GGKxy4/her-fosser-vannet-ned-trappene> [Read 18. September. 2019].

- Pelling, M. (2011) *Adaptation to Climate Change: From resilience to transformation.* USA, Canada: Routledge.

- Ramboll (2015) *Overvannsflom – metodar for kartlegging og analysar.* M-424/2015. Alta: Ramboll. Available from: <https://www.miljodirektoratet.no/globalassets/publikasjoner/M424/M424.pdf> [Read 03. June. 2020].

- Rawls, W.J., Brakensiek, D.L. and Miller, N. (1983) Green-ampt Infiltration Parameters from Soils Data, Journal of Hydraulic Engineering, 109(1), pp. 62-70. DOI: 10.1061/(ASCE)0733-9429(1983)109:1(62)

- Solgrids (n.d.) *Soilgrids.* Available from: <https://soilgrids.org/> [Read 01. October. 2019].

- Statistisk Sentralbyrå (2018) *Kommunefakta: Bergen* [Internet]. Available from: <https://www.ssb.no/kommunefakta/bergen> [Read 28. November. 2018].

- The Climate Workspace (n.d.) *IDF Curve.* Available from: <http://www.glisaclimate.org/node/2341> [Read 15. February. 2020].

- The Flood People (2018) *What makes good elevation data for national-scale flood mapping?* Available from: <https://www.jbarisk.com/news-blogs/what-makes-good-elevation-data-for-national-scale-flood-mapping/> [Read 15. January. 2020].

- UNESCO (n.d.) *Bryggen.* Available from: <https://whc.unesco.org/en/list/59/> [Read 12. June. 2018].

- USDA (n.d.) *Soil texture calculator.* Available from: <https://www.nrcs.usda.gov/wps/portal/nrcs/detail/soils/survey/?cid=nrcs142p2_054167> [Read 27. September. 2019].

- Varsom (n.d.) *Aktsomhetsnivåer for flom – og jordskredvarsling.* Available from: <https://www.varsom.no/flom-og-jordskredvarsling/aktsomhetsnivaer-for-flom-og-jordskredvarsling/?ref=mainmenu> [Read 27. March. 2020].

- Yin, J. et al. (2016) Evaluating the impact and risk of pluvial flash flood on intra-urban road network: A case study in the city center of Shanghai, China, Journal of Hydrology, 537, pp. 138-145. DOI: 10.1016/j.jhydrol.2016.03.037

8. Appendix

1. GRASS statements

a) g.region -p raster=DTM_Build_Nowater@PERMANENT res=3
save=DTM_NoWater3m

b) r.resamp.interp
input=DTM_Build_NoWater@PERMANENT output=DTM_NoWater_Resa
mp

c) r.mask --overwrite rast=DTM_NoWater_Resamp

d) v.to.rast input=Outlet_AllWater type=line
output=bctype_AllWater use=val value=4

e) v.to.rast input=Outlet_AllWater type=line
output=bcvalue_AllWater use=val value=0

f) t.create output=Regn2019(2100)_6h type=strds
temporaltype=absolute title="Rain at florida
14.09.19(2100) returnperiod 5Y" description="Uniform rain
in Bergen over 6 hours with return period of 5 years"

g) t.register -I input=Regn2019(2100)_6h type=raster
maps=(name of input maps in correct order)
start=2019(2100)-09-14 00:00:00 increment="1 hours"
separator=comma (create interval)

2-1. ITZÏ water-depth results with basemap (5th hour from each timeseries)

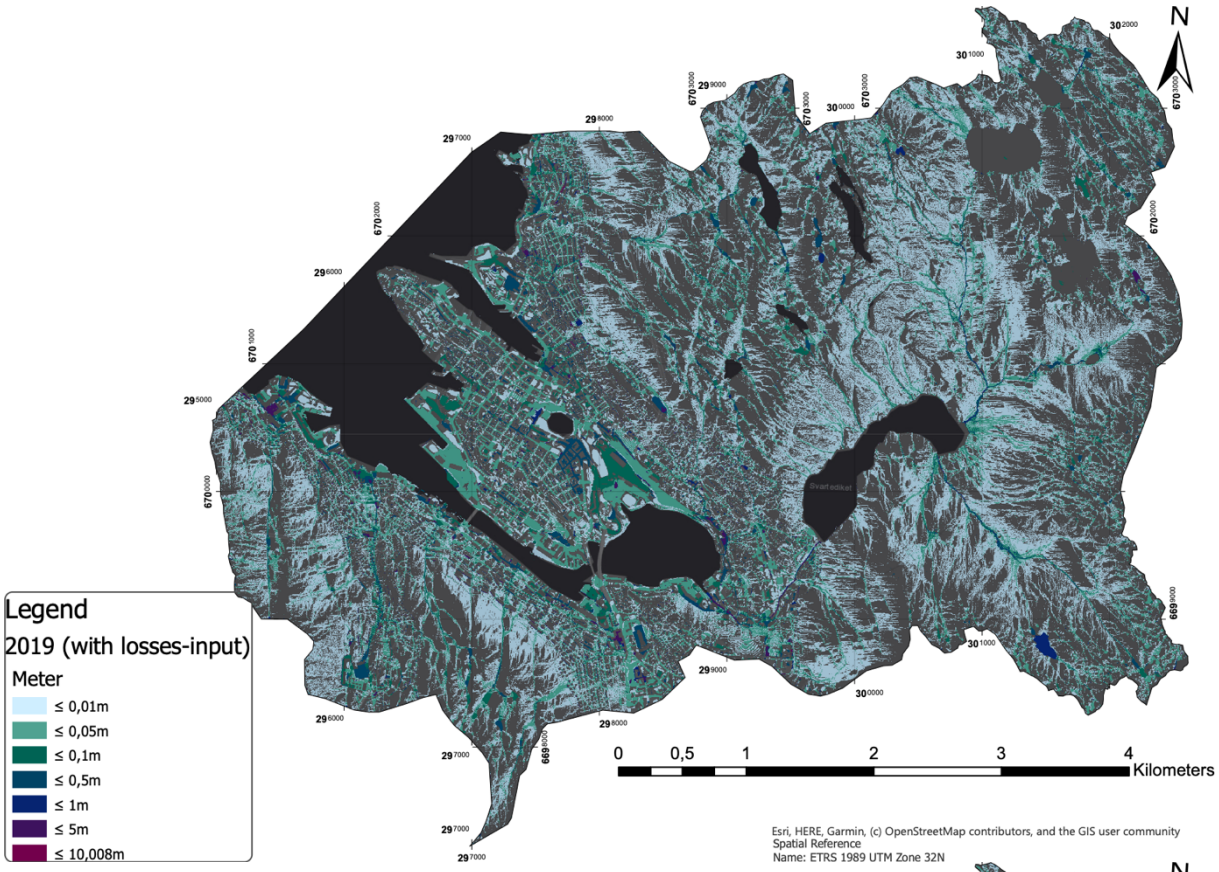

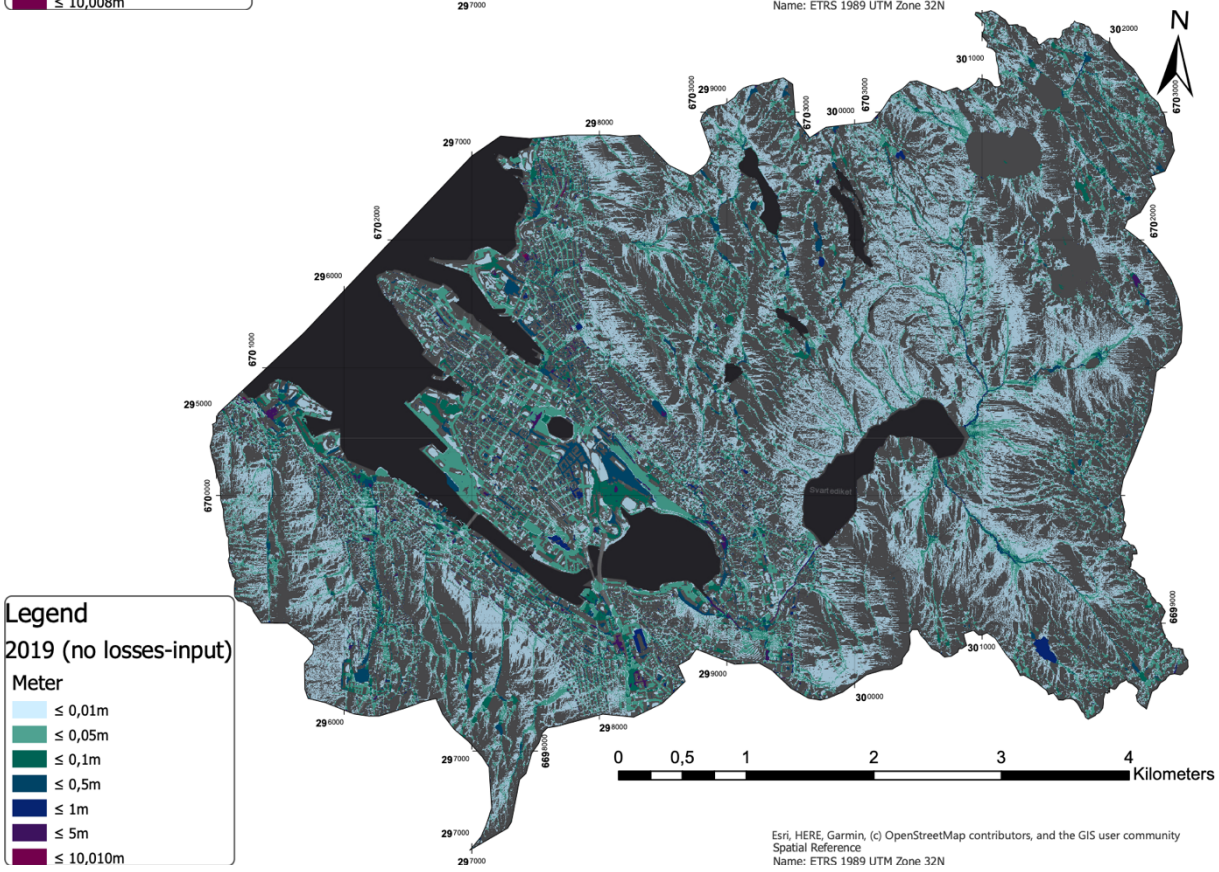

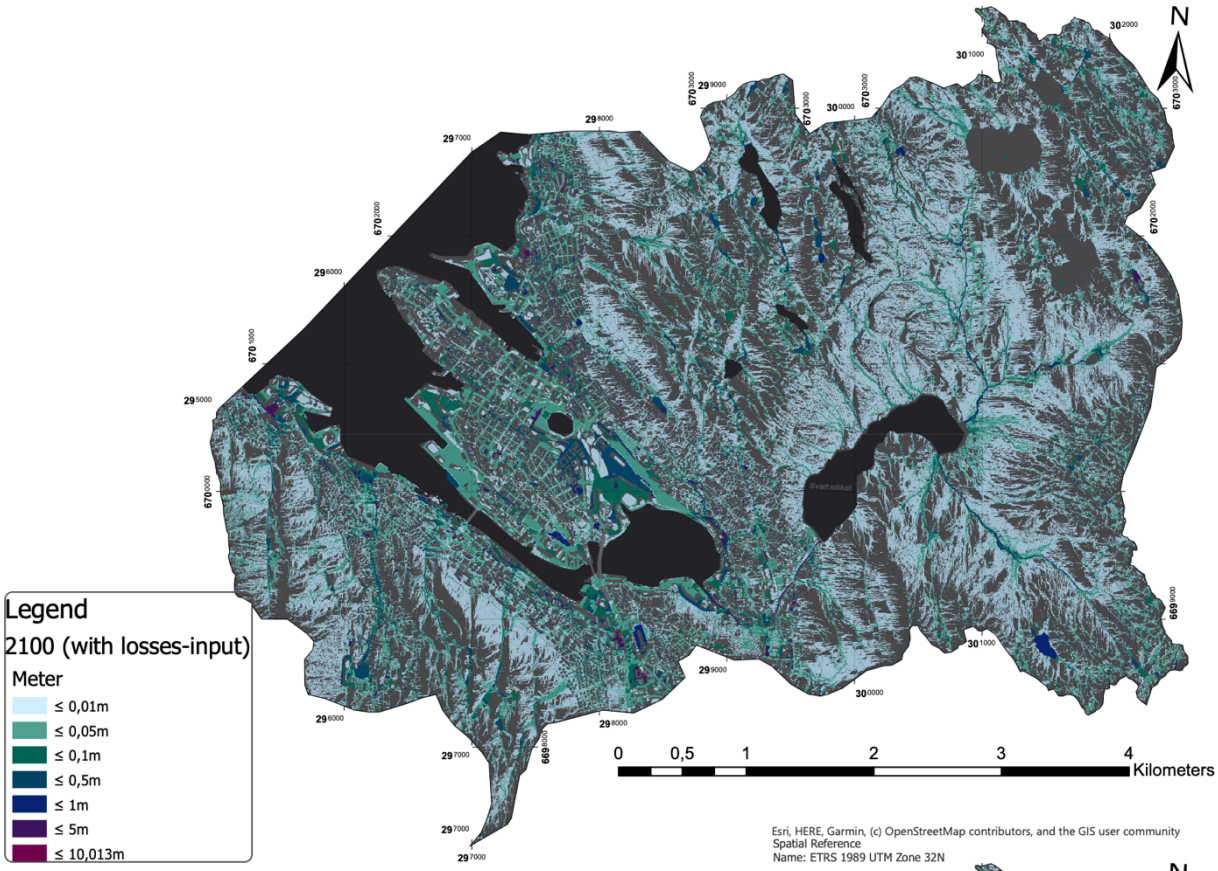
N
Legend
2100 (with losses-input)
Meter
≤ 0,01m
≤ 0,05m
≤ 0,1m
≤ 0,5m
≤ 1m
≤ 5m
≤ 10,013m
0 0,5 1 2 3 4
Kilometers
Esri, HERE, Garmin, (c) OpenStreetMap contributors, and the GIS user community
Spatial Reference
Name: ETRS 1989 UTM Zone 32N

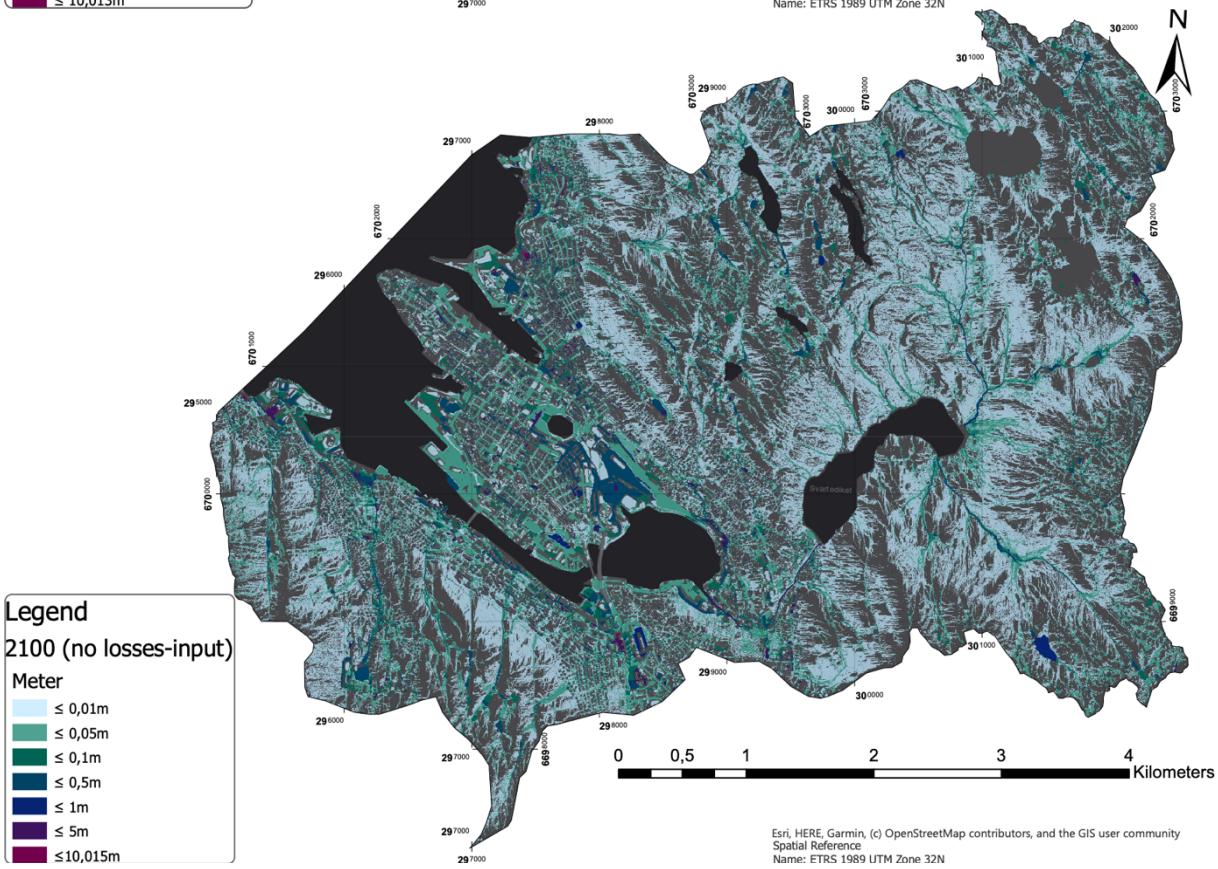
N
Legend
2100 (no losses-input)
Meter
≤ 0,01m
≤ 0,05m
≤ 0,1m
≤ 0,5m
≤ 1m
≤ 5m
≤10,015m
0 0,5 1 2 3 4
Kilometers
Esri, HERE, Garmin, (c) OpenStreetMap contributors, and the GIS user community
Spatial Reference
Name: ETRS 1989 UTM Zone 32N

2-2. Itzï water-depth results without basemap (5th hour from each timeseries)

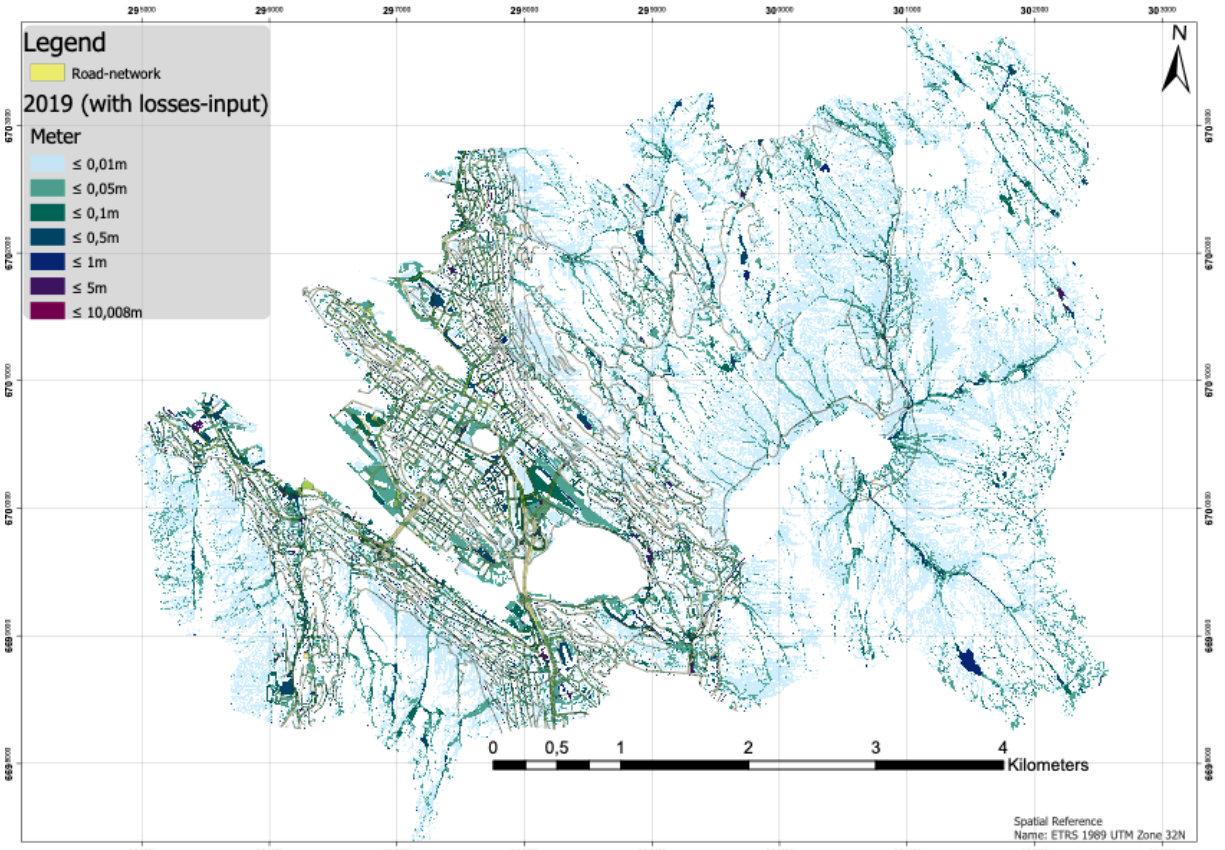

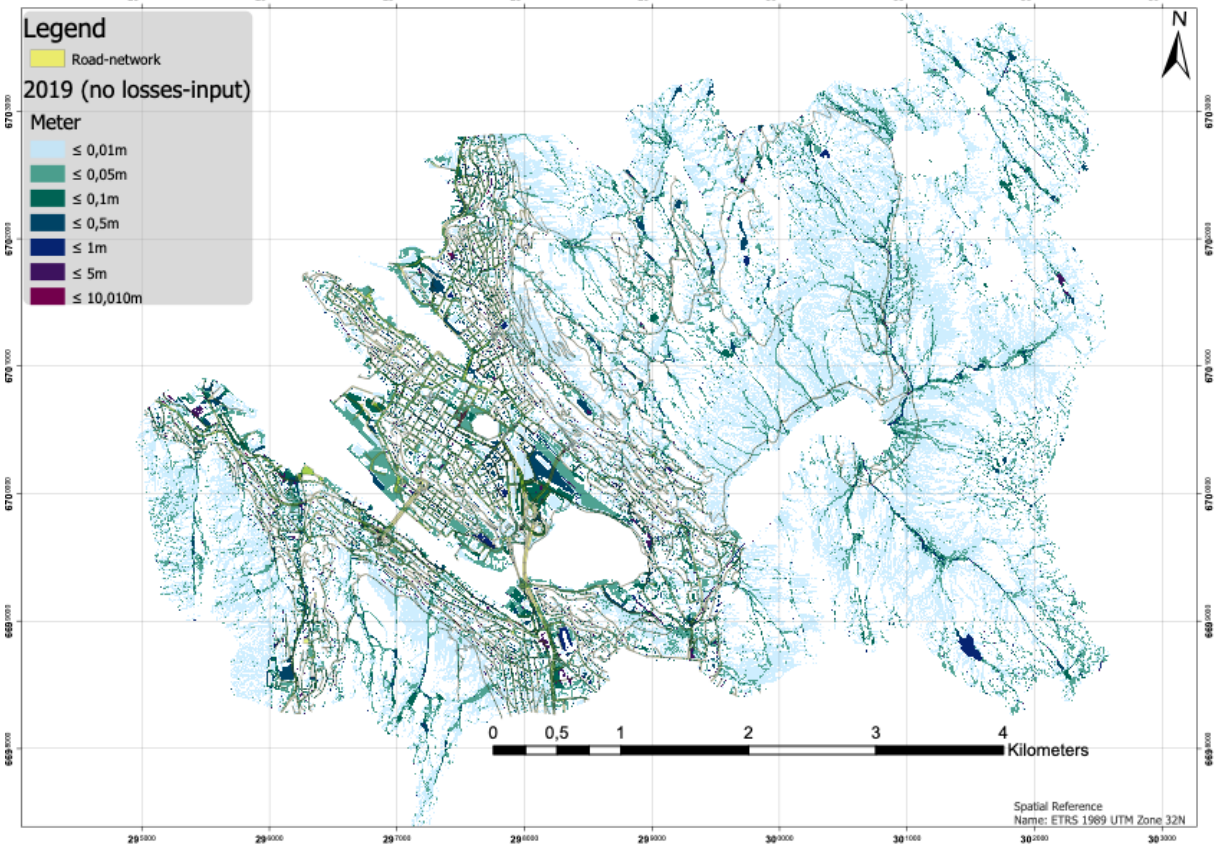

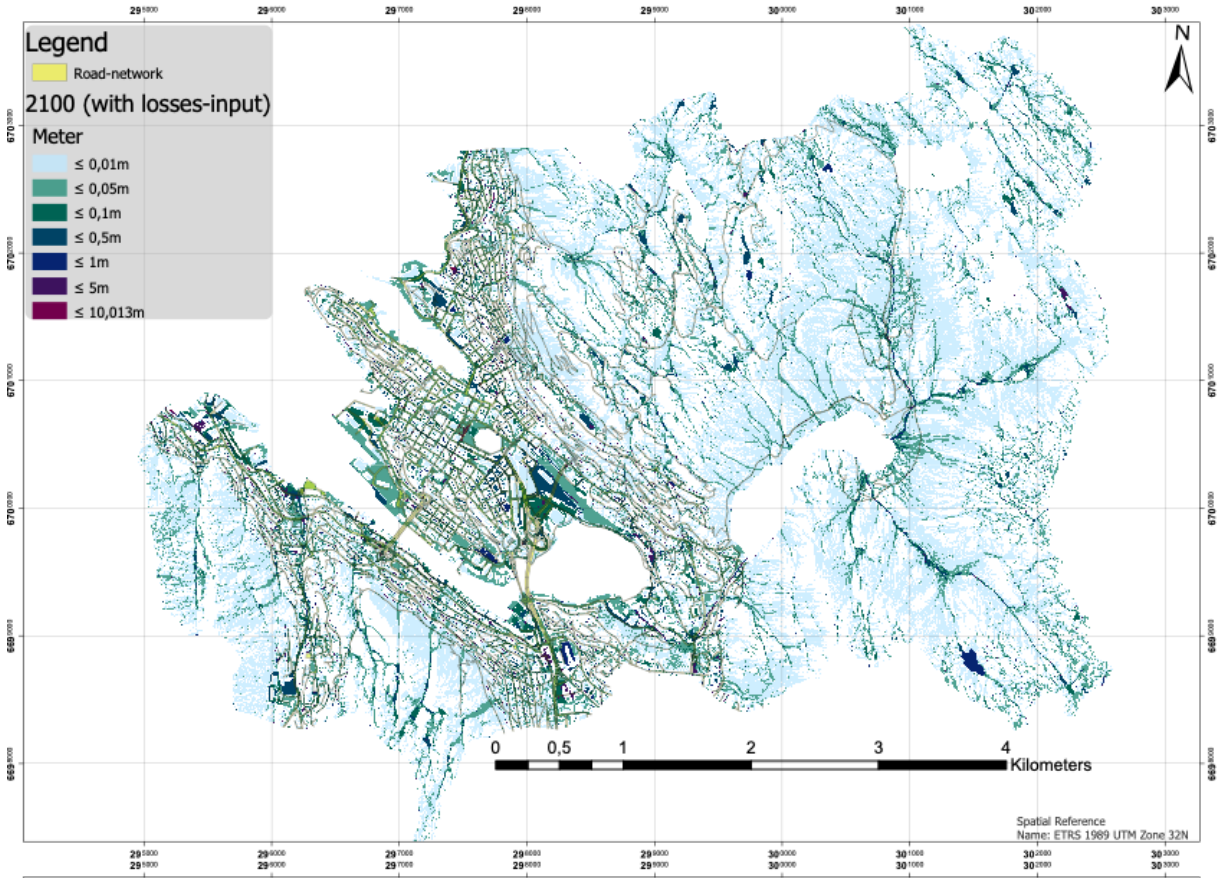
Legend
Road-network
2100 (with losses-input)
Meter
≤ 0,01m
≤ 0,05m
≤ 0,1m
≤ 0,5m
≤ 1m
≤ 5m
≤ 10,013m
N
0 0,5 1 2 3 4
Kilometers
Spatial Reference
Name: ETRS 1989 UTM Zone 32N

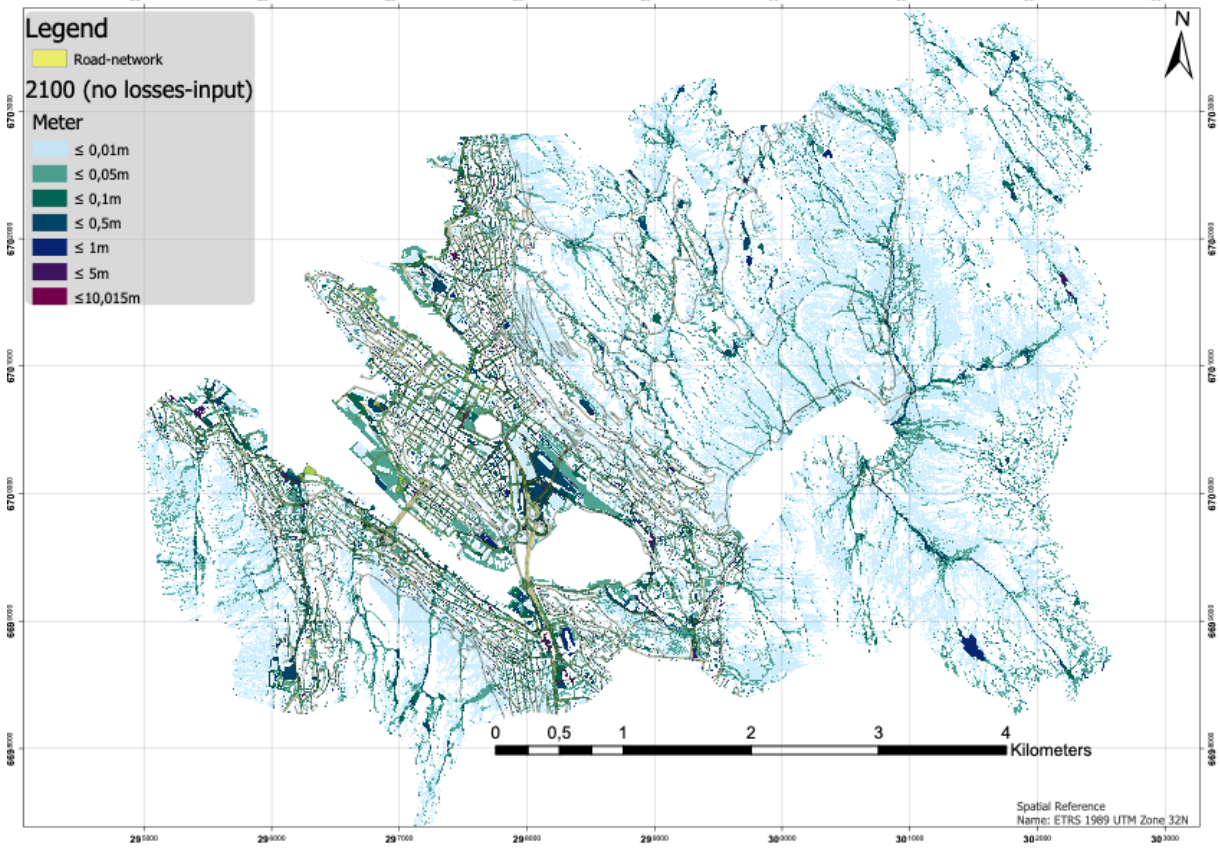
Legend
Road-network
2100 (no losses-input)
Meter
≤ 0,01m
≤ 0,05m
≤ 0,1m
≤ 0,5m
≤ 1m
≤ 5m
≤10,015m
N
0 0,5 1 2 3 4
Kilometers
Spatial Reference
Name: ETRS 1989 UTM Zone 32N

3-1. Itzï velocity results (5th hour from each timeseries)

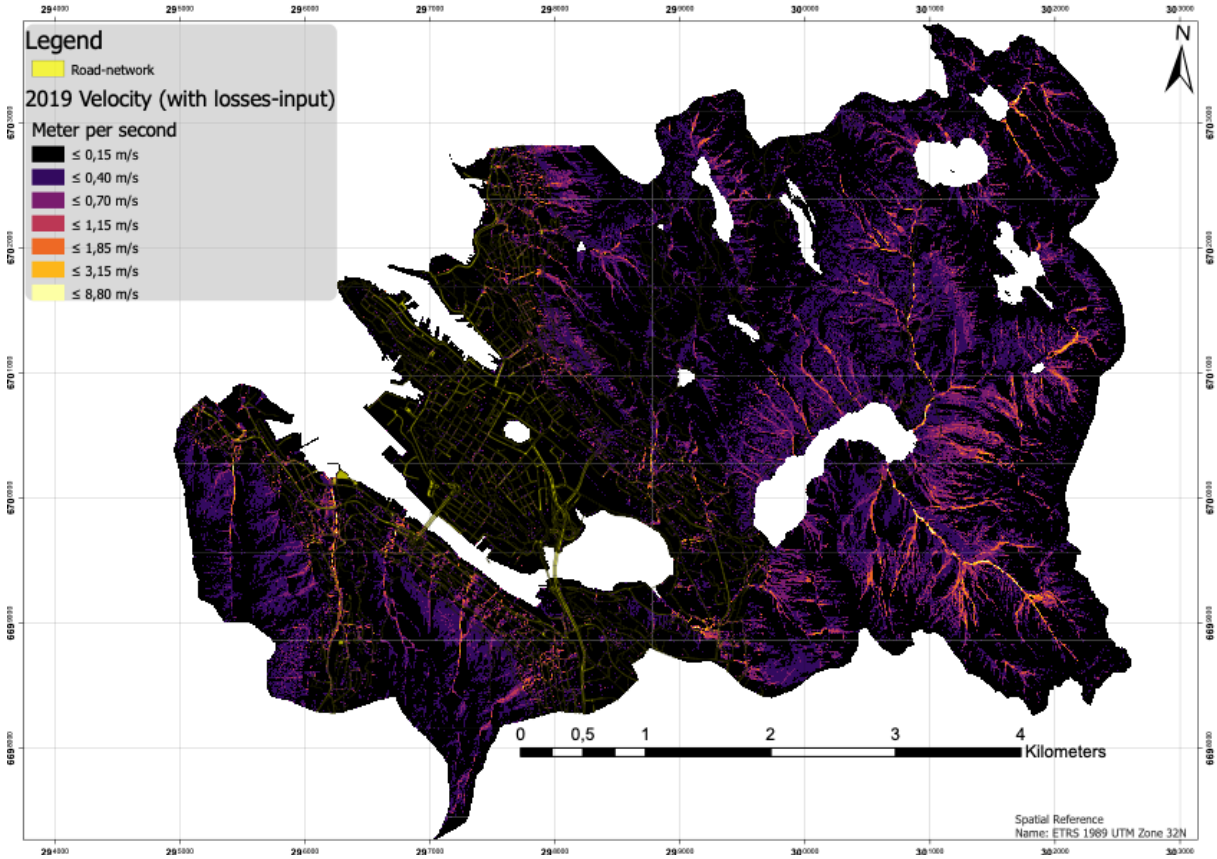

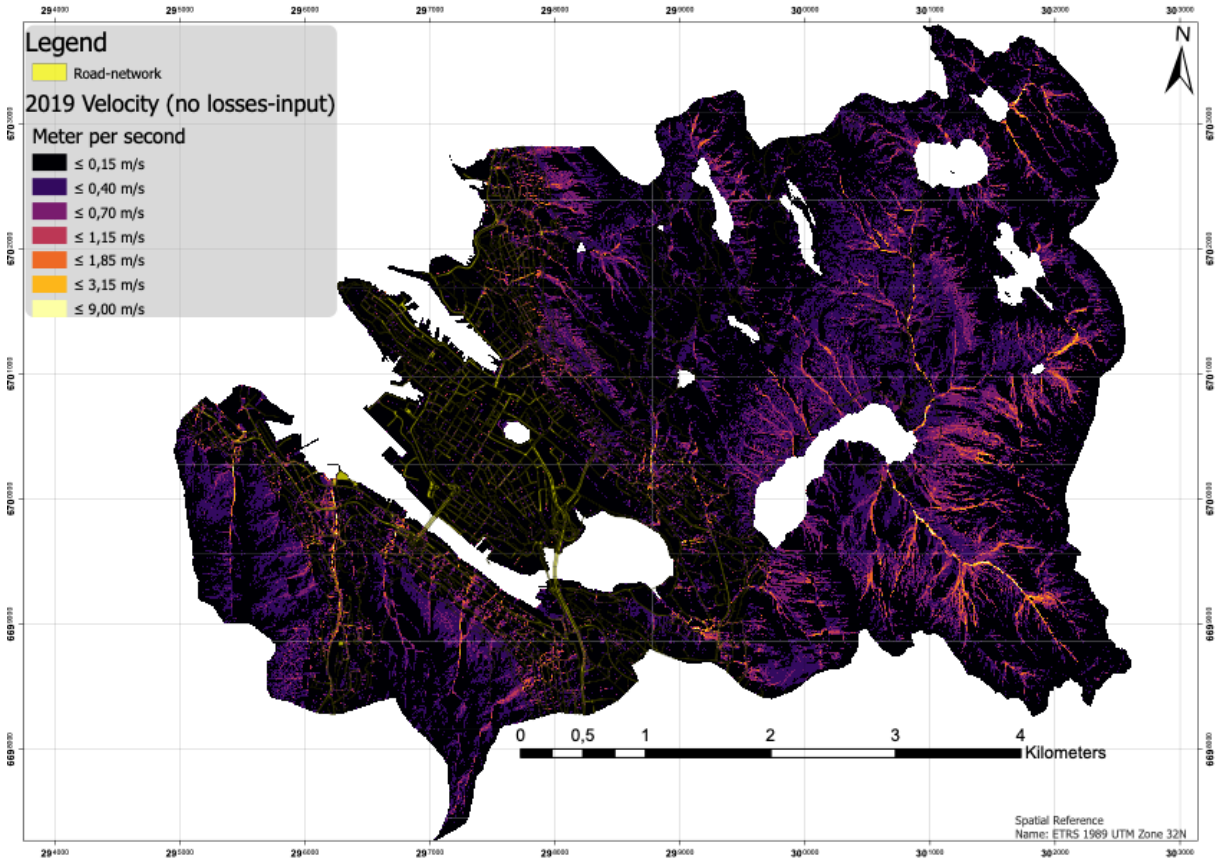

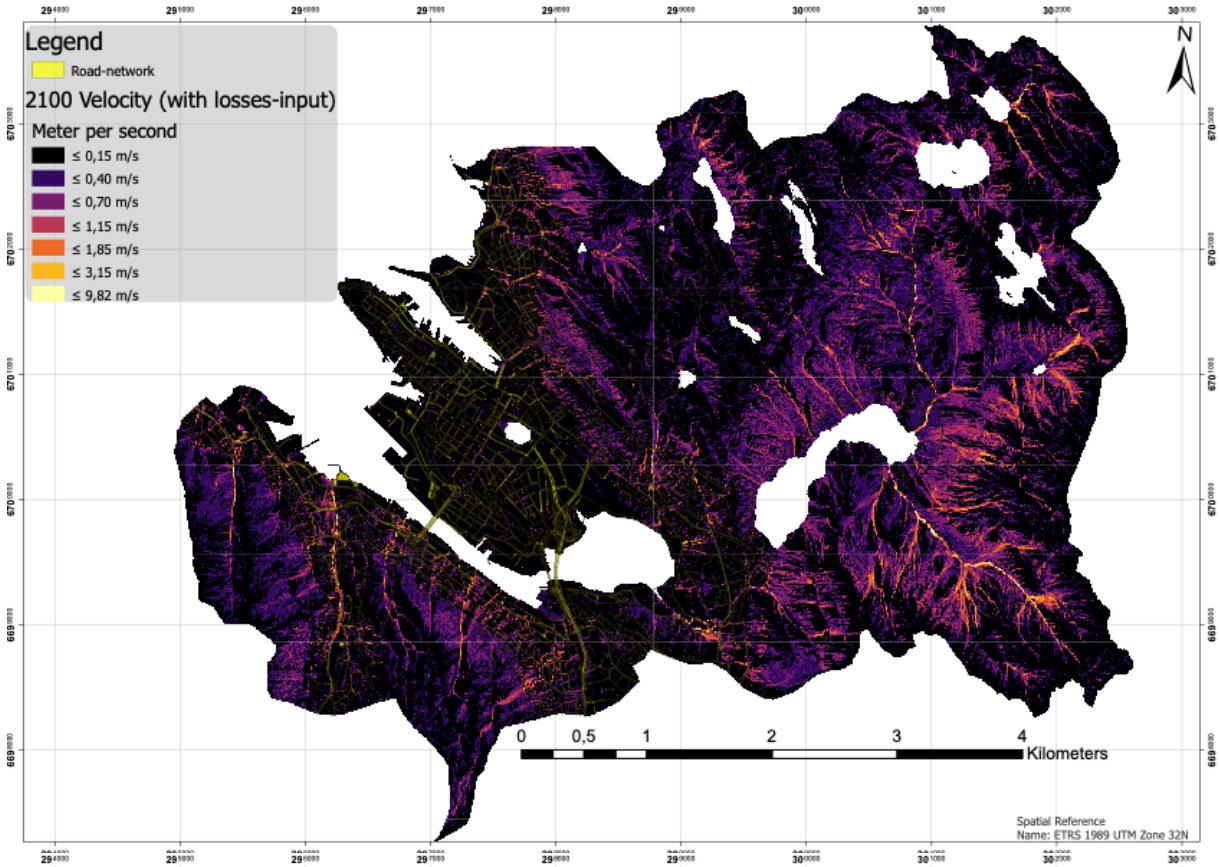
Legend
Road-network
2100 Velocity (with losses-input)
Meter per second
≤ 0,15 m/s
≤ 0,40 m/s
≤ 0,70 m/s
≤ 1,15 m/s
≤ 1,85 m/s
≤ 3,15 m/s
≤ 9,82 m/s
N
0 0,5 1 2 3 4
Kilometers
Spatial Reference
Name: ETRS 1989 UTM Zone 32N

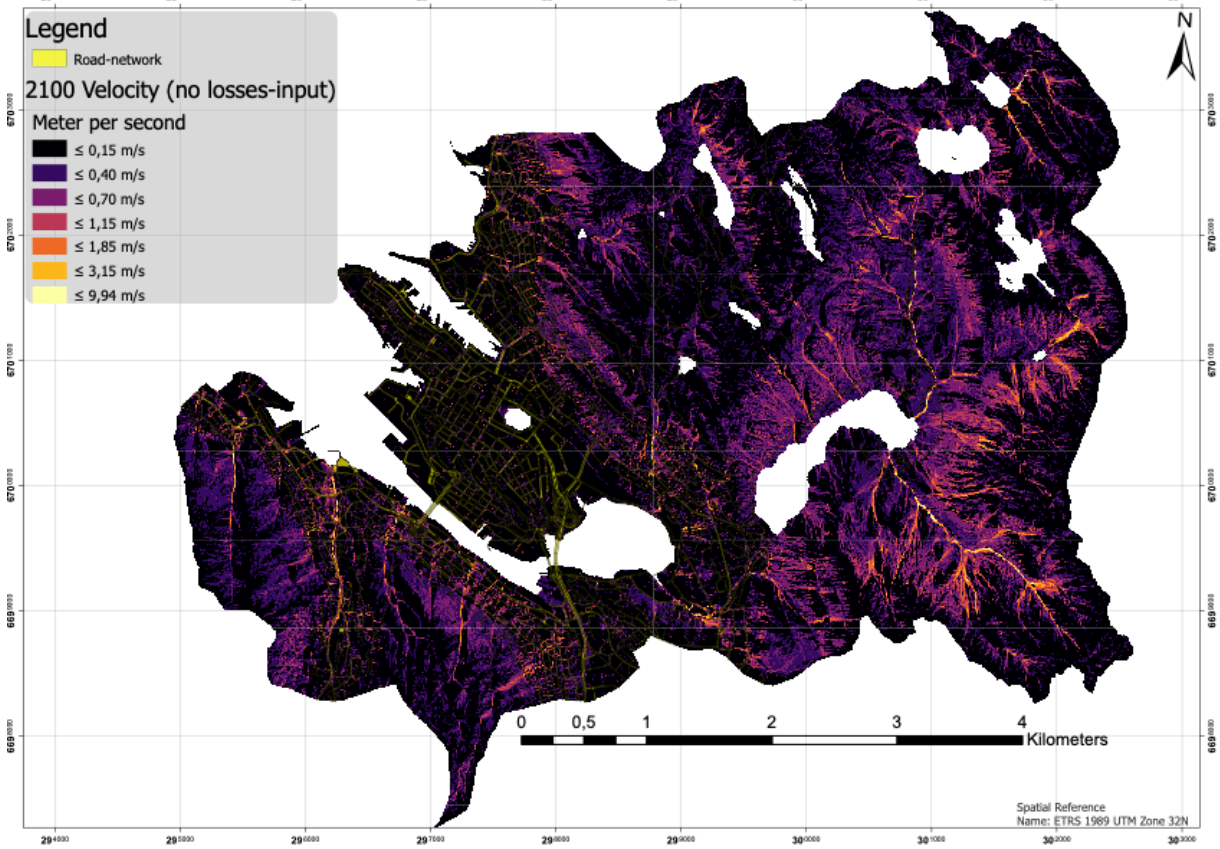
Legend
Road-network
2100 Velocity (no losses-input)
Meter per second
≤ 0,15 m/s
≤ 0,40 m/s
≤ 0,70 m/s
≤ 1,15 m/s
≤ 1,85 m/s
≤ 3,15 m/s
≤ 9,94 m/s
N
0 0,5 1 2 3 4
Kilometers
Spatial Reference
Name: ETRS 1989 UTM Zone 32N

3-2. Itzï velocity result (5th hour from year 2100 with no losses-data) compared to runoff-water dataset from Bergen Municipality